Chemoarchitectural studies of the rat hypothalamus and zona incerta. *Chemopleth 1.0* – A downloadable interactive *Brain Maps* spatial database of five co-visualizable neurochemical systems, with novel feature- and grid-based mapping tools

Vanessa I. Navarro[1–3,6,8–10], Alexandro Arnal[1,4,7], Eduardo Peru[1–3,6,9], Sivasai Balivada[1–3,10,11], Alejandro R. Toccoli[1, 2, 8, 9], Diana Sotelo[1,2,8,9], Olac Fuentes[4,5] and Arshad M. Khan[1–3,8–10*]

[1] UTEP Systems Neuroscience Laboratory, [2] Department of Biological Sciences, [3] Border Biomedical Research Center, [4] Vision and Learning Lab, [5] Department of Computer Science, [6] PhD Program in Bioscience, [7] PhD Program in Computational Science, [8] RISE Program, [9] HHMI PERSIST Brain Mapping & Connectomics Undergraduate Teaching Laboratory, [10] Interdisciplinary Group for Neuroscience Instruction, Training, and Education (IGNITE), [11] Lower Brainstem Group, The University of Texas at El Paso, El Paso, TX 79968.

Abbreviated Title

Census of rat hypothalamic/ZI chemoarchitecture

Key words

data visualization tool, digital overlay, grid-based mapping, neuronal nitric oxide synthase, hypocretin/orexin, melanin-concentrating hormone, copeptin, alpha-melanocyte-stimulating hormone, atlas, vector graphics

Address correspondence to:

Arshad M. Khan, Ph.D. (amkhan2 [at] utep.edu); Tel.: +1-915-747-8436, or
Vanessa I. Navarro (vinavarro [at] miners.utep.edu)

Abstract

The hypothalamus and zona incerta of the brown rat (*Rattus norvegicus*), a model organism important for translational neuroscience research, contain diverse neuronal populations essential for survival, but how these populations are structurally organized as systems remains elusive. With the advent of novel gene-editing technologies, there has been a growing need for high-spatial-resolution maps of rat hypothalamic neurochemical cell types to aid in their functional interrogation by virus-directed cell type-specific gene manipulation or to validate their expression in transgenic lines. Here, we present a draft report describing *Chemopleth 1.0*, a chemoarchitecture database for the rat hypothalamus (HY) and zona incerta (ZI), which will eventually feature downloadable interactive maps featuring the census distributions of five immunoreactive neurochemical systems: (1) vasopressin (as detected using its gene co-product, copeptin); (2) neuronal nitric oxide synthase (EC 1.14.13.39); (3) hypocretin 1/orexin A; (4) melanin-concentrating hormone; and (5) alpha-melanocyte-stimulating hormone. These maps are formatted for the widely used *Brain Maps 4.0* (BM4.0) open-access rat brain atlas. Importantly, this dataset retains atlas stereotaxic coordinates that facilitate the precise targeting of the cell bodies and/or axonal fibers of these neurochemical systems, thereby potentially serving to streamline delivery of viral vectors for gene-directed manipulations. The maps will be presented together with novel open-access tools to visualize the data, including a new Python programming language-based workflow to quantify cell positions and fiber densities for BM4.0. The workflow produces "heat maps" of neurochemical distributions from multiple subjects: 1) *isopleth maps* that represent consensus distributions independent of underlying atlas boundary conditions, and 2) *choropleth maps* that provide distribution differences based on cytoarchitectonic boundaries. These multi-subject cartographic representations are produced in Python from exported atlas maps first generated in the Adobe® Illustrator® vector graphics environment, which are then reimported and placed directly into the *Brain Maps* atlas. The soon-to-be-released files can also be opened using the free vector graphics editor, Inkscape. We also introduce a refined grid-based coordinate system for this dataset, register it with previously published spatial data for the HY and ZI, and introduce *FMRS* (Frequencies Mapped with Reference to Stereotaxy), as a new adaptation of long-used ephemeris systems for grid-based annotation of experimental observations. This database, which includes all data described in greater detail in Navarro (2020) and Peru (2020), provides critical spatial targeting information for these neurochemical systems unavailable from mRNA-based maps and allows readers to place their own datasets in register with them. It also provides a space for the continued buildout of a community-driven atlas-based spatial model of rat hypothalamic chemoarchitecture, allowing experimental observations from multiple laboratories to be registered to a common spatial framework.

Introduction

In this initial draft report, we describe *Chemopleth 1.0*, a soon-to-be-released downloadable database of maps of medial and lateral hypothalamic and zona incerta cell populations. Two sets of scientific developments in the 1990s – one, a set of careful labeling experiments, and the other, a set of rigorous technical innovations – form the basis for this database, which provides novel spatial data for five neurochemical systems.

First, experiments described over twenty-five years ago (Broberger et al., 1998; Elias et al., 1998), reported the relationship between neuropeptide-expressing cell populations in the medial hypothalamus (e.g., αMSH) and those in the lateral hypothalamus (e.g., H_1/O_A, MCH). These seminal findings, which included mRNA-label cell body distributions and select photographs of cellular interactions between some of these populations, were a high-water mark for hypothalamic chemoarchitectural studies, providing critical evidence linking first-order leptin-sensitive neuronal populations to downstream, second-order communication nodes (Sawchenko, 1998; Elmquist et al., 1999).

Second, the introduction by Swanson of digital atlas templates in the form of vector graphics files (Swanson, 1993) as a companion software package to his *Brain Maps* rat brain atlas (Swanson, 1992), marked a quiet turning point for neuroscientists seeking to create electronically formatted maps of neuroanatomical data they obtained from their own experiments for this model organism (reviewed in Swanson, 2001). One of the groups cited above (Broberger et al., 1998) used the *Brain Maps* atlas templates to map the distributions of cell bodies for medial and lateral hypothalamic neuronal populations, and additional groups have provided cell body maps of these populations in more recent versions of the *Brain Maps* reference space (Swanson et al., 2005; Hahn, 2010).

The *Chemopleth 1.0* database extends these developments – identifying medial and lateral hypothalamic cell groups and mapping their distributions to the *Brain Maps* atlas – in several important ways to better facilitate the precise targeting of these systems and their anatomical registration with other data for contemporary usage. First, unlike previous maps, the immunoreactive protein (i.e., immunohistochemical) maps in this database chart not only the cell bodies but also the axons and, in some cases, the terminal fields specific to these neurochemical systems in a standardized format. This is important for those interested in delivering retrogradely transportable vectors into axonal terminal fields (e.g., retro-AAV tracers), the locations for which are not provided by mRNA-based maps. Second, the cell bodies and axons charted in our database are mapped with respect to stereotaxic space, coordinates for which should be valuable to any experimentalist seeking to have a basic starting point to target vectors in the rat brain. At the time of this writing, such stereotaxically guided information is lacking in 2-D models at the spatial resolutions mapped here, let alone 3-D models of rodent hypothalamus produced by light sheet microscopy. Third, we provide computational tools that permit analysis and visualization of spatial information for each system in more than one subject and in more than one graphical representation to showcase the extent of variability for the distribution patterns observed, and to identify for the community the denser areas for each neurochemical system that can be experimentally targeted in stereotaxic space. Fourth, we present a new take on an older conceptual framework – grid-based annotation – that refines the existing stereotaxic coordinate system of the atlas and leverages its use for mapping and for gentle entry of outside datasets from the published literature into the database for the community to extend its contents.

Importantly, this study highlights the utility of the *Brain Maps* reference atlas as a *data repository*, taking advantage of the Adobe® Illustrator® (Ai) vector graphics workspace for the current *Brain Maps 4.0* (BM4.0; Swanson, 2018) digital atlas templates, and the ability of users to use, as an alternative workspace, the free vector graphics editor, Inkscape (www.inkscape.org) as another way to access this database in the near future. The foundation of *Chemopleth 1.0* consists of soon-to-be-released downloadable Ai (and Inkscape-compatible) files containing atlas templates for eight levels of the *hypothalamus (Kuhlenbeck, 1927)* and *zona incerta (>1840)* that form base maps in BM4.0. Building upon these base maps, we plan to provide the following tools/resources:

(1) *data layers* above the base map containing the mapped distributions of five chemically identified neuronal populations (both their cell bodies and their labeled neurites). These populations include the vasopressin gene product, copeptin; neuronal nitric oxide synthase (nNOS; EC 1.14.13.39), hypocretin/orexin (H_1/O_A), melanin-concentrating hormone (MCH), and alpha-melanocyte-stimulating hormone (αMSH);

(2) *choropleth maps*, which sort the relative abundance of distributions for the five neurochemical systems, in 3–7 subjects, by brain region;

(3) *isopleth maps*, which sort the relative abundance of distributions for the same neurochemical systems, in 3–7 subjects, independent of brain region; and

(4) *a grid-based coordinate system*, including the introduction of ephemeris tables for the distributions of these neuronal populations within this grid.

The Ai and Inkscape workspaces each allow for the interactive visualization of data layer overlays over each base map. Each data layer, which can be accessed using the *Layers* panel in Ai (*Layers and Objects* panel in Inkscape), can contain its own set of spatial data that is visualizable in relation to data present in other layers "in front of/above" or "in back of/under" the layer being examined.

After presenting methodological information about how the *Chemopleth 1.0* database and its tools were built, we describe the mapping innovations of the database and how to navigate the digital overlays within it. We then discuss the philosophy underlying the need for these tools, highlight the contents of the database in relation to previous visualization efforts, and discuss the design features of the database, including our conceptual framework for grid-based annotation. Because this study is presenting visualization tools (downloadable vector-formatted maps with digital overlays; open-source code for spatial averaging) for a structural model (a standardized brain atlas) of a complex object in nature (the brain), our narrative draws from an eclectic set of disciplines (cartography, geosciences, computing), as well as programs in the humanities and arts – all of which include scholarly and artistic efforts to visualize, register, and annotate complex information in time and space.

Materials and Methods

2.1 Naming conventions

Chemopleth 1.0 contains data populating brain regions named in accordance with Swanson (2015), as applied to the rat brain in *Brain Maps 4.0*, an open-access rat brain atlas (Swanson, 2018) and includes standard terms. Each term is set in italics and includes the named neuroanatomical structure and the associated author-date citation that first uses the term as defined, e.g., "*lateral hypothalamic area (Nissl, 1913)*". For those terms where assignment of priority was not possible, they are assigned the annotation "*(>1840)*", i.e., "defined sometime after the year 1840", a year which roughly marks the introduction of cell theory in biology, e.g., "*dorsomedial hypothalamic nucleus (>1840)*". Standard terms for *gray matter regions (Swanson & Bota, 2010)* can be found in "Table C: Rat CNS Gray Matter Regions 4.0 (Topographical Histological Groupings)" from the Supporting Information available online for Swanson (2018), which is based on the scientific literature and cytoarchitectonic features of Nissl-stained tissue sections. Similarly, *white matter tracts (Bell & Bell, 1826)* are listed in "Table D: Rat CNS White Matter Tracts 4.0 (Topographic Histological Groupings)" from the same Supporting Information, e.g., "*hypothalamic postcommissural fornix (Swanson, 2015)*". Importantly, any citation included within the standard term is included in the list of cited references in this study. A list of the standard terms and the abbreviations used in this study is provided in the Abbreviations section.

2.2 Early lessons

2.2.1 Settling on a mappable label

This project has its antecedents in our early student-driven efforts to characterize activation patterns for hypocretin/orexin-immunoreactive neurons in the lateral hypothalamic area in rats receiving glycemic challenges (Nham & Khan, 2009a, b), which led to exploration of additional cell types in this region (Agostinelli et al., 2010; 2011). These efforts, which were undertaken using immunofluorescence histochemistry, evolved to include a systematic photomicrographic analysis of several tissue biomarkers in the hypothalamus from 2012–2015 (Pinales et al., 2012; 2013a,b; 2014; Pennington et al., 2014; Wells et al., 2014a, b). By this time, we had also started examining the utility of axonal mapping for optogenetic applications and for examining putative synaptic interactions between labeled systems in the hypothalamus (Escapita et al., 2015; Wells et al., 2015a–c). While additional fluorescence-based efforts continued within our two-semester Brain Mapping & Connectomics undergraduate laboratory course as part of student-driven research (D'Arcy et al., 2016; Flores-Robles et al., 2017; Burnett et al., 2018; Martinez et al., 2018; 2019), the learning outcomes and curriculum for which also have been reported (D'Arcy et al., 2019; Khan et al., 2021), signal longevity and other challenges from the fluorescently-labeled tissue sets led us to realize that these patterns were best *mapped* using archival, non-labile staining that could be better controlled, signal-wise, across time (some of these issues have been detailed by Wells, 2017). Therefore, alongside these efforts, we used immunoperoxidase-based labeling methods, which yield signals that remain relatively stable over time (Guzman et al., 2019; Sotelo et al., 2019; Navarro et al., 2019; Peru et al., 2019; Navarro, 2020; Peru, 2020; Sotelo et al., 2020/21; Toccoli et al., 2020/21).

2.2.2 Settling on a feasible workflow for mapping density estimations

Originally, for our immunohistochemical labeling patterns, we wanted to estimate densities

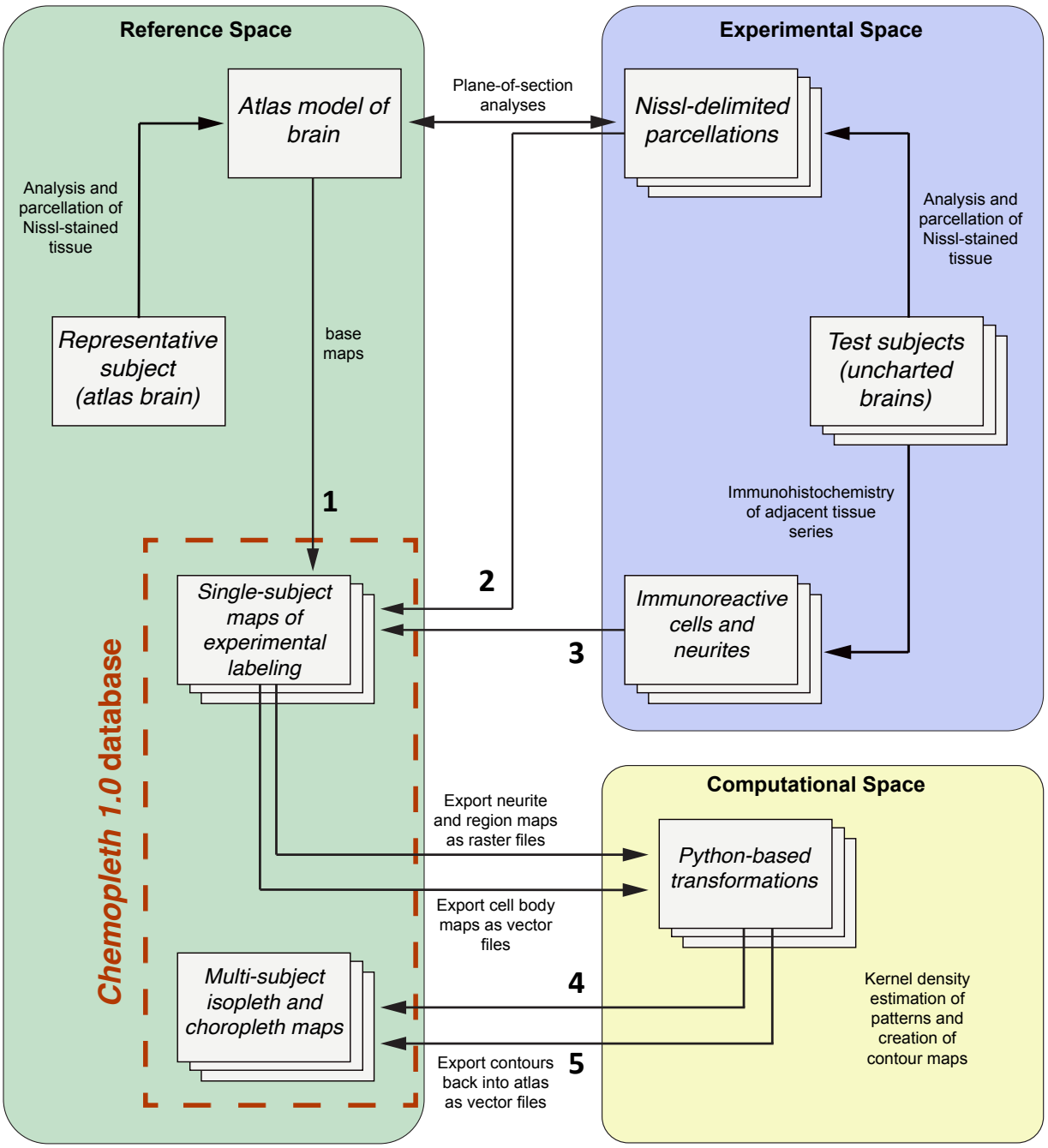

Figure 1. Workflow used by our laboratory to generate content for the *Chemopleth 1.0* database. Five steps (each numbered **1–5** in bold within the schema above) feed data into the database (dashed red box): (**1**) base maps from the *Brain Maps 4.0* rat brain atlas in *Reference Space*, for which (**2**) Nissl-stained series from experimental brains (*Experimental Space*) provide critical context-of-plane boundaries for parcellated regions, that, in turn, allow us to map (**3**) immunoreactive cells and neurites from adjacent series of tissues from these subjects onto the base maps. These single-subject maps can collectively be exported as raster or vector files into a Python-based *Computational Space*, where a custom-coded algorithm allows for their spatial averaging using kernel density estimation and their import back into *Chemopleth 1.0* (Steps **4** and **5**) as heat maps of multi-subject information on a single base map. These maps can either be choropleths (heat maps based on atlas territories), or isopleths (heat maps based on distributions independent of the underlying base map). See text for details.

of labeled elements within brain regions delineated on BM4.0 atlas maps. This led to an attempt to draw each vector-delimited area in BM4.0 base maps as a "shapefile" within a Geographic Information System (GIS) framework. Initial shapefiles were constructed in Mar 2020 by SB by exporting Ai files as .dxf AutoCad files for use in QGIS open-access software and plots of density distributions were created within the *R* framework (SB, unpublished laboratory blog post, 15 Apr 2020). Our initial efforts "were successful, as far as they went" (Hatton, 1984, p. 342). It soon became apparent, however, that the vector files from Ai needed to have closed polygons and exporting raster images of those regions would be more efficient than manually drawing shapefiles. It also became clear that we needed a tool "to take a published [BM4.0 atlas] map used by someone to populate their data and render it back into vector format so we can align [it] with current vector maps" (Khan, unpublished laboratory blog post, 21 May 2020). Therefore, we decided upon a workflow that would take vector-based shapes and *export them* for raster-based analysis and *return them* as vector graphics at the user level within the Ai graphical user interface. To achieve this, we settled upon the workflow described in the next section.

2.3 Overall workflow

Our workflow used to generate the data and populate the database operates within three major conceptual spaces: *Reference*, *Experimental*, and *Computational* (**Figure 1**). The *Reference Space* includes the *Chemopleth 1.0* database, which provides new content for the rat brain atlas reference, the *Brain Maps 4.0* (BM4.0) rat brain atlas (Swanson, 2018). Included in this *Reference Space*, therefore, is the actual animal subject which forms the basis of the BM4.0 atlas, an adult male 315-g Sprague Dawley rat ("representative subject"), along with the Nissl-stained brain tissue which was studied by Swanson to produce cytoarchitectonic boundaries for all major cell groups of the rat brain ("atlas brain"); these were drawn as vector objects to form atlas maps ("atlas model of the brain"). These atlas maps, in turn, serve as the *base maps* for the *Chemopleth 1.0* database (**Input 1** in **Fig. 1**).

The *Experimental Space*, in contrast, contains the test subjects we wanted to map chemoarchitectural labeling for within the BM4.0 atlas, which would form the basis of *Chemopleth 1.0*. In this space, we sectioned brain samples, collecting 30 μm-thick tissue sections into two adjacent series, the first of which was stained with thionine to generate a Nissl-stained series for reference, and the other series stained for a neuropeptide or neural enzyme of interest using immunohistochemistry (detailed in Navarro, 2020; Peru, 2020). The Nissl series provides labeling patterns that reveal the overall cellularity of the tissue and allows for cytoarchitectonic parcellation of stained cell clusters into nuclei and areas. We used that spatial information to infer what the boundary conditions were for nuclei and areas for those sections immunostained in the companion series, for which full labeling was never observed as it was with the Nissl series, but which were in tissue sections close enough to the Nissl section to permit the transfer of its boundary assignments.

In **Figure 1**, we have noted these processes in the *Experimental Space* with the Nissl-delimited parcellations and drawings of immunoreactive cells and neurites serving as Inputs **2** and **3**, respectively, to create the single-subject maps in the *Choropleth 1.0* database within the *Reference Space*. Thus, the single-subject maps of chemoarchitecture in *Chemopleth 1.0* were a product of: (**Input 1**) BM4.0 digital-format base maps; overlaid with (**Input 2**) Nissl-delimited boundaries to guide the mapper in drawing (**Input 3**) the labeling patterns of immunoreactive cells and neurites for the neurochemical systems we examined over the right locations on the base map.

Finally, we sought to develop cartographic methods that allow us to visualize immunoreactivity patterns in the same atlas level for more than one subject, so that consensus locations on the map could be identified across subjects where labeling was observed. To achieve this goal, we developed a Python-based workflow that allowed the cell and fiber maps from single-subjects to undergo a conversion into file formats that could then be exported out of the database and processed in *Computational Space*, re-entering the *Reference Space* as multi-subject "heat maps" showcasing the concordance of distributions of immunoreactivity for any given molecule we labeled. Two types of "heat maps" were generated (**Inputs 4 and 5** in **Fig. 1**). The first type was a *choropleth map* (Dixon, 1972), which scores the density of labeling as a color-coded gradient over a base map of defined territories; these vector-object territories on the base map first had to be 'closed' to form discrete polygons (see *Section 2.5.2*). The second type was an *isopleth map* (Mackay, 1951; Schmid & MacCannell, 1956; Barnes et al., 1970), which did not bin densities based on cytoarchitectonically bounded regions on the base map, but rather, was a computationally produced pattern based on kernel density estimation, which allows for distributions to be shown independent of the bounded cytoarchitectonic regions of the base map underneath them.

2.4 Data sources

In principle, as with other transformation workflows (e.g., see Oguchi et al., 2011; Khan et al., 2018) a variety of data sources, analog or digital, could potentially enter the proposed workflow as input data with the appropriate transformations. For this study, the most basic input data consisted of single-subject maps drawn in the commercially available (for-purchase software) workspace, Adobe® Illustrator® (Ai), as data layers over a base map. These are produced within the vector graphics application itself and registered to the *Brain Maps 4.0* base map (Swanson, 2018) which is the bottom layer ("base maps"; **Fig. 1**) making up the database (**Inputs 1 + 2 + 3, Fig. 1**). A second, more derived set of data populating our database is in the form of "heat maps" that are created by first exporting several individual maps of a single atlas level as .PNG or .SVG files, then processed by a Python program to create the heat maps using a Gaussian filtering form of kernel density estimation, after which these maps are re-imported into the database (**Inputs 4 and 5, Fig. 1**). Note that we used the Ai workspace to create these files, but they can, in principle, be generated within (or imported from) the free vector graphics editor, Inkscape (www.inkscape.org). Guidance for downloading, installing and using Inkscape can be found online at the Inkscape Beginner's Guide. All procedures described below were performed within or in relation to use of Ai workspace, and hence will be discussed mainly in that context, but readers using Inkscape should be able to utilize the database, once it is released, just as readily.

2.5 Tissue processing, parcellations, alignment, mapping, and semi-quantitative analysis

These procedures, which were required for us to produce atlas maps of the chemoarchitecture, will be described in detail elsewhere, and have been described thus far within our student dissertations forming the basis of this project (Navarro, 2020; Peru, 2020; also see Wells, 2017 and pp. 6–9 of Arnal, 2022). Below, we describe our spatial analysis of these maps to produce our final dataset that forms the *Chemopleth 1.0* database; we also show how to navigate the dataset and

Figure 2 (next page). Summary of bounded regions provisionally finalized for the *Chemopleth 1.0* database. Regions with visually apparent cytoarchitectonic boundaries were provisionally assigned closed boundaries to allow us to compute across them to produce areal densities for choropleth mapping. See text for details.

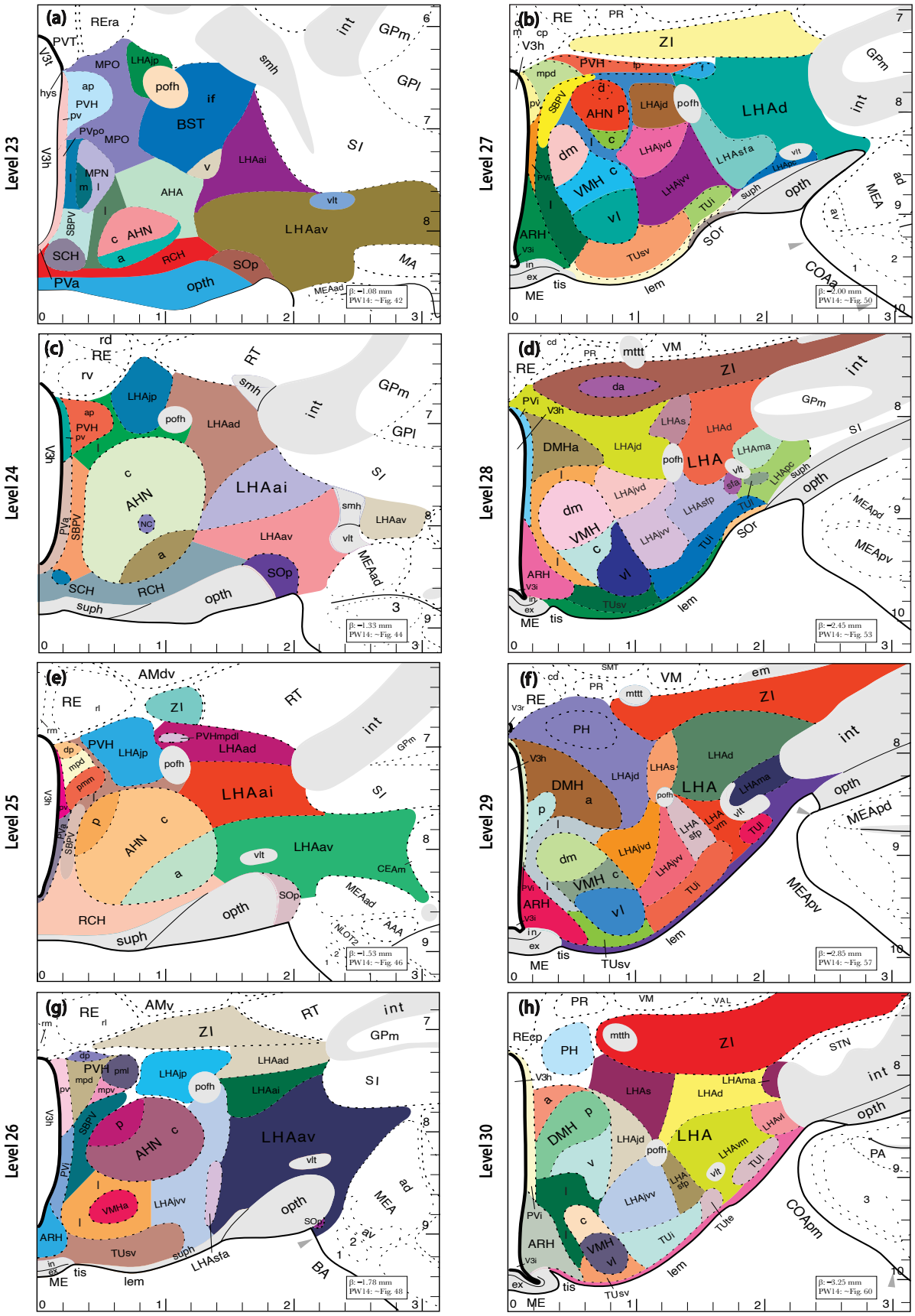
Level 23
(a)
β: −1.08 mm
PW14: ~Fig. 42
Level 27
(b)
β: −2.00 mm
PW14: ~Fig. 50
Level 24
(c)
β: −1.33 mm
PW14: ~Fig. 44
Level 28
(d)
β: −2.45 mm
PW14: ~Fig. 53
Level 25
(e)
β: −1.53 mm
PW14: ~Fig. 46
Level 29
(f)
β: −2.85 mm
PW14: ~Fig. 57
Level 26
(g)
β: −1.78 mm
PW14: ~Fig. 48
Level 30
(h)
β: −3.25 mm
PW14: ~Fig. 60

import/register user-generated data.

2.6 Preparing the dataset for spatial analysis

Our maps of immunoreactive perikarya and neurites, present within the Ai vector graphics workspace as digital overlays, were spatially analyzed outside of this workspace ("Computational Space" in **Fig. 1**) to produce novel data visualizations and tabulated measurements using Python programming language (Van Rossum, 1993; see Van Rossum (2009–2018) for a history of Python). To prepare the data for use in Python, a script was written in JavaScript (JS) programming language (Wirfs-Brock & Eich, 2020) that could be accessed and run within the Ai workspace to export the maps into a usable format. The JS script, *Swanson Data Exporter.js*, is available on GitHub.

2.6.1 Exporting data

Individual data layers from the BM4.0 dataset were exported from the template files within the Ai workspace by running the JS script as described above. Perikarya mapped on the electronic atlas templates were exported as scalable vector graphic (SVG) files. Each SVG file contained the mapped antigen from one animal on one level of the atlas and the Ai artboard of the atlas level, which served as the spatial reference frame across files.

Neurite maps on the atlas were exported as portable network graphic (PNG) files. Unlike the perikarya maps represented by coordinates, neurite paths were represented by raster images, with discrete bins or pixels marking the neurite trajectory. The artboard also served as a spatial reference frame across files, and the stroke width of all paths was set to approximately 5 μm before exporting.

Rationale for our export methods. For perikaryal analysis, to prevent us from being limited by the size of the circle glyph in vector space used to mark the cells, we kept the SVG vector format of the map rather than exporting the raster. Instead, once imported as an SVG into the Python program, a raster was generated internally to represent those cells which was then computed upon to generate counts and/or to perform Gaussian blurring. For neurite maps, the entry into Python of the PNG (raster) format obviated the need for any further processing to perform the same analysis.

2.6.2 Exporting regions of the BM4.0 base map for choropleth analysis

Brain region and stereotaxic grid boundaries were exported to compute region-dependent measurements for each atlas level to produce choropleth maps (as described in *Section 2.7.2*). However, some brain region boundaries in *Brain Maps 4.0* are only visually implied and had to be fully closed to enable proper data binning by the Python programs. Therefore, before exporting them, we converted these visually implied regions to closed polygons in Ai **(Fig. 2)**. We found that the easiest way to obtain these polygons without manually redrawing boundaries was to use the *LivePaint* feature in Ai, which interpolates between existing paths that are close to each other. The feature takes a user-defined "gap" parameter to automatically close paths that may not be fully intersecting or touching. Lastly, we cleaned up the final regions by merging polygons that belonged to a single region such that the number of polygons equaled the number of brain regions. Then, after closing visually implied regions, we addressed the brain regions in the atlas that shared a continuous space with other regions, such as the *internuclear hypothalamic area (Swanson, 2004)* (I). For these cases, our team members (AA, VIN, SB, AMK) conferred to draw new boundaries provisionally. In this manner, all regions had discrete boundaries, which enabled region-dependent

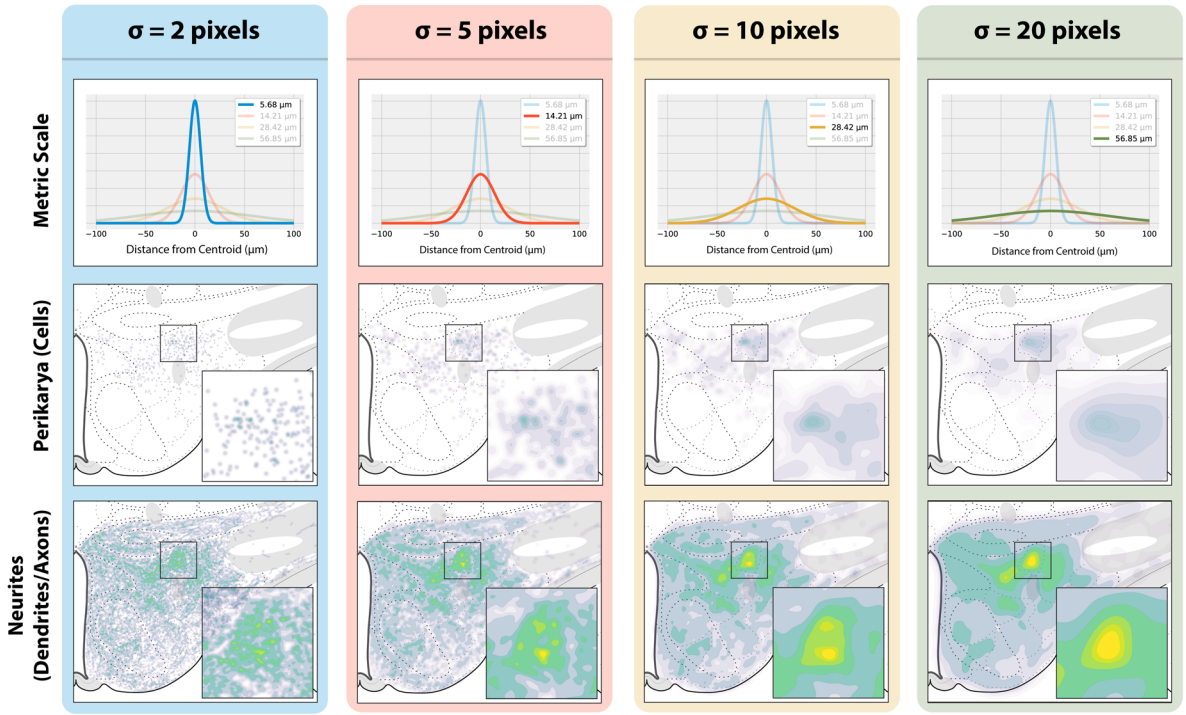

Figure 3. Comparison of kernel density estimation parameters and their resulting isopleth maps. The columns from left to right are sorted by increasing values for sigma (in pixels), which is a value that signifies the spread of the normal distribution curve for any mapped perikaryon. **Top row**: The normal distribution curves resulting from the sigma value assignments, as measured in microns. **Middle row**: Isopleth maps of the mapped perikaryon profiles from multiple subjects averaged together and plotted on the base maps of the *Brain Maps 4.0* rat brain atlas (Swanson, 2018), with the box outlining the enlarged area containing a portion of the *lateral hypothalamic area (Nissl, 1913)*. **Bottom row**: Isopleth maps of the neurite profiles from the same subjects, with the box outlining the same region as for the middle row (cell body) maps. For the *Chemopleth 1.0* database, all isopleth maps were generated with a sigma value of 10 pixels (*third column from the left*). See text for details.

quantification of perikarya and neurite profiles. For *Chemopleth 1.0*, these boundaries are a necessary starting point for our analyses, but we anticipate that the boundary assignments will change as new data about the regions come to light or if further discussion warrants a redrawing of the boundaries based on new information. Readers must be aware that any boundaries they may wish to redraw would likely necessitate a re-analysis of choropleth scores, since such scores are computed over the total area occupied by each polygon.

2.7 Spatial analysis of data

2.7.1 Importing data into Python for further computational analysis

The raster approach described in *Section 2.6.1* allows binning the perikaryon centroid points and neurite profiles to a uniform grid of pixels ("control areas") to facilitate cell and neurite counts for choropleth mapping. A useful reference to guide readers on setting such "control areas" is provided by Barnes (1978). The approach also allows for density estimation of perikaryon and neurite profiles by Gaussian blurring to produce isopleth maps.

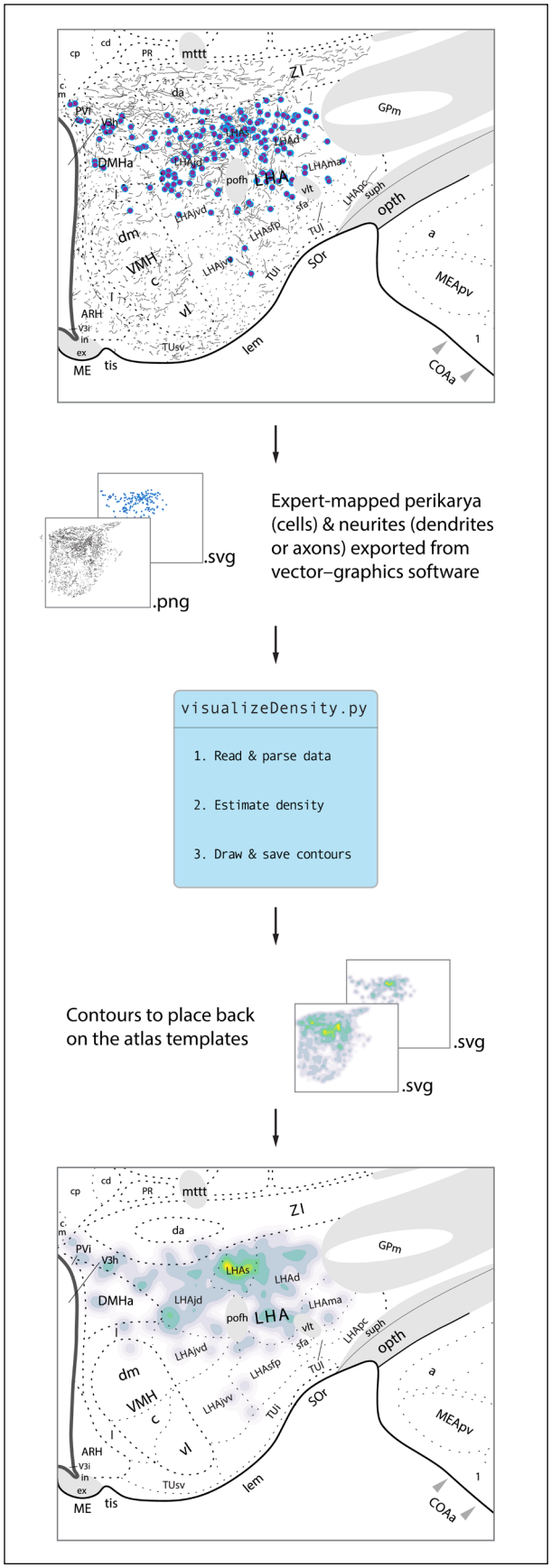

2.7.2 Generating isopleth maps for mapped immunoreactive perikarya and neurites

To visualize spatial trends of immunoreactivity in a manner that considers subtle differences in the exact atlas map placements of filled circles for perikarya that would statistically occur because of the mapper, we decided to represent each instance of an immunoreactive perikaryon and neurite segment as a normal distribution curve in two dimensions. The normal curve has a long history of describing error distributions, dating back to its mathematical formulation in 1808 (Adrain, 1808; Gauss & Davis, 1857; Stahl, 2006; Pontes, 2018). Suitably, the normal curve is an appropriate representation of a mapped perikaryon (or neurite segment) since it embodies the distribution of errors, with the peak of the curve assigned as the centroid point of the plotted perikaryon and the possible alternative positions on the plot assumed to be within a normal distribution. Specifically, the sigma value (σ), which determines the spread of the normal curve, can be considered a proxy for errors incurred when mapping a particular perikaryon (or neurite) to an atlas template. Based on sampling of various hypothalamic regions and measuring the diameters of perikarya (10–15 perikarya/region), we found the average diameter of perikarya to usually range between 10–20 µm. We therefore set σ to ~14 µm, which would place any perikaryon's mapped circle centroid point at ~28 µm from the first standard deviation of the Gaussian curve (third column (10 pixels) in **Fig. 3**), thus conservatively blurring the location information for 1–3 mapped perikarya. Now, if a perikaryon is ~28 µm in diameter, this means that a region with a diameter of ~28 µm can physically only contain information about one perikaryon's position. Put another way, the only time a region

Figure 4 (*left*). Process of generating isopleth maps of chemoarchitecture from multiple subjects based on individual single-subject maps exported and computed upon by a custom Python workflow. See text for details.

of 28 μm can contain information about more than one perikaryon is if there is an overlap of perikaryon positions from multiple experimental subjects. We found the probability value, or the height of the curve at the first standard deviation and used multiples of that height as thresholds to draw contours. This effectively gave us a contour for regions where densities were similar. Of course, depending on the needs of the mapper and the sizes of the cells to be mapped, one could adjust the sigma value to reflect the dimensions of other perikarya. We suggest that readers try different values based on their region of interest, the size of the perikarya in that region, and the desired granularity of the isopleth map needed.

In our implementation, we used the gaussian_filter method of the Python library, SciPy, which takes as input 1) the raster image of the mapped distributions from a BM4.0 atlas template and 2) the σ value and produces a blurred version of the input image or raster. Mathematically, the blurring occurs after computing a 2-dimensional normal curve of pixel intensities at every pixel position. Moreover, this Gaussian blur method is faster than the traditional stepwise kernel-density estimation method of iterating over all perikarya and neurite segment centroids and computing the density of every point while progressively adding them together (Gray & Moore, 2003; Virtanen et al., 2020). Once the program computed the density estimation maps, the maps were passed to a contouring function to draw contours at 10–100% of maximum density in 10% increments. The program then saved the contour as an SVG file which we then placed back on the map in the Ai workspace **(Fig. 4)**.

We also extended this process to visualize spatial trends of cell and fiber distributions for a given neurochemical system from multiple cases. To achieve this, we computed each density map, and before passing them to the contouring function, we combined the density maps by averaging. Then, for multiple levels, we looped through the final density maps of each level and recorded the minimum and maximum values across all levels. Finally, we generated a contour map for each level. However, this time, we provided the minimum and maximum values to the contour function, allowing the color scheme to capture the relative distribution among levels.

2.7.3 Generating choropleth maps for mapped immunoreactive perikarya and neurites

To streamline the process of counting perikarya or estimating neurite density per region, we developed a Python program that utilizes raster brain regions and stereotaxic grid regions to automatically calculate the number of perikarya and approximate area of neurites. The data loading process for this method is identical to that used for the isopleth analysis, except that brain regions of the BM4.0 atlas were first prepared for export as described earlier in *Section 2.5.2*. Once the raster versions of the data were ready, we loaded the region files and iterated through all the regions across the corresponding level. At each step, we calculated the number of pixels in each data raster that overlap with the region raster.

For perikaryon profiles, we tabulated the number of overlapping pixels representing the direct perikaryon profile count and applied a sampling correction (Abercrombie, 1946). For neurite profiles, we tabulated their approximate area by scaling the count of overlapping pixels by the metric conversion factor of approximately 8×10^{-6} mm^2/pixel (i.e., 1 pixel represents that much space in vector space). We then calculated the averages of counts or areas per level across cases of the same marker. Subsequently, we utilized the tabulated information to generate choropleth maps with brain regions serving as the bins of the map. However, instead of simply using the counts of perikarya or the area of neurites per region to color the choropleth regions, we normalized all

values by the area of their respective brain regions. The final choropleth maps were saved as raster or PNG files and then placed on a data layer within the Ai atlas workspace. Next, we iterated across the averaged levels to record the lowest and highest values, which were used to assign colors that captured the relative distribution among levels of a given marker.

2.8 Spatial referencing of profile counts

2.8.1 Feature-based spatial referencing

As described previously (*see* Fig. 6 of Khan et al., 2018), the spatial distributions of the data plotted in the maps generated in this study were determined by superimposing the drawn boundaries of *gray matter regions (Swanson & Bota, 2010)* [see *Section 2.1* for naming conventions] of the HY and ZI, determined by cytoarchitectural criteria revealed by adjacent Nissl-stained tissue sections. The cytoarchitectural criteria used in this study are based on those used by Swanson (2004), which draw upon a wide variety of studies for each of the HY *gray matter regions (Swanson & Bota, 2010)* presented. In summary, these are the morphology, staining intensity, orientation, packing density and distribution as revealed by Nissl-stained sections. The scope of the current study includes BM4.0 atlas templates (levels 23–30), which cover two of the four major rostrocaudal divisions of the *hypothalamus (Kuhlenbeck, 1927)* (HY) (anterior and tuberal). For each of these levels, the entire mediolateral and dorsoventral extents of the HY were analyzed, and many of these levels also included the *zona incerta (>1840)* (ZI) within the *ventral thalamus (His, 1893)* (TH) (see *Section 3.1*). Cytoarchitectural boundaries of tissue sections were used to identify them as corresponding to one of the atlas levels observed in this study (plane of section analysis), which then allowed for the transfer of data from immunohistochemically stained sections to atlas templates. These same cytoarchitectural boundaries established with the use of photomicrographs of Nissl-stained tissue sections are overlaid onto the photomicrographs of immunohistochemically stained sections using Ai software to organize them into transparent layers (digital overlays). Overlays in Ai also allowed for the migration of data from tissue sections to approximate locations of all mapped perikarya and neurites onto atlas templates in this study.

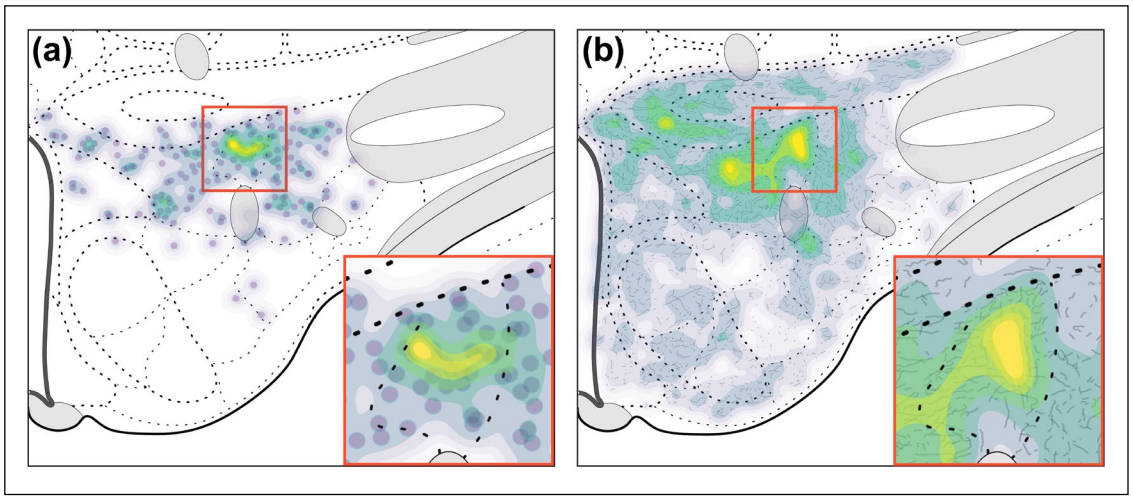

Figure 5. Qualitative validation of isopleth accuracy. Isopleth maps were overlaid over **(a)** perikarya maps or **(b)** neurite maps from single subjects to compare the distribution patterns between the maps. Notice that the brighter areas, which reflect greater average density, tend to be over single-subject maps also showing areas of higher density, accurately reflecting those patterns.

We distributed our profile counts across the hierarchical list of brain regions found in Table C: Rat CNS Gray Matter Regions 4.0 (Topographical Histological Groupings) from the Supporting Information available online for Swanson (2018). Counts were made from the mapped glyphs denoting immunoreactive neuronal profiles and tabulated.

2.8.2 Grid-based spatial referencing

Complementing our feature-based spatial referencing, we reasoned that indexing the quantitative data to an atlas-independent spatial reference system would allow the data to be readily migratable to other atlas reference spaces indexed to the same format, as we have discussed previously (see §4.6.2.2 of Khan, 2013; Khan et al., 2018a; Perez et al., 2018). Accordingly, we are proposing a system to tabulate the distributions of our profile counts within a stereotaxic, grid-based spatial referencing system. This was facilitated by Swanson's inclusion of the stereotaxic coordinate system of Paxinos and Watson (1986) as a data layer in the electronic vector-formatted templates of his atlas. The *FMRS annotation system* presented in the Results (*Section 3.5.4*) is essentially a refinement of the existing atlas feature and modifies the existing data layer containing the original atlas stereotaxic grid.

2.9 Validation of methods

Several checks were made of our processes for generating the datasets or use of the tools presented in *Chemopleth 1.0*. First, for counting procedures, our automated quantitative analysis was checked against expert, manually annotated counting (e.g., comparisons between the two methods for counting H_1/O_A-ir cell bodies). Second, for our isopleth map constructions, we aligned the isopleth generated for a given chemical system with the underlying single-subject maps to see if higher densities in any given subject generally reflected the trends marked by the spatial averaging of the isopleth corresponding to that chemical system **(Fig. 5)**. Finally, though this was not *a priori* intended to be a validation of our maps, we found that the registration of legacy datasets from the published literature, carried out by careful replotting of the data onto base maps and aligning these with our isopleths (described next), demonstrated a marked correspondence between datasets from the pairs of studies (see Results).

2.10 Migration and registration of legacy datasets to Chemopleth 1.0

To migrate the datasets from Yao et al., (2005) and Kerman et al., (2007), we cropped digital photos of the older maps from the publications and placed each of them as a transparent overlay over the base map of BM4.0 that corresponded to the atlas level we imported. These were then overlaid with an additional transparent layer to mark the locations of the perikarya by placing a glyph over the underlying location where the original was mapped, taking care that the maps were aligned precisely. So re-plotted, the data of the imported study, along with the relevant overlay for our isopleth map of the same chemical system, were prepared as figures for this study in Ai.

3. Results

3.1 Chemopleth 1.0 dataset files, source code, and documentation.

Chemopleth 1.0 will be eventually be made accessible from a standalone data repository holding a stable version of the dataset that enables further versioning (e.g., Zenodo), and the link will be provided in subsequent revisions of this draft report. The base maps forming *Chemopleth 1.0* are digitally cropped portions of electronic files from the open-access *Brain Maps 4.0* (BM4.0) rat brain atlas (the unpopulated base maps can be found in the Supplementary files accompanying Swanson, 2018). The mapped datasets populating these base maps were produced by our laboratory and have been reported in Peru (2020) and Navarro (2020); these have been prepared for viewing within Ai/Inkscape as eight individual files, each representing a unique atlas level, in .svg format. Each file contains a BM4.0 base map of a specific atlas level and digital overlays of our maps, produced for multiple experimental subjects, for these neurochemical systems. Source code for our workflow is available as a public repository on GitHub. The source code repository contains the JavaScript (JS) and Python programs to analyze shapes and data in BM4.0. The JS programs are used to export data from Adobe Illustrator (Ai), and the Python programs are used to generate summaries, choropleth maps, and isopleth maps of the data, described in greater detail in the sections that follow. The repository also includes documentation on how to navigate the files.

3.2 Summary of database contents

Chemopleth 1.0 contains a full datasets for five immunoreactive neuronal populations through a circumscribed portion of the *hypothalamus (Kuhlenbeck, 1927)* (HY) and a portion of the *zona incerta (>1840)* (ZI) within the *ventral thalamus (His, 1893)* (TH) in multiple subjects. The database includes the profile distributions of perikarya (cell bodies) and neurites (axons and/or dendrites) that were observed to be immunoreactive for one of the following macromolecules: (1) the pre-pro-vasopressin gene product, copeptin; (2) neuronal nitric oxide synthase (nNOS; EC 1.14.13.39); (3) hypocretin 1/orexin A (H_I/O_A); (4) melanin concentrating hormone (MCH); or (5) alpha-melanocyte-stimulating hormone (αMSH). Within the BM4.0 reference atlas (Swanson, 2018), the HY is represented by 22 coronal-plane atlas levels (abbreviated here as 'S' with superscripted level numbers), containing boundaries derived directly from Nissl-stained sections (from 22 companion plates) in the same atlas. These levels, $S^{15–36}$, are samples of a 5.45 mm-long anteroposterior expanse of tissue located between +0.45 and –5.00 mm from Bregma (β) (from a rat inferred to be in the flat-skull position). Similarly, the portion of the TH containing the ZI is

Figure 6 (*next page*). Coverage of hypothalamic and zona incerta within this dataset. (**A**). (*top*) sagittal silhouette of a rat brain from the Swanson (2018) *Brain Maps 4.0* (BM4.0) atlas, with the box outlining the enlarged area containing the approximate extents of the *hypothalamus (Kuhlenbeck, 1927)* (HY) and *zona incerta (>1840)* (ZI). *Blue lines* indicate the planes of section through both structures representing levels 23–30 in the atlas (designated as $S^{23–30}$). (**B**). A more granular view of the coverage of the HY and ZI in our dataset, with the vertical axes to the left and right marking the bregma coordinate (in mm). *Filled black circles* at the left mark individual atlas levels in BM4.0 with positions calibrated to bregma. The top and bottom axes show, in approximate rostral to caudal order, individual brain regions (marked by their atlas abbreviations) that are included in the HY and ZI. From left to right, the clusters of regions are organized by the longitudinally arranged *periventricular*, *medial* and *lateral zones (Nauta & Haymaker, 1969)* of the HY (Swanson, 2018; see Bedont et al., 2015; Xie & Dorsky, 2017), followed by the ZI. *Filled blue circles* indicate those regions in the BM4.0 base maps, at their particular atlas levels, that are populated within *Chemopleth 1.0*. Note that the most rostral ($S^{15–22}$) and caudal ($S^{31–39}$) levels are not yet populated (*pale yellow circles*).

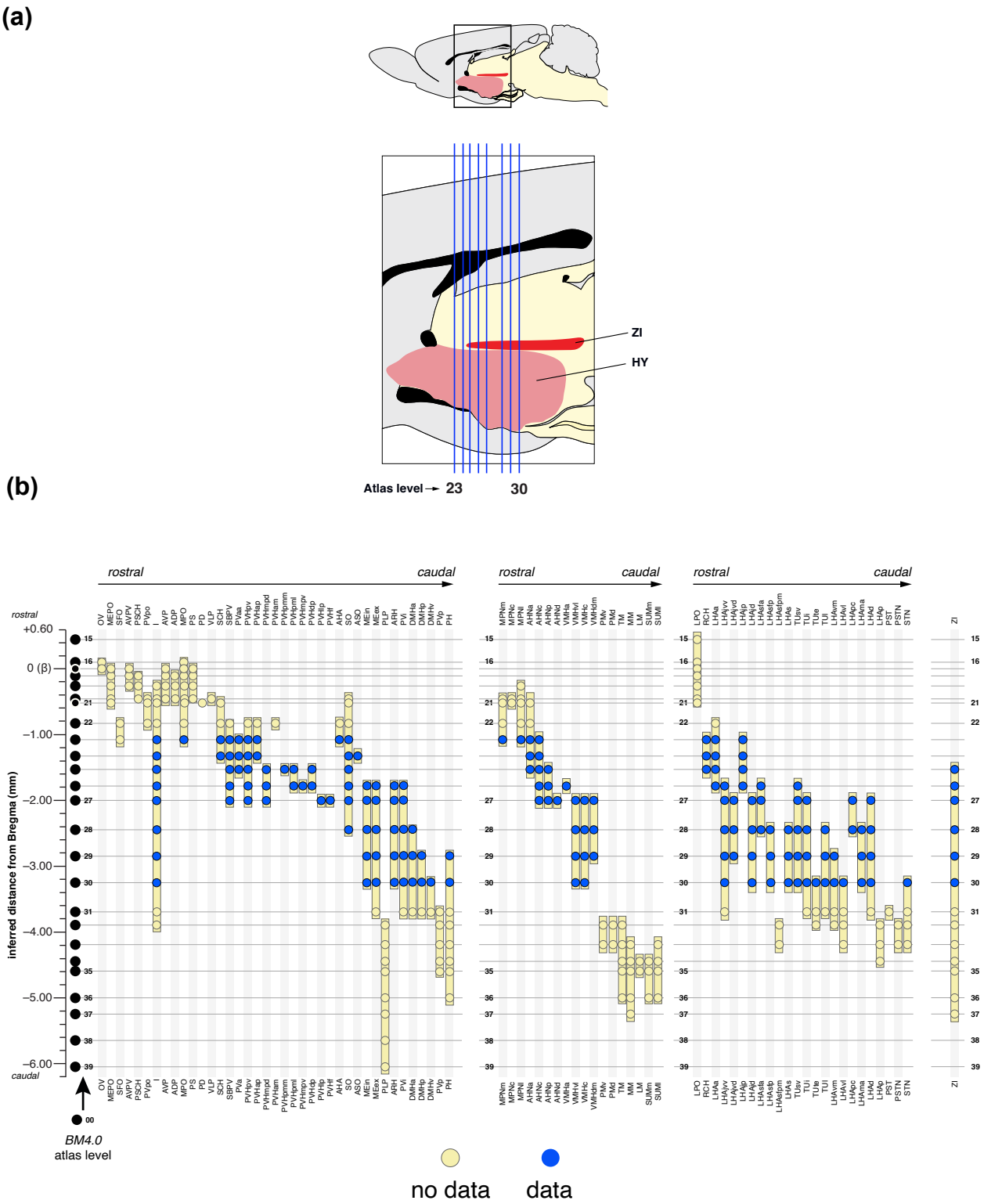
(a)
ZI
HY
Atlas level → 23
30
(b)
rostral
caudal
inferred distance from Bregma (mm)
+0.60
0 (β)
−1.00
−2.00
−3.00
−4.00
−5.00
−6.00
BM4.0
atlas level
no data
data

represented through a 3.72 mm-long anteroposterior expanse of tissue by 13 atlas levels ($S^{25–37}$) located between –1.53 and –5.25 mm from β.

In this study, we elected to create standardized maps for the distributions of immunoreactive perikarya and neurites through eight levels of BM4.0 ($S^{23–30}$), ranging from –1.08 to –3.25 mm (from β), which represents 39.8% coverage (2.17 mm) of the HY, and 46.2% coverage of the ZI (1.72 mm, between –1.53 and –3.25 mm from β) (**Figure 6**). This selected expanse of tissue falls approximately within that which has been apportioned as the anterior and tuberal regions of the HY (Swanson, 1987; after Clark, 1938; also see Simerly, 2015; Xie & Dorsky, 2017). In the narrative that follows, we use "anterior" to refer to HY represented within $S^{23–25}$ and "tuberal" to refer to HY represented within $S^{26–30}$.

3.3 Major data visualizations in Chemopleth 1.0

The soon-to-be-released *Chemopleth 1.0* database is a collection of different maps of immunoreactive chemoarchitecture for the rat *hypothalamus (Kuhlenbeck, 1927)* (HY) and *zona incerta (>1840)* (ZI). This chemoarchitecture includes immunoreactive cell bodies (perikarya) and neurites (axons and/or dendrites). We classify axons and/or dendrites as "neurites" and do not distinguish between them for two main reasons. First, the immunoreactivity we observe does not always allow us to distinguish between the two protoplasmic extensions based on morphological assessment. Second, since there are instances reported in the HY where an axon can extend from a primary dendrite rather than the cell body (Armstrong and Stern, 1997), some of the neurites, as drawn, may be portions of both (hence, the "and/or" designation; also, see Goaillard et al., (2020) for examples of certain hypothalamic peptidergic systems, not studied here, that also have hybrid extensions).

There are two main classes of maps, either for a single subject or for multiple subjects.

3.3.1 Single-subject maps

These maps are of two kinds: 1) a *single-label* map of immunoreactive cells and fibers for a neurochemical system (e.g., nNOS), representing data from the study by Peru (2020); and 2) *dual-label maps,* where two neurochemical systems were stained and mapped in the same tissue section (e.g., nNOS and aMSH), representing data from the study by Navarro (2020). Each single-subject map includes separate maps for cell bodies (perikarya) and neurites (axons and/or dendrites). Thus, for the single-label map, we have separate maps for cell bodies and neurites (two maps). For the dual-label maps involving two neurochemical systems, we have four maps (two for cell bodies and two for neurites). Additionally, we went further with the dual-label maps as described in Navarro (2020) and added an additional (fifth) map which marks locations where putative synaptic appositions between the two neurochemical systems were checked under bright field illumination at high power. **Figure 7a** provides an example of *several single-label, single-subject maps* (each for MCH-immunoreactive neurites) visualized together on a base map (these single-subject maps were superimposed on a single base map, with each map on its own transparent data layer; read more about data layers in *Section 4*).

3.3.2 Multi-subject maps.

These maps are also of two main kinds. First, *choropleth maps* are area-delimited "heat maps" providing color-coded magnitudes for distribution densities of cell bodies or neurites for each neurochemical system we investigated. **Fig. 7b** shows an example of how multiple single-

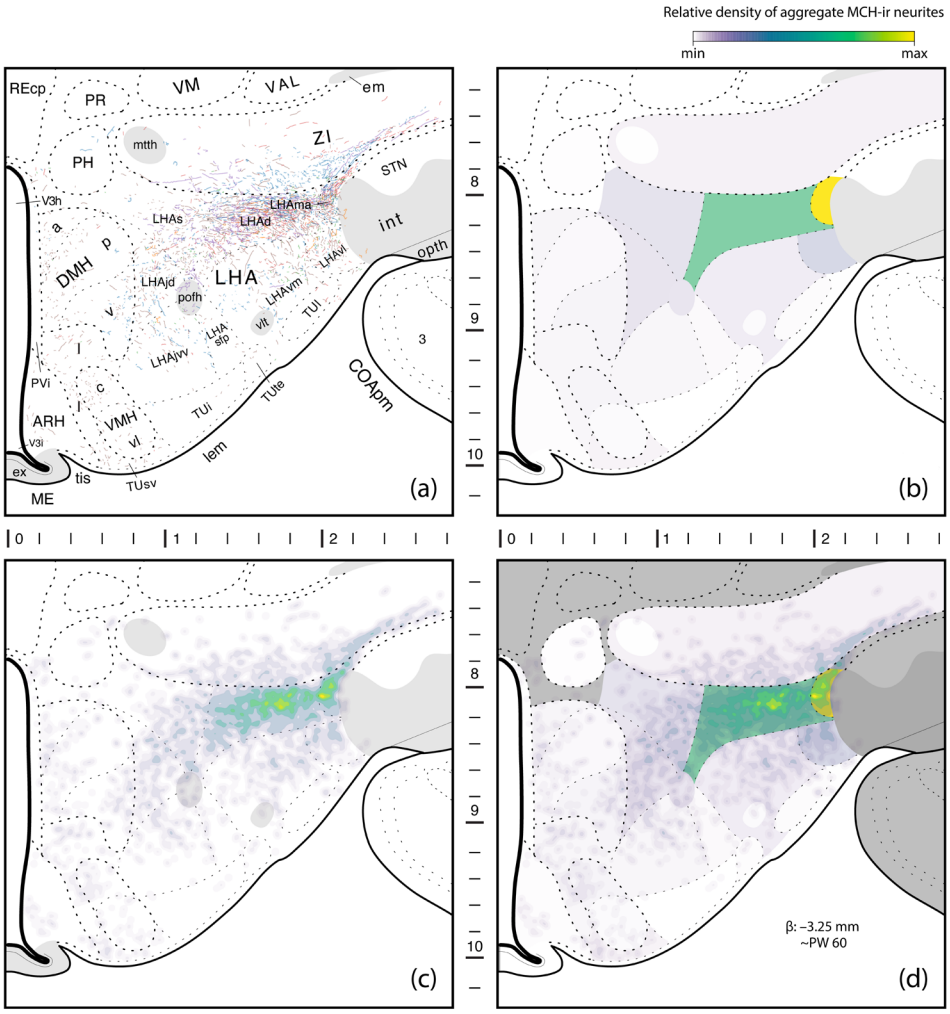

Figure 7. Examples of map types in the *Chemopleth 1.0* database. The maps shown are for neurites (axons/dendrites) immunoreactive for melanin-concentrating hormone (MCH). Single-subject distributions are superimposed from multiple animals onto a base map to produce a profile of immunoreactive populations in **(a)**, which are scored for areal density within cytoarchitectonically defined territories of the *Brain Maps 4.0* base map to produce choropleth maps **(b)**. In contrast, the distribution patterns shown in **(a)** are shown as isopleth maps **(c)**, which are based on a spatial contouring of consensus distributions based on kernel density estimation of local spatial conditions of individual distributions, independent of the underlying boundaries of the base map. These two types of "heat map" are superimposed in **(d)** to illustrate how the "hottest" territories scored in the choropleth map (LHAd, LHAma) overlap with those in the isopleth map. The color bar indicates that the scores reflect relative density of the neurites and the scale in between the panels marks inferred stereotaxic coordinates, in millimeters.

subject MCH-immunoreactive neurite representations shown in **Fig. 7a** become represented as areal densities across subjects. Each atlas region on the base map is coded by a different color depending on the magnitude of areal density of the immunoreactive fibers within that bounded region. These regions were first prepared for choropleth analysis as described in *Section 2.5.2* and then the analysis was performed on these regions as described in *Section 2.6.2*. Thus, choropleth maps provide heat map assignments confined by cytoarchitectonic region and divided over the

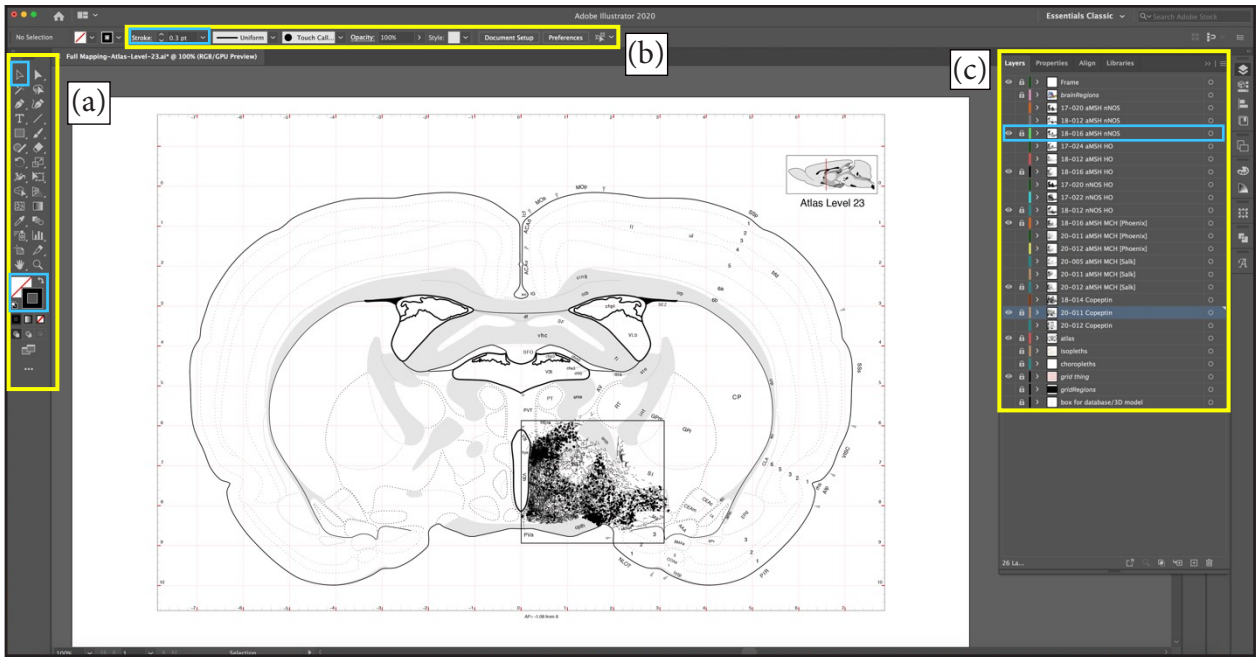

Figure 8. An example of an atlas level with mapped data, which together are part of the *Chemopleth 1.0* database, opened within the Adobe® Illustrator® (Ai) workspace. The artboard displays a base map of a transverse section of the rat brain from the open-source *Brain Maps 4.0* (BM4.0) atlas (Swanson, 2018). In this example, BM4.0 atlas level 23 is shown, with the contents of the database shown in the boxed outline on the base map (*black rectangle*), which consist of patterns of immunoreactivities drawn from photomicrographs of several experimental subjects directly onto the base map (here colored black to simplify the view). (**a**). *Tools panel* for Ai outlined in *yellow*, with the *Direct Selection Tool* outlined in *cyan* toward the top of the panel and the *Fill and Stroke Tool* outlined in *cyan* toward the bottom of the panel. (**b**). *Control panel* for Ai outlined in *yellow* with the *Stroke Tool* outlined in *cyan*. (**c**). *Layers Panel* for Ai outlined in *yellow*, with data for one of the specific experimental subjects shown in the map outlined in *cyan*. See the text for an explanation of these panels.

areal limit of that region.

Second, a separate type of multi-subject representation within *Chemopleth 1.0* is in the form of an *isopleth map*, which is a heat map providing color-coded locations of sparse versus dense distributions of cell bodies or neurites *independent* of the underlying boundaries for regions on the base map (i.e., the density is *not* divided over the area of a specific bounded brain region). An example of an isopleth map of MCH-immunoreactive neurites is shown in **Fig. 7c**. This map is a collection of contours which mark the *average densities* of perikaryon or neurite locations on the base map across multiple subjects. Areas which are color-coded in yellow in the figure are denser and reflect greater spatial consensus of the immunoreactive elements across all experimental subjects; those areas coded lighter and duller in shading are areas of lower density, where the presence of immunoreactive elements was found in only one or a few experimental subjects. While the overall isopleth map reflects the *consensus* of mapped immunoreactive elements from multiple subjects, it must be borne in mind that these maps should not be considered as "probabilistic" maps, since the sample sizes are low and therefore the relative contributions of any single subject's distributions to skew the overall distribution patterns is greater when samples are fewer in number (in our study, n=3–7 subjects).

Keeping this caveat in mind, and consistent with the appearance of a bright region on the choropleth map shown in **Fig. 7b**, the isopleth map in **Fig. 7c** reflects bright (i.e., denser) consensus distributions on the base map that, when superimposed on the choropleth map, agree with it (**Fig. 7d**). Notice that while the bright yellow color-coding of the isopleth distributions falls within the bounded territory color-coded as bright green in the choropleth map, the yellow distributions do not completely occupy this green territory but, rather, mark a subset of immunoreactive elements in this area, illustrating how the isopleth distributions provide finer spatial resolution of the distributions at the σ value we assigned (see *Section 2.7.2*). Having understood these types of data visualization, we next turn to how readers can utilize the Adobe® Illustrator® (Ai) vector graphics platform to access and use our database files. We note, however, that users can also visualize *Chemopleth 1.0* files in the freely downloadable software, Inkscape.

3.4 Navigating Chemopleth 1.0 files using the Adobe® Illustrator® (Ai) graphical user interface

To accurately use the master files when they become available in a subsequent version of this report, it is important to keep the dimensions of the original Ai files downloaded from the *Brain Maps 4.0* (BM4.0) publication (Swanson, 2018). There are eight atlas levels (numbered 23–30) from BM4.0 covering the anterior and tuberal *hypothalamus (Kuhlenbeck, 1927)* (HY), and portions of the *zona incerta (>1840)* (ZI), of an adult male rat. An example of a database file opened in Ai is provided in **Figure 8**, where BM4.0 level 23 was opened (using Adobe® Illustrator® 2020). Note that the layout might look slightly different depending on what workspace option you choose. Here we have the workspace set in "Essentials Classic mode"; however, any workspace will have the same tools, just with a different layout. To change your workspace, go to Window > Workspace > [Essentials Classic]. In **Figure 8**, three panels are highlighted in yellow, within which key control are outlined in cyan:

Tool panel **(Fig. 8a)**: contains all the tools to use Ai. By hovering over the icon tools, you can see the name of the tool and a keystroke or keystroke sequence in parentheses which is the shortcut for the tool. Two tools are highlighted in cyan: (1) the *Direct Selection Tool* (at the top), the icon is a black arrow. This tool will help you select your object on the artboard/canvas. (2) the *Fill and Stroke Tool* (at the bottom) represents the fill color (top black open square) and stroke color (background white square) of any selected text or object.

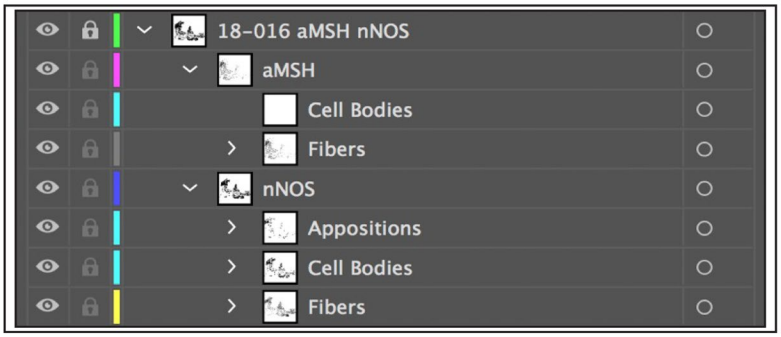

Figure 9. An enlarged view of the Layers panel in the Ai workspace, listing the data layers for subject #18-106 within the *Chemopleth 1.0* spatial database. The label for the main layer (*top row*) shows that the data are for dual immunoreactivity labels for the neuropeptides alpha-MSH (aMSH) and nNOS. Clicking on the *arrowhead* (>) to the left of the main layer label opens sublayers for each biomarker, under which additional nested sublayers appear if the *arrowheads* (>) to the left of each sublayer label are toggled in turn: those for cell bodies (perikarya) and neurites (axonal fibers and/or dendrites), and in some cases, appositions.

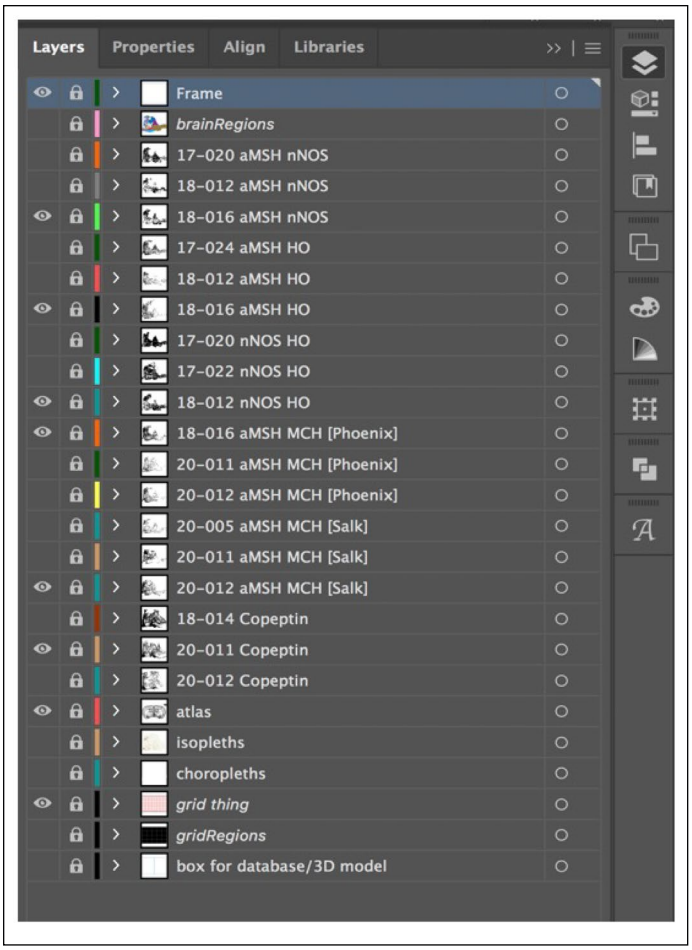

Figure 10. Detail of the *Layers Panel* in Ai workspace, showing various layers and their arrangement within the *Choropleth 1.0* database.

Explanation of select layers: *Frame*, square surrounding the area of the *hypothalamus (Kuhlenbeck, 1927)*; *brainRegions*, enclosed brain regions enabling the tabulation of cell counts and fiber area estimates by regions. *atlas*, base map from BM4.0; *isopleths*, trends by average counts; *choropleths*, average counts by region; *gridthing*, stereotaxic grid lines; *gridRegions*, regions covered in this study by grid lines; *Box for database/3D model*, frame embedded in the database for future registration of additional data in 2-D or 3-D. See Abbreviations for details concerning the immunoreactive labels (aMSH, nNOS, HO, MCH). Please note that soon-to-be-released *Chemopleth 1.0* data files will consist of eight levels, with each level saved as a separate .svg file that can be opened in Adobe Illustrator or the freely available graphic editor, Inkscape. Please refer to the text for details. Note that the layer names displayed in this screenshot may undergo revisions in subsequent versions of this report.

Control panel **(Fig. 8b)**: according to the tool you are using from the *Tool panel*, this panel will display additional specific tools for objects or text you have selected. In this example, the *Stroke Tool* is outlined in cyan, which lets you choose the size of your stroke (outer thickness).

Layers panel **(Fig. 8c)**: This is where all the objects in your artboard are listed. Each row is a data layer (transparent digital overlay) and you can toggle on or off the visibility of the data for that layer on the base map by toggling on the *eye icon* to the left of each layer or by leaving it toggled off, respectively. The *lock icon* is to lock the layer, preventing any moving or deleting of data on that data layer.

3.5 Detailed contents of the database

Chemopleth 1.0 is accessed via the *Layers panel* in the Ai platform. There are three experimental subjects per pair of immunoreactive antigen, and each will have sublayers with their corresponding antigen, with additional nested sublayers for appositions, cell bodies, and fibers **(Fig. 9)**. Layers contain artwork (i.e., the data) and are arranged in a stack. As shown in **Figure 10**, content on layers located at the top of the *Layers panel* (e.g., "Frame", "brainRegions") appear *on top of* content on layers that are lower in the *Layers panel* (e.g., "atlas", "isopleths", "grid"). Isopleths show spatially averaged density maps of the distributions of immunoreactive elements, showing regions of consensus (and discordant) distributions across multiple subjects independent of cytoarchitectural boundaries marked on the underlying base map. In contrast, choropleth maps

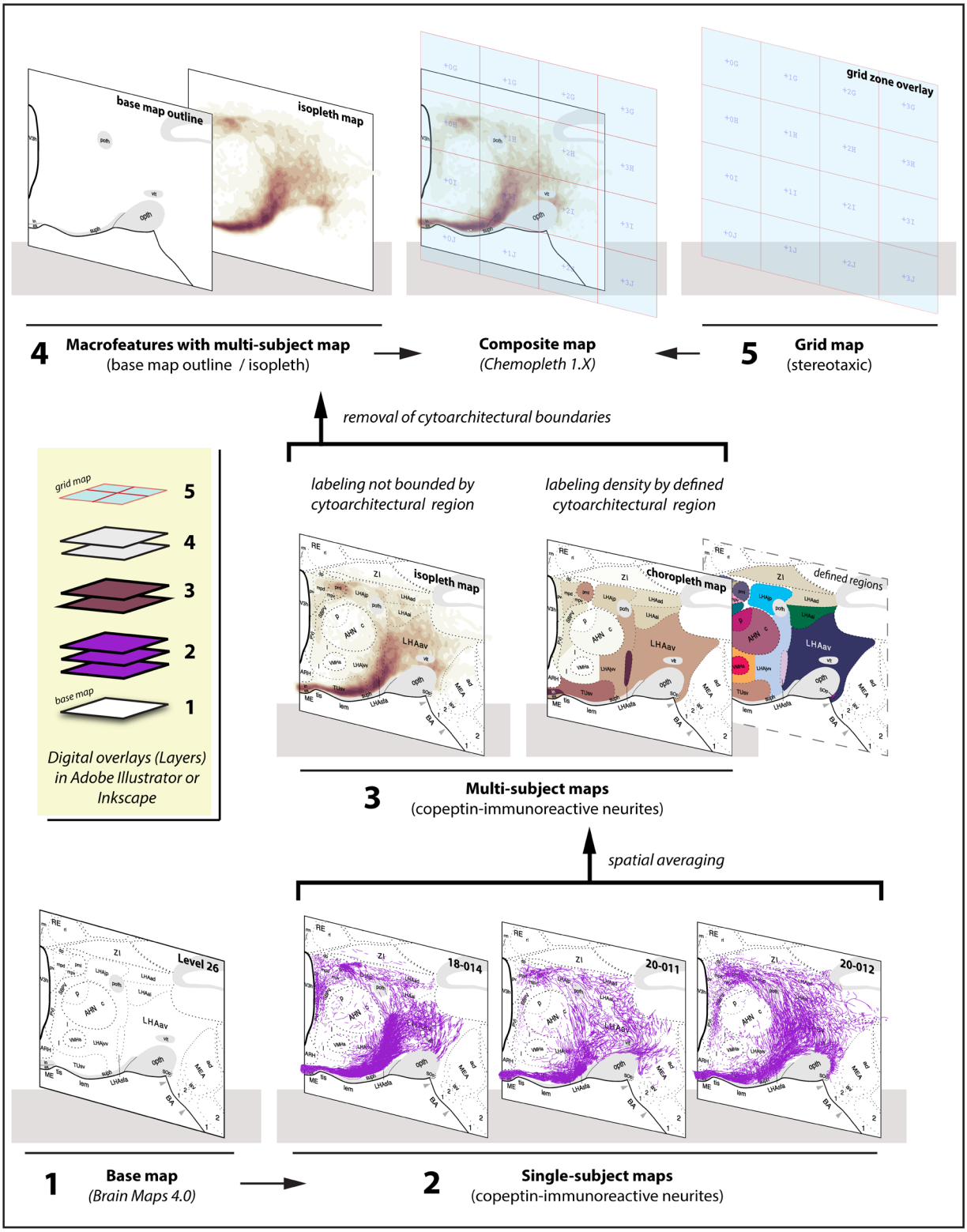

Figure 11. Illustration of the relationship among the base map, single-subject maps, and multi-subject maps of the *Chemopleth 1.0* database. The base map (**1**) from the *Brain Maps 4.0* atlas forms the base layer in the Layers stack shown (*yellow outlined stack, middle left*). Stacked as transparent overlays on this base map are single-subject maps (**2**) and multi-subject maps (**3**). Macrofeatures of the data (**4**) along with a stereotaxic grid map (**5**) form the final composite map of the database. See text for details.

provide distribution gradients normalized and bounded by the cytoarchitectural boundaries of the underlying base map. See Peru (2020) and Navarro (2020) for details concerning the distributions of these immunoreactive biomarkers and their biological significance.

3.5.1 Single-subject maps of immunoreactive perikarya and neurites

Fig. 11 provides a summary of how *Chemopleth 1.0* contains a base map for each BM4.0 atlas level (see **1** in **Fig. 11**), upon which single-subject maps were produced for each immunoreactive system we labeled, using copeptin-immunoreactive neurites as the example (**Fig. 11**, **2**) (in this instance, only the neurites immunoreactive for copeptin are made visible by toggling off the visibility for the layer with copeptin-immunoreactive perikarya).

3.5.2 Multi-subject isopleth and choropleth maps

Fig. 11 also shows two types of multi-subject map, which were produced by exporting the single-subject maps (as described in the **Fig. 1** workflow) and computing across them to produce averaged "heat maps". The color-coded density scorings of these maps were binned by cytoarchitectonic region (to produce a choropleth map) or sorted into a distribution that was independent of the cytoarchitectonic boundaries of the base map (thereby producing an isopleth map) (**Fig. 11, 3**).

3.5.3 Interaction maps

For certain experimental subjects (see **Figure 9**) we also performed a spatial analysis of the locations for putative synaptic appositions between two neurochemical systems. For these cases, an additional map was placed in a Layer called "Appositions".

3.5.4 Grid-based coordinate system

3.5.4.1 Definition of the coordinate system

This coordinate system is displayed as an 8.0 × 12.0 mm grid overlay (layer) within each Ai-formatted electronic BM4.0 atlas level template used in this study, with the origin located on the lower left corner of the coronal plane hemi-section **(Figure 12a)**. The *x*-axis of this grid (which marks the mediolateral (ML) stereotaxic coordinates of each atlas map) is 8.0 mm in length, and the *y*-axis of the grid (which marks the dorsoventral (DV) stereotaxic coordinates of the map) is 12.0 mm in length. Note, however, that the maximal dimensions vary depending on the position of the brain section within each specific atlas level (i.e., some levels will have tissue expanses spanning fewer lengths.

We define the lines parallel to the *y*-axis (sagittal lines, or *sagittals*) by the numerals 0–7, with 0 marking 0.0 mm ML (the ML coordinate at the origin), 1 marking 1.0 mm ML, and so on, until the final numeral 7, which marks the penultimate sagittal at 7.0 mm ML. Sagittals located on the right-hand hemisphere of the map are denoted by a plus sign (+) before their respective numeral, and those on the left-hand hemisphere are denoted by a minus sign (–). For example, +5 marks the sagittal located +5.0 mm along the ML stereotaxic axis in the right-hand hemisphere map of a given BM4.0 atlas map. In similar fashion, we assigned alphabetical designations (A–L) for the lines parallel to the *x*-axis (horizontal lines, or *horizontals*), which correspond to numerical values of the dorsoventral coordinate (–1.0 to –12.0 mm). Note that these numbers grow more negative in value from dorsal to ventral along the map. Thus, J denotes the position of the horizontal that is 10.0 mm ventral (i.e., –10.0 mm DV) to the most dorsal edge of the map (which is located at position 0.0).

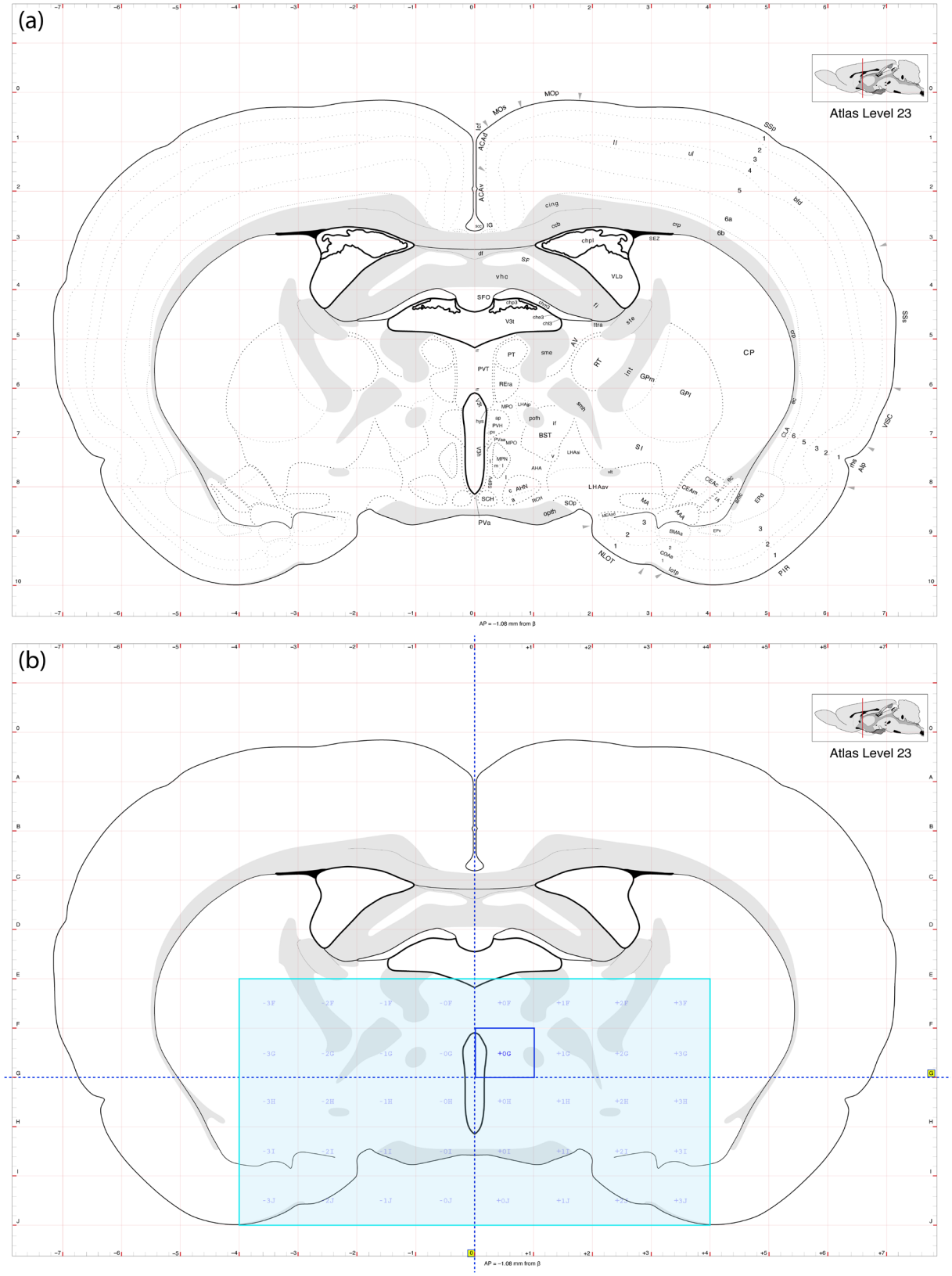
(a)
Atlas Level 23
AP = −1.08 mm from β
(b)
Atlas Level 23
AP = −1.08 mm from β

Figure 12 (previous page). (**a**). Feature-based map with stereotaxic coordinates. Detail of the *Chemopleth 1.0* data layers showing the BM4.0 base map for atlas level 23 and feature-based boundaries (such as parceled brain regions). Also shown is the digital overlay for the sterotaxic grid included in the original BM4.0 atlas template (*red-lined grid*). (**b**). Grid-based map with stereotaxic coordinates. Detail of *Chemopleth 1.0* data layers showing the basic outline of the BM4.0 base map for atlas level 23 along with white matter tracts. A new grid zone system (*light blue tiles and labels*) is shown over the base map, dividing portions of it according to a new naming system for each zone, based on sterotaxic grid (*red-lined grid*) position of the tile (see text for details).

Together, the sagittal and horizontal designations can be used to identify specific *grid zones* or *tiles* within the map, with the convention adopted to name each *tile* based on the ventromedial corner intersection of each sagittal and horizontal. The notation for *grid zones* for our database based on the 1.0 × 1.0 mm squares created by the stereotaxic lines follows the format: ± (numeric signifier (0.00 – 8.00 mm) of the ML coordinate; alphabetical signifier (A–L) of the DV coordinate), with + marking coordinates on the right-side of the atlas map and – marking coordinates for the left side of the atlas map. For example, tile +8E denotes the tile that has its *lower left corner* marking the intersection of sagittal +8 with horizontal E. Note that ventromedial positioning means that the left side of the atlas map would have the corresponding tile (–8E), with the *lower right corner* marking the intersection of sagittal –8 with horizontal E, since the lower right corner would be more medial than the lower left corner **(Figure 12b)**. We opted to designate the ventromedial corner rather than an absolute direction (e.g., "lower left" corner), since selection of the medial corner for corresponding locations on both hemispheres ensures that each grid zone in one hemisphere has the identical but opposite-sign grid zone name in the contralateral hemisphere. Thus –4G and +4G would mark grid zones in the left and right hemispheres for bilaterally corresponding territories of brain tissue space.

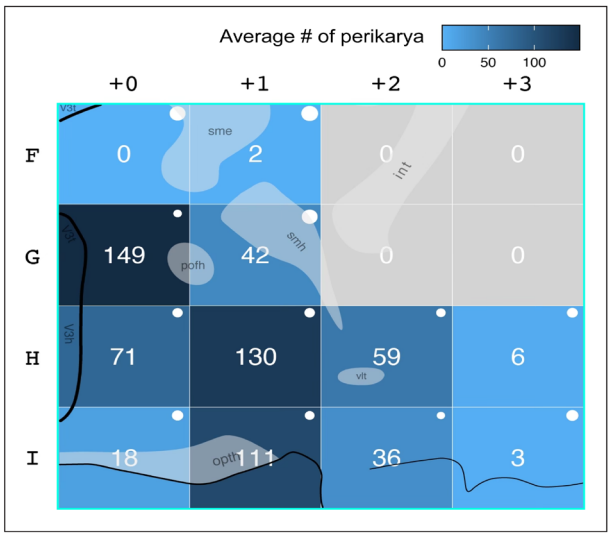

Figure 13. An FMRS for neuronal nitric oxide synthase-expressing perikarya counted by grid zone. Note that each zone is color-coded according to the density gradient shown at the top right, and that the macro features of the brain are visible under the grid zones as a reference to the underlying features from the BM4.0 base map for Atlas Level 23 (see text for details). The sizes of white dots mark relative standard error of the mean (SEM).

3.5.4.2 Populating stereotaxic space: Creation of the FMRS annotation system

Using this refined grid-based stereotaxic coordinate system, we tabulated our counts for immunoreactive perikarya and/or neurites within this grid using a new annotation system we call the *FMRS annotation system* (FMRS = "Frequencies Mapped with Reference to Sterotaxy), which essentially are counts of these immunoreactive elements *binned by grid zone* as opposed to brain regions **(Figure 13)**. An *FMRS*, an acronym we use as a noun and pronounced similarly to the word *ephemeris* (see *Section 4.2.3.2* for rationale), is a table of positions of spatial data points (in this case, profile counts) in stereotaxic coordinate space obtained from a single observation or a few observations (i.e., a single subject or a few subjects), with each entry in the FMRS consisting

of the following values: anteroposterior (bregma) coordinate (in mm), grid zone or tile defined by a specific sagittal and horizontal intersection, and profile count (frequency of perikaryon profiles or a pixel-density score for neurites) in that zone.

We generated several FMRS, each keyed to a single bregma coordinate. To construct each FMRS from any data-populated BM4.0 atlas level within Ai, the visibility of the data layer featuring the vector-formatted cytoarchitectonic boundaries was toggled off, and the visibilities of the data layers with glyphs for immunoreactive perikarya or neurite profiles and the Paxinos & Watson-derived stereotaxic grid were toggled on, allowing the profile counts to be parsed by grid zone within Swanson (2018) reference space.

3.5.5 Legacy datasets in register with new data

Figures 14–19 show the results of placing legacy data in register with our current maps in *Chemopleth 1.0*. Specifically, we migrated the data from Kerman et al., (2007), which was mapped in BM3.0 reference space, into BM4.0 reference space and placed their data in register with our datasets for MCH- and H_1/O_A-immunoreactive perikarya distributions **(Figs. 14, 15)**. We also migrated data in Yao et al., (2005) from BM2.0 space to BM4.0 space **(Figs. 16–19)**.

4. Discussion

In this study, we populate the base maps freely available from the *Brain Maps 4.0* rat brain atlas ("BM4.0"; Swanson, 2018) with new datasets to create *Chemopleth 1.0*, an interactive spatial database of chemoarchitecture for portions of the rat hypothalamus and zona incerta. *Chemopleth 1.0*, which, when released with a subsequent version of this report, will be accessible using Adobe Illustrator (Ai) or the free software platform, Inkscape (www.inkscape.org), and will provide a detailed view of the cell body and axonal fiber distributions of five neurochemical systems to aid in their targeted functional examination in stereotaxic space. As part of this new resource, a programmed workflow was developed that allows the user to export cell and neurite data from the atlas in tabular and raster formats, compute on these data, and export data visualizations of spatially averaged "heat maps" derived from individual data maps from multiple subjects. These maps are produced in a file format that is compatible with their re-importation into the native atlas environment. The database includes two types of these maps, one providing density estimates by cytoarchitectural region ("choropleth" maps) and the other providing density patterns that are computed across territory in a manner independent of the underlying cytoarchitectural boundaries ("isopleth" maps). Additionally, we introduce a new grid-based annotation system, based on the stereotaxic grid provided in the atlas, to allow non-expert neuroscientists to map their own data within the atlas without needing training in detailed cytoarchitectural mapping methods. Finally, we provide guidance in this report on navigating the Ai workspace to access and make sense of the spatial data contained in the database.

Below, we discuss the need for this database, and then focus on its contents and design features. Throughout, we reflect upon the database's design, environment and assumptions with discussion that draws upon programs in geology, geography and geographical information sciences, the humanities, and the visual, literary, and performative arts. The net is deliberately cast wide to emphasize the shared 'experimental entanglements' (Fitzgerald & Caillard, 2015) of our collective efforts to model, visualize, and make sense of complex, spatiotemporal data and to also learn how such tasks are carried out by those outside of our immediate discipline.

Data Migration/Registration – Kerman *et al.*, (2007)$^{S04 \rightarrow S18}$ (re-plotted from their Fig. 7)

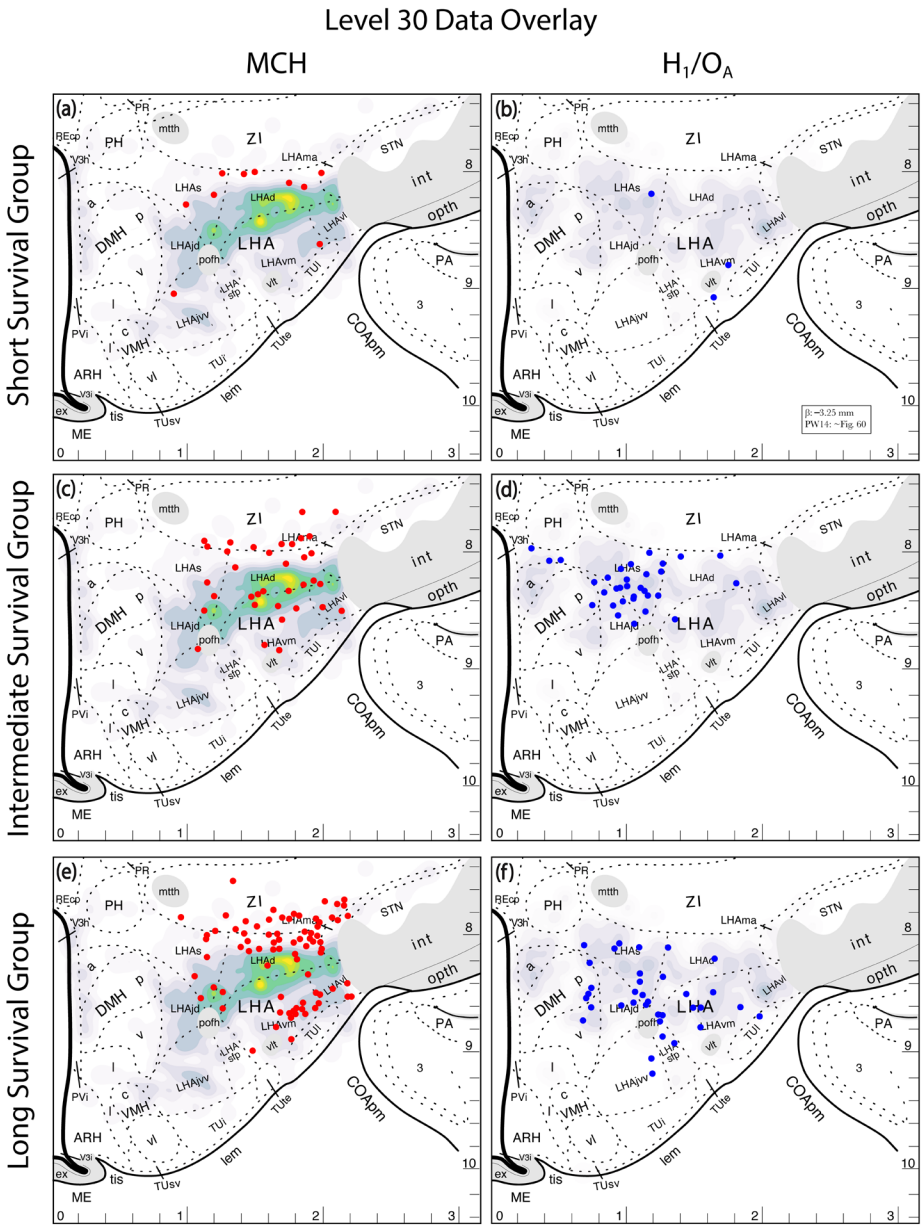

Registered datasets	Color: Mapped data	Descriptor: Mapped data
Kerman *et al.*, 2007	●	presympathetic-premotor MCH$^+$ perikarya
	●	presympathetic-premotor H_1/O_A^+ perikarya
This study	min – max	Relative density of MCH [Salk]$^+$ or H_1/O_A^+ perikarya

Figure 14 (this page and next page). Example of data migrated and redrawn from Kerman et al., (2007) into *Chemopleth 1.0* and placed in registration with the database's relevant datasets.

Data Migration/Registration –

Kerman *et al.*, (2007)$^{S04 \rightarrow S18}$ (re-plotted from their Fig. 8)

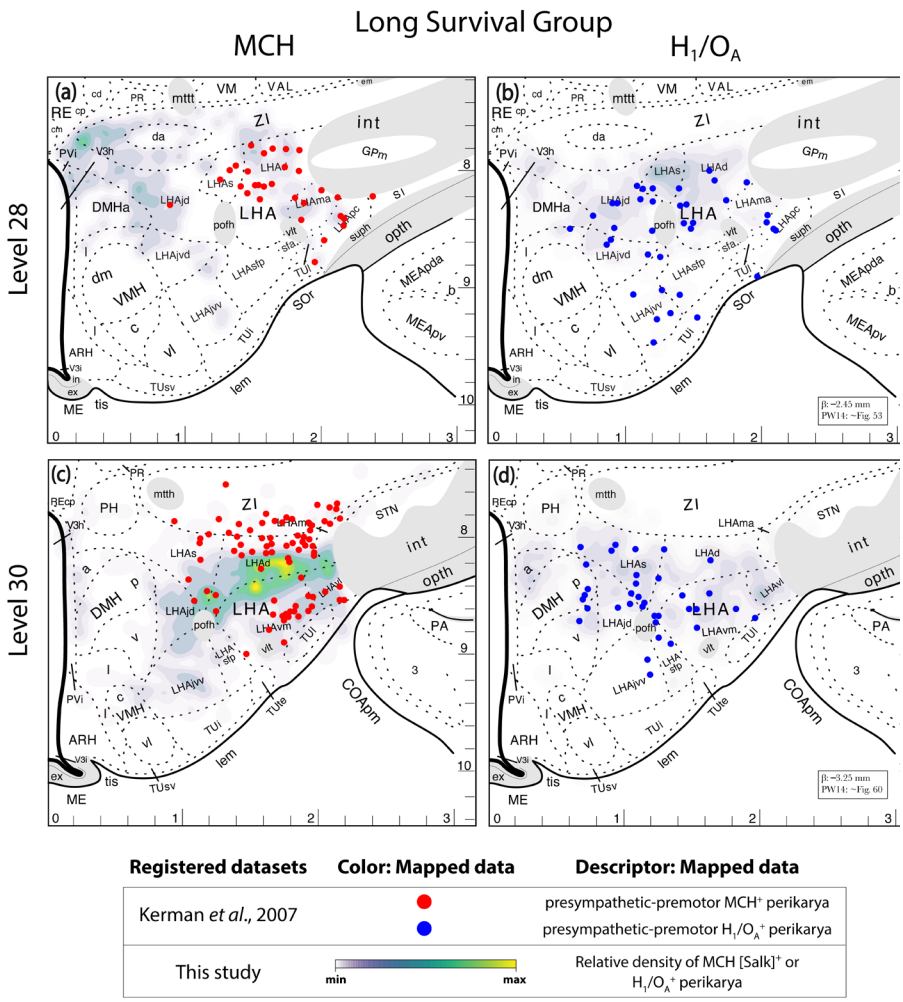

4.1 Why do we need *Chemopleth 1.0*?

4.1.1: Limitations of extant maps

In the past three decades, the identification of molecular constituents of hypothalamic and zona incerta systems has outpaced their spatial mapping. This identification has involved transcriptomic, proteomic or peptidomic analyses of sampled tissues from these regions. Most of the detailed published molecular studies of this kind have either been performed in laboratory mice, were not intended to (and therefore do not) provide actual *mapped* spatial information but only dimensionality reduction visualizations (e.g., tSNE plots), and/or have sampled denser nuclei at the expense of more diffusely organized areas (reviewed by Khan et al., 2018). In contrast, older, more concerted mapping efforts have provided maps of rat brain chemical systems, but these have largely done so as part of larger whole-brain survey efforts (this is exemplified by the excellent *Handbook of Chemical Neuroanatomy* series, many volumes of which remain out of print at the time of this writing). These studies included the hypothalamus and zona incerta, but they often lack

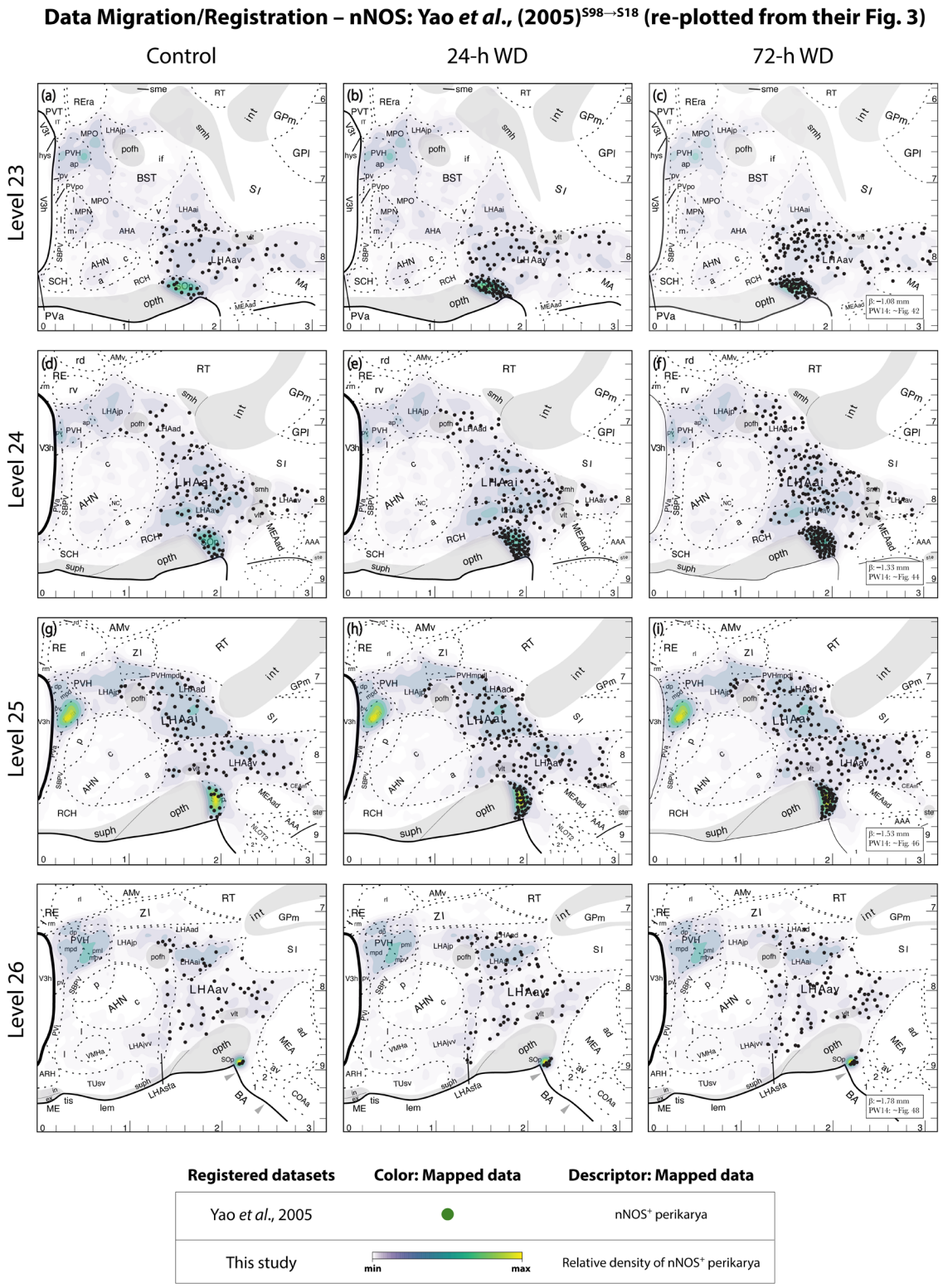

Figure 15 (above and next page). Example of data migrated and redrawn from Yao et al., (2005) into *Chemopleth 1.0* and placed in registration with the database's relevant datasets.

Data Migration/Registration – nNOS: Yao *et al*., (2005)$^{S98 \rightarrow S18}$ (re-plotted from their Fig. 3)

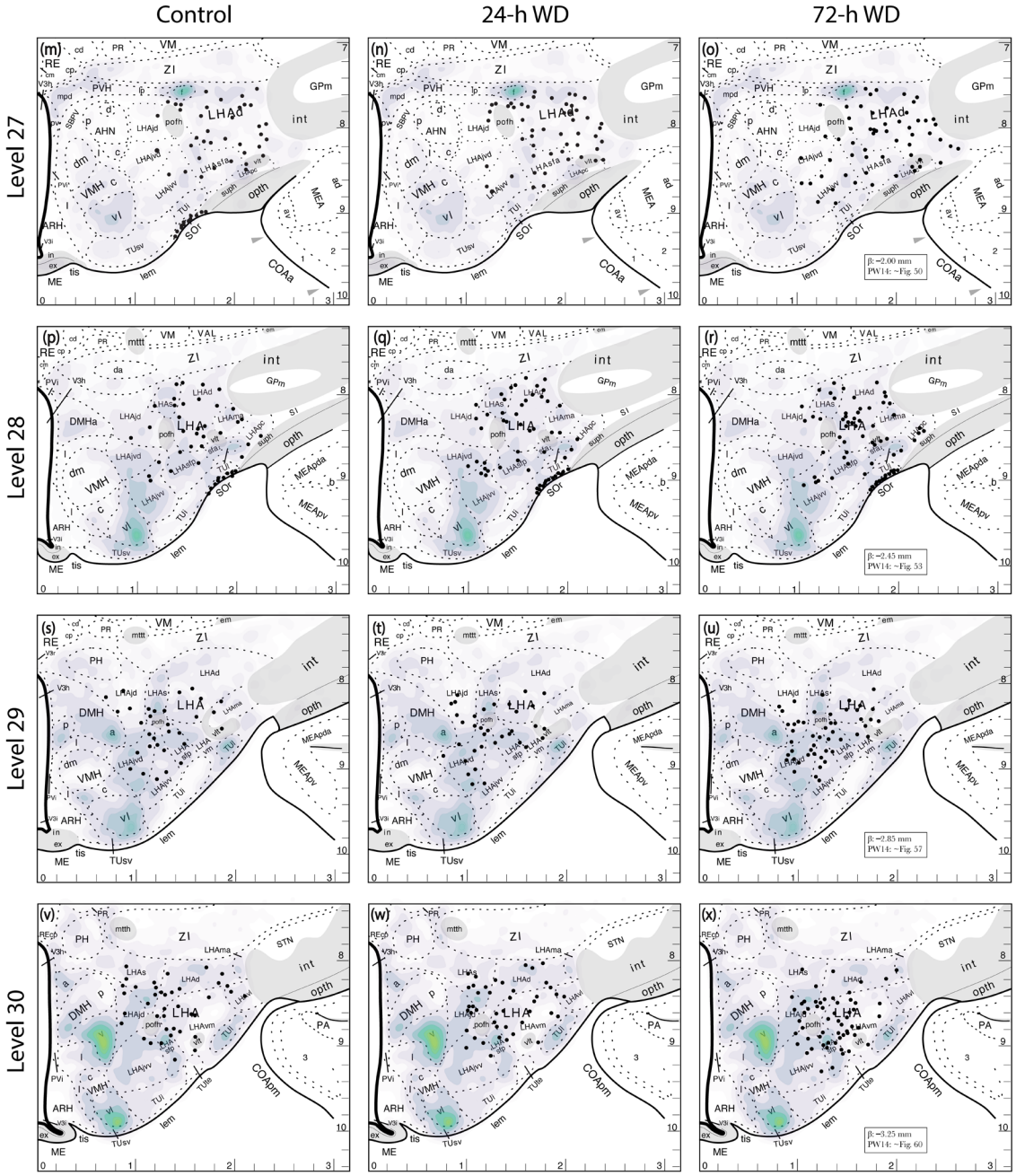

Registered datasets	Color: Mapped data	Descriptor: Mapped data
Yao *et al*., 2005	●	nNOS^{+} perikarya
This study	min → max	Relative density of nNOS^{+} perikarya

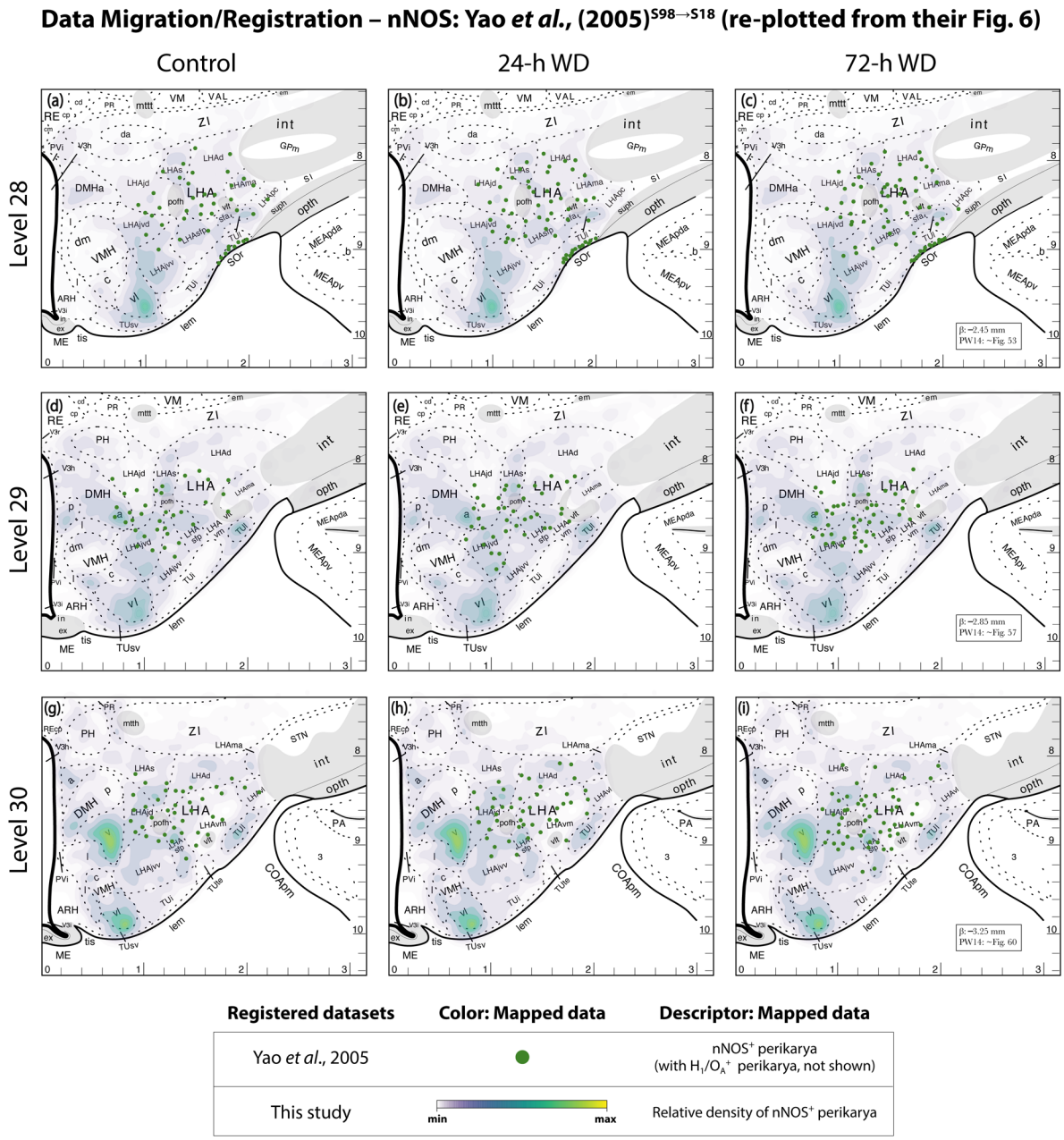

Figure 16 (this page and next page). Example of data migrated and redrawn from Yao et al., (2005) into *Chemopleth 1.0* and placed in registration with the database's relevant datasets.

the spatial resolution or coordinate space to facilitate precise targeting of the chemical systems with virally directed tools; such tools aid in targeting neurochemical systems in the rat, which has few transgenic lines (see *Section 4.1.2*). Finally, most published reports of chemoarchitecture for the rat hypothalamus and zona incerta have focused on mapping cell bodies; only a few have mapped axonal fibers, the locations for which are important to map in order to target retrogradely transportable vectors.

Data Migration/Registration – H_1/O_A: Yao *et al.*, (2005)$^{S98 \rightarrow S18}$ (re-plotted from their Fig. 6)

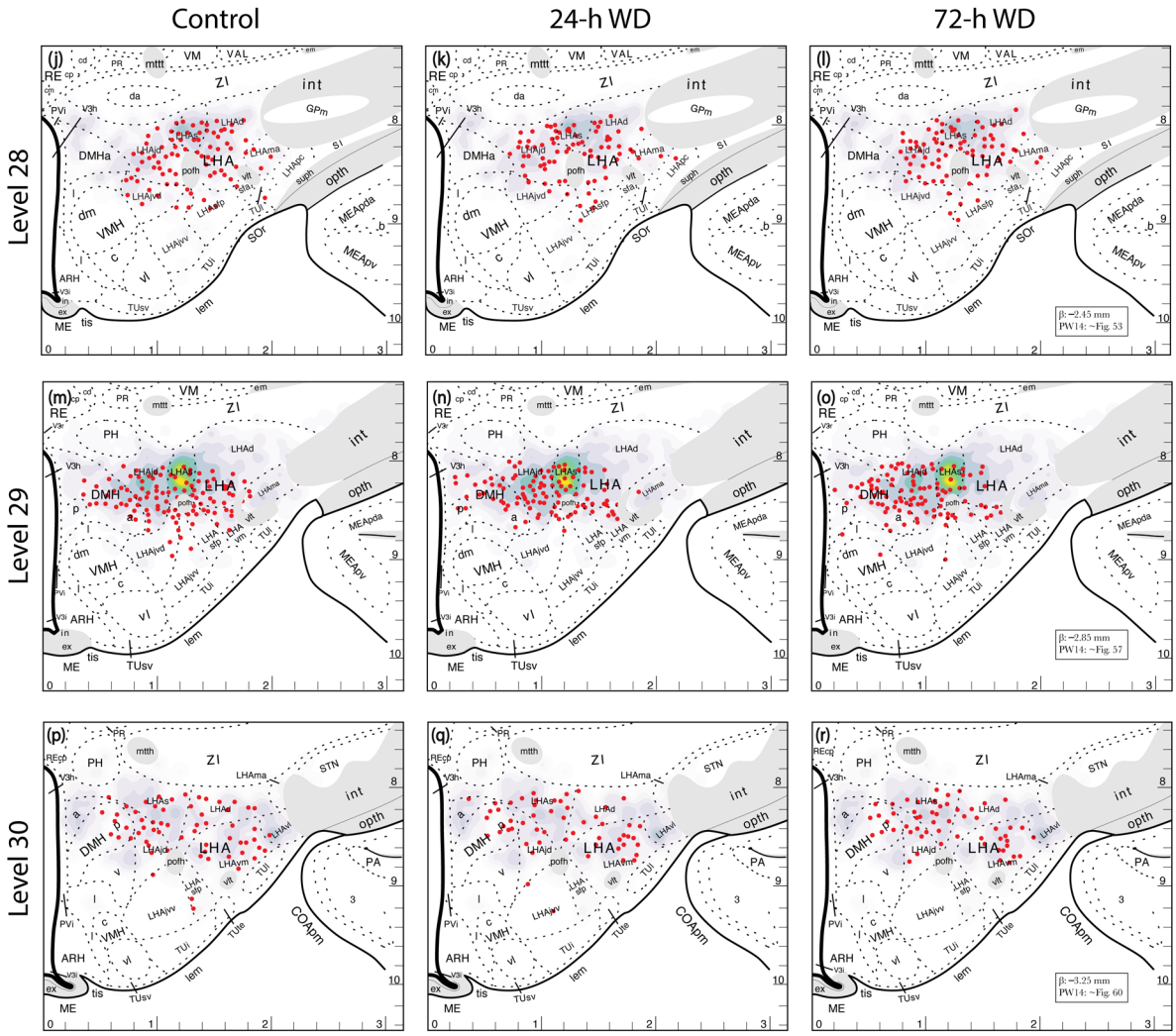

Registered datasets	Color: Mapped data	Descriptor: Mapped data
Yao *et al.*, 2005	●	H_1/O_A^+ perikarya (with $nNOS^+$ perikarya, not shown)
This study	min → max	Relative density of H_1/O_A^+ perikarya

Recently, Paxinos and colleagues published the third edition of their chemoarchitectonic rat brain atlas (Paxinos et al., 2022), which contains photomicrographs of tissue immunostained with eight neuronal markers, two of which are well-established proxy markers for known bona fide neurotransmitter systems (tyrosine hydroxylase for catecholaminergic neurons) and NADPH-diaphorase (for nitrergic neurons). *Chemopleth 1.0* complements this effort by providing detailed hypothalamic and zona incerta maps in the rat for neuronal nitric oxide synthase-immunoreactive neurons (another means to identify presumptive nitrergic neurons) as well as for four additional neurochemical systems.

4.1.2: Limitations of current transgenic rat lines

The laboratory rat has been a mainstay of neuroscientific research for over a century (e.g., King, 1910; Huber, 1915; see Oglivie (2007) for a nuanced historical contextualization), with a rich scientific literature concerning neural substrates and their causal links to behavior and physiology. While leveraging this information affords scientists with immense benefits when probing deeper into structure-function relationships for the nervous system, there historically have been limitations in the genetic tractability of this model organism. This, however, appears to be changing dramatically as new programmable nuclease tools gain currency.

Thus, at the time of this writing, a few transgenic rat lines exist to aid in labeling and identifying specific chemoarchitecture in the rat brain (Witten et al., 2011; Bäck et al., 2019; Zallar et al., 2019; Iwasaki et al., 2023), and more lines are being generated, especially using the CRISPR/Cas9 gene editing tool (reviewed by Ma et al., 2017). In most cases, however, detailed comparisons of transgenic neuropeptide expression patterns with wild-type controls are still lacking, and no detailed standardized atlas-based mapping for transgenically expressed rat chemoarchitecture has yet been reported. In the more rigorously characterized lines, such as the TH-Cre rat, unexpected germline recombination with a parental sex bias has been reported (Liu et al., 2016). This is also a wider problem for numerous transgenic lines of mice and zebrafish used in neuroscientific research (Luo et al., 2020), reinforcing the calls for observing careful breeding and genotyping procedures when using these important and valuable model organisms (Song & Palmiter, 2018). Maps of wild-type rat brain chemoarchitecture, therefore, will be important for validating transgenic patterns of expression, even as the models undergo refinement and improvement, and such datasets begin coming online. *Chemopleth 1.0* provides a useful starting point to facilitate such comparisons against five different neurochemical systems in wild-type rats.

4.1.3: Limitations of automated and semi-automated mapping methods

The need for maps of wild-type rat chemoarchitecture is also evident in the field of machine learning and computer vision, where efforts to automate or semi-automate the mapping of chemoarchitectural systems will require deep learning algorithms to improve their performance by computing on enough training data that can serve as ground truth. While a small amount of histological data can be bootstrapped to increase the amount of training data (e.g., Straathof et al., 2020; Arnal, 2022), and for certain deep learning approaches a small training set of macroscale histological data (MRI images) may suffice for effective neural network performance (Zoghby et al., 2024), it is also evident from other studies that a large amount of such data can be a better means to achieve accuracy in computer-vision-based pattern recognition methods (Sun et al., 2017). At the time of this writing, mesoscale histological datasets, such as the ones we are providing here, have not yet been evaluated to determine the minimal effective amount of training data needed for robust pattern recognition to facilitate their mapping to a standardized atlas.

4.1.4: Limitations of current 3-D visualizations

Finally, current methods to label and visualize rat chemoarchitecture in 3-D (for example, by light sheet microscopic imaging) need spatial validation from 2-D tissue sets produced by separate methodology (Quintana et al., 2024), particularly with respect to cytoarchitectural patterns where Nissl stains have long served as a gold standard and for which compatible methods in cleared whole tissue samples are still undergoing refinements.

4.2 Database Contents and their Biological Considerations

In *Chemopleth 1.0*, we provide single- and multi-subject chemoarchitectural data visualizations for five neurochemical systems across eight *Brain Maps* atlas levels through the anterior and tuberal *hypothalamus (Kuhlenbeck, 1927)* and parts of the *zona incerta (>1840)*. Each atlas level from *Brain Maps 4.0* (Swanson, 2018) is represented by a single base map of the hypothalamus/zona incerta that can be opened in Adobe® Illustrator® (Ai) or in Inkscape. The atlas file consists of a stack of data layers placed over the base map. The data layers are labeled according to experimental subject and the neurochemical immunoreactivity patterns being shown, with sublayers sorted according to the type of data being shown (immunoreactive patterns for cell bodies, neurites, and appositions). In addition to base maps and evidence-based cytoarchitecture, the database also includes the following contents:

4.2.1: Feature-based maps

The first major class of map produced from these efforts are called *feature-based maps* because they not only document the features of the immunoreactive patterns we are seeking to map, but also because these patterns are drawn with respect to brain regional boundary assignments that are first drawn as a *base map* in the atlas from the cytoarchitectonic features of Nissl-stained tissue series serving as the reference. Indeed, both the boundaries and the immunoreactive patterns are basic features of the landscape and are manually drawn by observation of photomicrographic data or, as in the case of other disciplines (e.g., Hill, 1991), drawings from direct lens-based observations. These feature-based maps are for single subjects (see next section) but can be transformed into multi-subject consensus maps of two kinds (see *Section 4.2.1.2*).

4.2.1.1 Single-subject maps of data elements (cell bodies, neurites, putative appositions). Strictly speaking, the mapped elements on the base map mark the locations of *profiles* of cell parts: perikaryal profiles, axonal or dendritic profiles, putative apposition profiles. The locations of the perikaryal profiles drawn over the base map are represented in 1:1 registration with the location of the profile observed in photomicrographs of the native immunostained tissue. In the case of a putative apposition, the drawn profile marked the location that was in registration with the location observed on the actual tissue slide as it was visualized under a ×100 oil objective lens through the *z*-axis by a trained student. Thus, one circle glyph marks the position of one profile for each perikaryon or putative apposition. To the extent possible, this approach was also followed for immunoreactive neurite profiles but was not always maintained for especially dense regions of neurites, where it was difficult to distinguish individual elements from each other. In those instances, the overall trends of density and directionality were drawn to represent the overall spatial organization of the data overlaid on the base map.

4.2.1.2 Multi-subject maps. One way in which neuroanatomical mapping between subjects can be reconciled is using deformation or warping algorithms that normalize a subject's brain anatomy to fit a standardized template. Such efforts require validation by comparing "before" and "after" dispositions of known landmarks within the tissue, as has been performed for human MRI images (e.g., Grachev et al., 1999) and for mouse and rat brains (e.g., Gaser et al., 2012; Sergejeva et al., 2015). In such instances, the landmarks selected are identified using an expert human actor trained to recognize such landmarks, providing a expert-guided validation. An alternative approach, where the comparison across subjects occurs without warping but through structural analysis, has also been conducted by various groups and formally described (Riviére et al., 2022).

We opted for a hybrid approach for *Chemopleth 1.0*; in this case, each subject was *first* mapped by an expert to the BM4.0 standardized atlas *and then* the final map from each subject for a given atlas level was spatially averaged to produce the two classes of multi-subject maps described below. With this approach, the need to warp was obviated by the direct intervention of an expert mapper to transfer neuroanatomical data to atlas templates with the aid of Nissl-based parcellation and manual registration.

4.2.1.2a. Choropleth mapping. We opted to include choropleth-based mapping to follow traditional approaches to tabulating distribution differences with respect to cytoarchitectonic boundary conditions set in place by Nissl-delimited brain region assignments that produced the atlas reference space we are using as a model. The data visualization in this format should be considered as a semi-quantitative assessment of densities bounded by cytoarchitectonic region within the base map (i.e., the density values were normalized by bounded area). Automated quantitative analysis is dependent on the boundary conditions we set for those regions without explicit boundary knowledge available from the Nissl-based cytoarchitecture. These determinations, therefore, should be considered purely as a starting point, and the datasets can be re-analyzed under different boundary delimitations in the future to refine these assessments.

4.2.1.2b. Isopleth mapping. A new tool introduced in this database is the isopleth map. Like choropleth maps, isopleth maps denote differences in areal density for the cell populations being mapped across multiple subjects, with the concentrations in darker shading denoting "core" population densities, surrounded by lighter shaded territories representing sparser densities of the cells. However, unlike choropleth maps, isopleth maps display density distributions that are not confined to cytoarchitectonic boundaries of the base map. The design features of this mapping method are discussed in *Section 4.3*; here, we focus on what the maps might be revealing about the native distributions of these neuronal populations.

Economy of space is believed to consolidate cellular populations apart from fiber systems (Nieuwenhuys, 1998), and the lateral hypothalamic reticular pathways have been described to contact leptodendritic cells which are more sparsely distributed within perpendicularly oriented configurations with respect to ascending and descending fiber systems (Rámon-Moliner, 1969; Nieuwenhuys, 1998; see Geser et al., 2022). Recently, evidence has been furnished that lateral hypothalamic populations in the mouse form ultra-sparse connections among themselves (Burdakov & Karnani, 2020); this may be true for the rat as well.

Some of the lightly shaded areas in our isopleth maps are likely marking regions that actually harbor cell populations, but which were not immunostained and therefore not mapped in our studies. However, apparent cell-sparse zones may reflect a true dearth of perikarya in the territories traversed by the main ascending and descending fiber components of the medial forebrain bundle (Veening et al., 1982), which has been observed to be "coextensive" with the lateral hypothalamic area (Krieg, 1932, p. 67). Our preliminary investigation into fiber contributions to the mfb has demonstrated that corticohypothalamic projections from the infralimbic area arise within the several subregions of the LHA, with >60% of these connections forming putative appositions with hypocretin/orexin (H_1/O_A)-immunoreactive perikarya ipsilaterally (Negishi and Khan, 2019). It is noteworthy that we observe relatively sparse distributions of H_1/O_A neurons in the LHAd in the vicinity of these fibers, underscoring the idea that the ultra-sparse connectivity reported in this region in the mouse may also extend to spatial organization in the rat.

What would the functional significance of sparse connectivity in this region be? One possible explanation is that these relatively sparser areas may be sources of information flow outside of the main centers of cellularity, evoking patterns strikingly reminiscent of *karesansui,* or Japanese dry landscape gardens (Keane, 2004; Wicks, 2004) and other representations of scattered particulate landscapes, where there may be discrete denser aggregates (Guidi, 2023) surrounded by areas of flow. Evidence is mounting that the brain's interstitial spaces include extracellular elements that may serve to synergize communication with the cytoarchitectonically defined areas they surround; these elements include not only glia, but blood vessels (Scremin, 1970; Yao et al., 2021), perineuronal nets (Blacktop & Sorg, 2018; Mirzadeh et al., 2019) and other non-neuronal cell types (Argente-Arizón et al., 2015). Local, non-point-to-point neuronal communication via neuromodulation (Katz, 1999) or graded neurotransmission that does not requires action potentials (Bullock, 1981; also see Shepherd, 1981; Strathern, 2021), or forms of volume transmission which may not involve neuronal elements (Alpár et al., 2019; Guidolin et al., 2022), may serve to interconnect all these elements as part of a larger hybridized or even "extra-connectomic" network (Bargmann and Marder, 2013). Even among neuropeptidergic cell clusters, for example, in the hypothalamus, the geometry of these arrangements may permit neurons to respond selectively to specific electrical oscillations in the surrounding tissue (Kosse & Burdakov, 2018).

In relation to neuronal geometry, blood vessel contributions also appear to be significant occupiers of interstitial space in the hypothalamus (Scremin, 1970; Ambach & Palkovits, 1982), and probably exert an influence on geometric determinations of clustered neuronal populations in the hypothalamus, given the reported synergy that blood vessels generally appear to have with neurons during development of shared pathways in tissue space (Weinstein, 2005; Larrivée et al., 2009). Indeed, there appear to be spatial correlations in the hypothalamus between dense neuronal clusters and dense vascular patterns, such as that reported for the hypothalamic paraventricular nucleus (Frahm et al., 2012). This is especially likely for the chemoarchitecture we examined, particularly copeptin, neuronal nitric oxide synthase and melanin-concentrating hormone, which appear to also occasionally aggregate in clusters around blood vessel cross-sections in the medial and lateral hypothalamic zones (Khan, unpublished observations; Silva and Khan, 2012). Clustered assemblies of neurons along vascular routes may provide alternative routes for communication, much as indigenous communities clustered around riverbanks have networks that bypass traditional overland routes (Comer, 2015). For melanin-concentrating hormone, for example, evidence for volume transmission through the vasculature and cerebrospinal fluid has been furnished (Noble et al., 2018). Understanding such neuronal-vascular relationships may contribute greatly to our understanding of how communication is carried out in the hypothalamus (e.g., see Roy et al., 2021), relationships that isopleth mapping and future registration of angioarchitectural datasets could help reveal.

Collectively, these considerations of extra-neuronal elements challenge our current understanding of whether cytoarchitectonically determined boundary conditions in the brain reflect functional distinctions, and may render such conditions irrelevant at larger scales of visualization and functional integration, much as boundary conditions established by political or colonial elements on the ground become less influential or even meaningless from the vantage point of higher elevations (Sayet, 2022; 2024). Indeed, at a fundamental level, it is evident that processes visualized at one scale do not necessarily have operations that are as salient at larger or smaller scales (Lima, 2011, pp. 91ff.) – the misunderstanding of which contributes to the so-called

"scaling fallacy" (e.g., see Lidwell et al., 2003, pp. 214–215; West, 2017, pp. 43–45). It is now well documented, for example, that cortical microstructure may not be reflected in the organization of macroscopic borders (Devlin & Poldrack, 2007). Indeed, it is also not yet clear that macroscale connectivity measures obtained from resting-state fMRI or diffusion tractography correlate with underlying mesoscale axonal connectivity, with some studies reporting poor correlations (Straathof et al., 2020; Benozzo et al., 2024) and others reporting stronger ones (see Straathof et al., (2020) for discussion).

The advantage of isopleth mapping, which we are performing here at the mesoscale, is that the distribution patterns we observe for these neuronal populations *are not constrained* to Nissl-defined boundaries and more accurately reveal the spaces in between nucleated aggregates of cells, the precise geometry of which, even if not yet discernible at the microscopic scale, could nevertheless undergird observable phenomena at larger scales. If larger-scale functions are in play that transcend cytoarchitectonic boundaries, the isopleth distributions could, in principle, either reflect such functions structurally in a way not yet known to us; alternatively, they can, at the very least, be placed in register with future structural maps that may better reflect such functional operations.

4.2.1.2b (i). Implications of isopleth mapping of intersubject variability. In addition to providing a liberation from Nissl-delimited cytoarchitectonic space, the isopleth mapping that we provide here for five immunoreactive neurochemical systems in the hypothalamus and zone incerta also provide for greater considerations of chemoarchitectural changes in time. The idea that there exist species-typical patterns of connectivity which break down at the individual level, where stochastic difference may account for variation is not a new one (e.g., see Mitra, 2014), and has been discussed by many biologists, including neuroscientists wrestling with the idea of how changes in the brain may be reflected as changes in external phenotype, whether this manifests in the form of structure or function.

In our isopleth maps, we may be looking at zones of constancy and zones of variability that have been selected for during evolution, which leads to the realization that we are juxtaposing mapped structures to reveal varying depths of change over evolutionary time. Areas that may confer survivability may in fact be also correlated with areas that display strongly concordant immunoreactive patterns across individual subject where the structure-function relationships of such areas are too critical for survival to change drastically over time. However, those variable regions that are evident may reflect areas of the brain that are selected for evolutionarily to remain plastic and changing to confer behavioral flexibility, what is termed the ability of natural selection pressures to allow for different evolutionary *strategies* over time. Much as scientists have painstakingly examined the morphological variations of the Galápagos finches and determined that they satisfy the salient conditions necessary for evolution to occur (i.e. variability in the population, heritability of these varied traits, and their contributions to the finches' reproductive success; Weiner, 1994), it becomes clear that atlas-based mapping of chemoarchitecture from multiple animals into a common reference framework allows for a constrained evaluation of morphological variation to be made lawfully. This exercise, in turn, sets the stage for formulating testable hypotheses as to whether such variations in immunoreactive distributions are state-dependent within the lifetime of the subject (as many of them most surely are), or are overlaid by longer-term factors that account for their variability across the subject's lineage over time (Khan, unpublished laboratory blog posts entitled "Ultraconserved Elements I, II, III", 25 Oct 19, 3 Nov 19, and 24 Feb 20). This question,

namely, the degree to which individual variation among subjects is the result of deep evolutionary change rather than individual lifetime-bounded state changes is one that is tackled routinely by scientists studying geometric morphometrics, which could be applied eventually to our datasets as well, once a suitable sample size is achieved.

4.2.3: Grid-based mapping

4.2.3.1: Stereotaxic grid. The original hard copy edition of *Brain Maps: Structure of the Rat Brain* (Swanson, 1992) included a transparent overlay that could be aligned to each base map which bore calibration marks for the stereotaxic coordinates for the Paxinos and Watson (1986) stereotaxic coordinate system. Their system is considered the gold standard coordinate system for targeting probes to brain structures mapped in their atlas or – in the case of *Brain Maps* – any reference atlas that is produced in register with the plane of the Paxinos and Watson atlas. Since that first edition, the *Brain Maps* reference atlas has included this stereotaxic coordinate system as a data layer embedded within each atlas file. The *Chemopleth 1.0* database retains this data layer of inferred stereotaxic coordinates, and we introduce a new, named coordinate system for this coordinate framework that allows grid-based mapping of data for the first time. *Section 4.3.4* describes this design feature in greater detail.

4.2.3.2: The FMRS System. We selected the acronym, FMRS, because it phonetically resembles the word *ephemeris*, which is the term for a table of positions of celestial objects (e.g., planets) that has been used by many civilizations and cultures since antiquity (Gingerich, 1997; also see *zij*: Kennedy, 1956; King and Saliba, 1987; see Banneker (1793) for a notable example of a published ephemeris). We use "FMRS" in the same way as "ephemeris" is used in a sentence (i.e., as a noun and not an adjective; thus "an FMRS", not "an FMRS table"). Also, we use "FMRS" as both a singular and plural noun: "one FMRS", "many FMRS". We opted to use FMRS rather than ephemeris for two reasons: (1) the acronym emphasizes its roots as a tabulation in stereotaxic space and not celestial coordinate space (i.e., Frequencies Mapped with Reference to Stereotaxy); and (2) it does not dilute, expand, or confuse the use of ephemeris, as used in astronomy, but still pays tribute to it as essentially the same concept: *an annotated tabulation of positional information for observed objects in a coordinate space*.

Also worth noting is the fact that ephemeris is closely related to "ephemeral", which denotes "short-lived" or "momentary"; ephemeris (and by extension, FMRS), therefore, emphasizes that the counts or frequencies recorded in each grid zone represent those of a *single experiment or observation* in one subject within a circumscribed set of space-time conditions, and that these frequencies are being used by a single laboratory to model such distributions as they may appear across subjects. Therefore, they should be treated as a limited representation of more generalized states or phenomena. In other words, FMRS notations are of *circumscribed experimental observations*. Much as positional information tabulated in an ephemeris is dependent on the local conditions where such observations were recorded from, so, too, are the frequencies binned to stereotaxic grid zones dependent on the laboratory making the observations, the condition of the experimental subject they are studying, the conditions and parameters of their labeling experiments, etc. In *Section 4.3.4.3*, we discuss the advantages the use of this grod-based annotation system may afford investigators seeking a general summary of which brain areas to target experimentally and how such a system is a straightforward way to map distributions without needing training or expert knowledge in feature-based (i.e., cytoarchitectonic) mapping.

4.2.4: Registered legacy datasets

We now turn to the published data we registered to our own datasets. Specifically, we have re-plotted the spatial positions of three neuronal populations reported in two studies: Yao et al., 2005 (hypocretin 1/orexin A, nitric oxide synthase) and Kerman et al., 2007 (hypocretin 1/orexin A, melanin-concentrating hormone). A few points are worth noting regarding this registration.

4.2.4.1: Aligning earlier and later work within a 'spatial commons' reveals concordance. First, the alignment of these data with our own isopleth maps of these populations reveals a strikingly concordant overlap across our collective studies. This alignment is striking because the methods used to map these populations were not shared between those laboratories and our own, nor were the methods used to generate the histological staining patterns identical. The registration underscores how standardized atlasing of data provides a means to readily explore similarities and differences among experimental results generated by investigators separated in time and space and who may use resources and methods that are similar, but not identical. Such investigators, who "share the same spaces" and are essentially "performing the same movements" (Farriss & Hutchence, 1990), can operate out of isolation and into a shared intellectual commons where they can help build, refine, and interrogate a shared spatial model of the brain (discussed in Khan, 2013; also see Leergaard & Bjaalie, 2022). Indeed, apart from the Swanson laboratory's own use of the *Brain Maps* reference space, many other labs report mapped data for the hypothalamus or zona incerta plotted in this space, including mRNA and/or protein expression patterns (Broberger et al., 1998; Kelly & Watts, 1998; Khan et al., 2000; Yao et al., 2005; Hahn, 2010), chemical/electrode lesions or electrode placements (Gallistel et al., 1996; Flores et al., 1997; Simmons et al., 1998; Radley, et al., 2006; Choi et al., 2007; Martínez et al., 2023), chemical microinjection sites (España et al., 2001; Khan et al., 2007), cellular activation patterns (Zséli et al., 2016), neuroanatomical tract-tracer injection sites and tracer-labeled cell bodies and fibers (Jansen et al., 1995; Abrahamson & Moore, 2001; Leak & Moore, 2001; Geerling et al., 2003; Uschakov et al., 2007; Kerman et al., 2007), and optogenetic fiber placements (Wood et al., 2019). It is hoped that *Chemopleth 1.0* allows for such a model to grow and evolve for the rat hypothalamus and zona incerta by collective efforts of the scientific community. Ultimately, the use of inference engines and artificial intelligence across such layered datasets could provide explicit linkages and hypothesis generation for future data-constrained experiments, as has been recently shown in archaeological research (Casini et al., 2023), and of relevance, in linking structural brain variations with down-scale genetics and larger-scale autism phenotypes (Kundu et al., 2024). The targeting of this mapped chemoarchitecture could literally and conceptually be refined by such linkages.

4.2.4.2: Digital overlays as a form of shorthand citation and preservation of evidentiary trails. Second, the use of artificial intelligence notwithstanding, the digital overlays afforded by the Ai environment (*see Section 4.3.1*) already reveal explicit evidentiary and historical relationships among disparate sets of data. **Figure 17** provides a simple example of how overlays can provide a shorthand form of citation that links a newly reported dataset (for example, the distributions of MCH-immunoreactive neurons; present study) with previous efforts "within" the same reference space (identification of premotor-parasympathetic MCH-immunoreactive neurons; Kerman et al., 2007). A prepared digital overlay of another laboratory's data is essentially a form of data curation from the literature that speeds up the process of understanding how such data relate to one's own during the process of literature-based study of previous work in one's field. This approach of registering published datasets to these BM4.0 base maps is very much in keeping with the standard

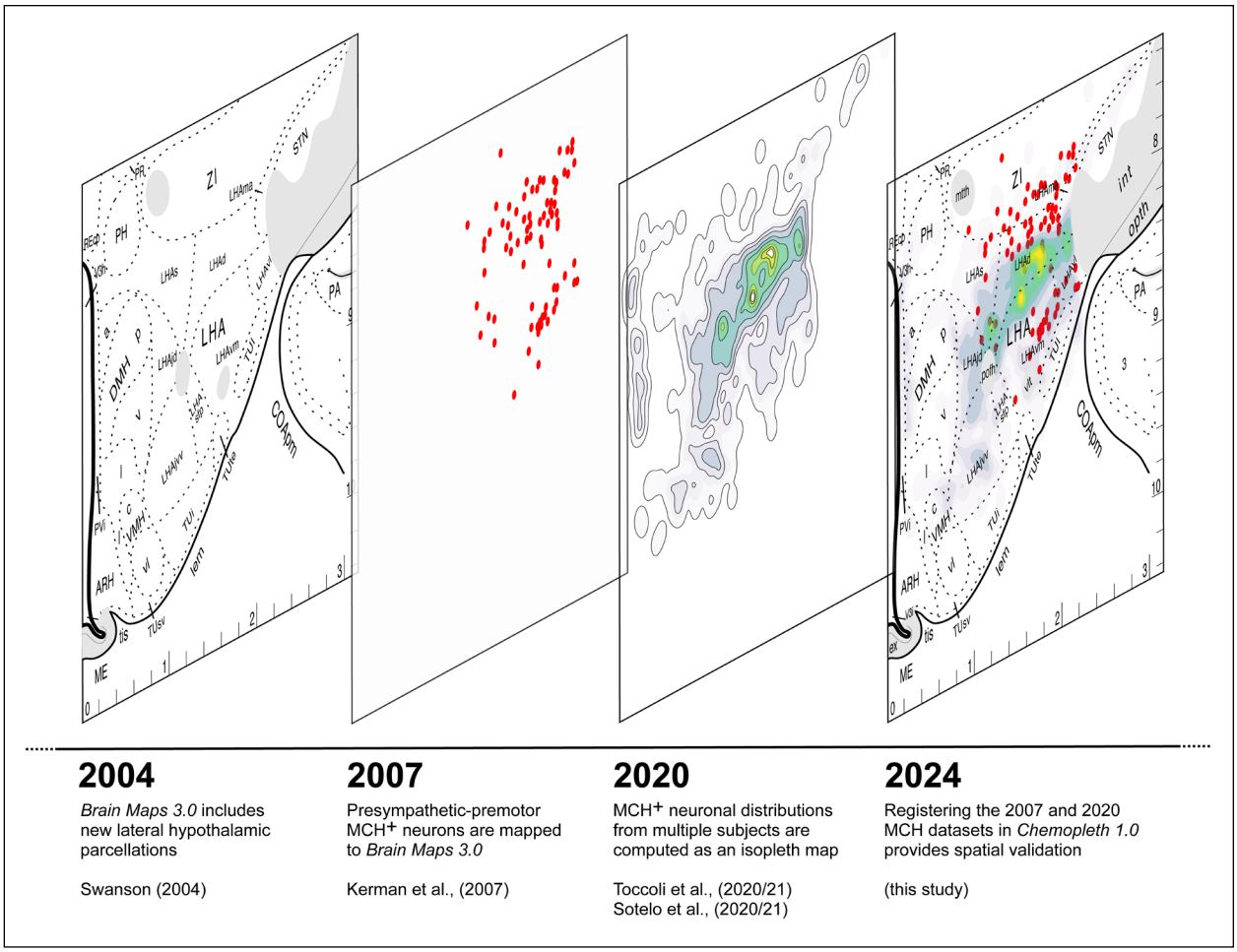

Figure 17. Community-based model building. An example of our data registration presented as a scientific chronology, illustrating a model-building process for the lateral hypothalamic area and zona incerta of the adult male rat in *Brain Maps 4.0* atlas reference space. In this example, the base map additions provided by Swanson (2004) allow finer-resolution mapping of traced MCH-immunoreactive populations in 2007 by Kerman et al. (presented as a separate data overlay in the database), which are supported by our successive isopleth analyses of multi-subject MCH-immunoreactivity patterns in 2020 (presented as a third overlay). The resulting model, shown at the far right, is, therefore, a community-built model of this chemoarchitecture. See text for details.

set by Swanson (2018) for the atlas itself, ever since its first edition (Swanson, 1992), where an appendix was included which relates the majority of all brain regions and areas to the published literature. As Swanson has himself stated, the atlas is essentially a hypothesis (Swanson, personal communication to AMK), with each region's boundaries undergoing refinements as more evidence furnished in the steadily accumulating scientific literature is brought to bear on that specific feature. This approach – that of linking structural features of the atlas maps to the published literature – also more formally underlies Swanson's published Foundational Model of Connectivity (FMC), which states as one of its arguments that it is based on evidence not authority (Swanson & Bota, 2010).

In many ways, then, by linking our spatial datasets to the published evidence in the literature and citing those previous scientists who have furnished this evidence, we explicitly build upon those findings as we disseminate our own to the next group of readers who, in turn, may build

upon what we have reported. This process is akin to the transfer of knowledge of spatial location in Polynesian cultures from one generation to the next in "a never-ending chain" (Foa'i & Miranda, 2016), only the difference is that their transfer is in oral, not written, form (Thompson, 2019). It also echoes the concept of 'time-binding' furnished by Korzybski (1950), as articulated by abstract artists such as Charles Biederman, where succeeding generations of human beings retain and build upon the knowledge and understanding from previous generations of how visualization of complex forms can be achieved (see p. 32–33 of Biederman, 1948). Complex and highly specific forms in art and music often find recurrences in later works, whether it be Greek key motifs in art or guitar riffs in songs (e.g., compare 0:48 of Bowie, 1971, with 6:19 of Burton et al., 1986); the re-embedding of these motifs in later works simultaneously traces evidentiary trails of their origins while at the same time redefining them for new audiences. Similarly, the linkage in time and space of different datasets explicitly points to recurring structure/function relationships in them; this includes re-contextualization of old datasets in relation to new ones, as we discuss next.

4.2.4.3. Older data fitted to newer models re-contexualizes them. Third, as an example of how data can be updated to fit new models, we note that the data maps in both Yao et al., (2005) and Kerman et al., (2007) were plotted in those studies using older editions of the *Brain Maps* atlases. Thus, Yao and colleagues used the second edition of the atlas (*Brain Maps 2*) and Kerman and colleagues used the third edition of the atlas (*Brain Maps 3*). In the present study, we migrated and re-plotted these datasets to the latest edition of *Brain Maps* (*Brain Maps 4.0*; Swanson, 2018). The specific atlas levels Kerman and colleagues mapped their datasets to did not undergo any major change in *Brain Maps 4.0*, making their migration from the third to the fourth edition simply a carryover of the data into a similar space. In contrast, the migration of the Yao et al., (2005) dataset from the second to fourth editions *re-contextualized* those data. Specifically, where there were minimal subregional parcellations of the lateral hypothalamic zone in the second edition, this region underwent a major re-analysis based on more detailed observations by Swanson of the original Nissl-stained tissue set on which the atlas is based (the editions are all based on the same brain: a single, 315-g male Sprague Dawley rat). These considerations lead us to consider next the importance of data layers in a temporal context.

4.2.4.4. Data layers as a chronological record. Much as data layers have been proposed for use by geoscientists to mark chronological events in geospatial datasets (Langran & Chrisman, 1988; pp 4, 9–11; also see Langran, 1993; Saint-Marc et al., 2014), including real-world geospatial processes ('world-time'; i.e., when the geological process took place) and their records/reported findings ('database-time'; i.e., when the observation regarding the geological process was recorded; again, see Langran & Chrisman, 1988), data overlays can provide the same advantages for brain mapping. Similar to what Langran and Chrisman (1993) state in their treatment of time in geospatial datasets, we propose that a similar system should be adopted for registering legacy datasets to current reference spaces, since this form of data migration is important to track and memorialize in terms of 'world-time' and 'database-time'. The salient difference between how geological processes and their documentation are handled in this fashion and how we might imagine neurological processes to play out is that the time between the occurrence of a neurological process and its observation is usually never very long. Thus, whereas geological and neurological processes can both occur quickly in real time (e.g., earthquakes, seizures) and measured the moment they occur (e.g., seismographs, electroencephalograms), the former can also occur over the scale of centuries (continental drift, seafloor spreading) and measured accordingly

(magnetic field inversions, isotope ratios). As a result, the 'database-time' (time when observations are recorded) can be far apart from 'world-time' of that event.

However, one way in which there are longer time frames in neuroscience (apart from lifespan in one organism or comparisons of lifespans of different organisms or evolutionary processes) is between sets of recorded observations in neuroscientific history. Thus, there is a need to consider that the time between world-time and database-time in experimental neuroscience will usually be short, but model-building will require multiple snapshots in database-time as the spatial model of the brain is further refined. A standardized atlas, which importantly, also ought to undergo revisions over time, can serve as such a model, and spatial mapping such as that presented here can be databased over time and various experimental observations so recorded.

In the case of our simple exemplars of legacy database registration (Yao et al., 2005; Kerman et al., 2007), we propose that a standard notation be used for data migration, and that this notation be included as a tag accompanying a given dataset. Thus, Yao et al., 2005 (based on *Brain Maps 2*) migrated to the current *Chemopleth 1.0* database (based on BM4.0) could be written in notation form as the following dataset name: Yao et al., $(2005)^{S98 \rightarrow S18}$, where S98 and S18 denote Swanson atlas editions from 1998 and 2018, respectively (as proposed by us earlier: Khan et al., 2018b) and the arrow denotes migration between the two atlas editions. We have used this notation for our data layers in *Chemopleth 1.0*.

4.3 Database tools and how they inform design and scientific representation

4.3.1 Digital overlays

Background. In neuroscience, certain fundamental issues associated with the visualization of neural elements in space naturally arose from the desire to examine – in three dimensions – information that was present in two-dimensional tissue sections under the microscope. Just as photographers needed to find some way of capturing relief features in flat photographs, scientists sought to refine ways to capture 3-D information from the *z*-axis of an otherwise *xy* plane. This was difficult with the first microscopes, which were monocular lenses with limited depths of field (Ford, 1985). However, these instruments eventually gave way to binocular lenses and stereoscopic views where images arriving at both eyes were merged or superimposed to produce greater depths of field. The invention of the stereoscope by Wheatstone in 1838 catalyzed the development of binocular lenses in microscopes, and Cajal's manual on color photography describes his use of stereoscopy to visualize the nervous system (Cajal, 1912; Santarén, 2014).

Paralleling this need was the corresponding need to represent and visualize drawn 2-dimensional representations of tissue elements viewed through their depth. This need also grew out of limitations imposed by the finite cache of labels one could employ to visualize tissues under the microscope: "the gains in brain are mainly in the stain" (Bloom, 1975). Early attempts to address problems of superimposition or composite imaging involved manual reconstructions via semi-transparent overlays of paper (e.g., Streeter, 1905). Later, sequential images of different structural information could be viewed simultaneously by taking advantage of film technology (e.g., Levinthal & Ware, 1972), breakthroughs for which allowed multiple photographs on film to be combined into a composite image using optical printing, as pioneered, for example, by Richard Edlund for *The Empire Strikes Back* (Lucas, 1980; discussed during 25:25–28:03 in Kasdan, 2022; also see Fordham, 2023). The history of the use of transparent overlays has proven to be elusive in its transition from analog to digital formats (e.g., see Cloud, 2005). In neuroanatomy, computer

graphics applications ("computer-assisted neuroanatomy"; see Woodward et al., 1985) largely supplanted film technology with digital data overlays, which were applied to neuroscientific data in the 1980s (e.g., Toga et al., 1984).

The *Chemopleth 1.0* database is based on a digital overlay system that is historically embedded within the Ai environment from the time of its early version in 1993 (Adobe Illustrator, version 3.1). The use of this overlay tool within the first release of the graphics files of the *Brain Maps* atlas makes this rat brain atlas likely the first to utilize digital overlay technology and atlas maps formatted in vector graphics. For this atlas, instantiations of a graphic user interface with digital overlay tools were reported by Dashti et al., (2001) and Burns et al., (2006). *Chemopleth 1.0,* in many ways, can be considered as a complementary resource.

Overlays allow for both raster- and vector-format data to be superimposable in the same reference space. Historically, as with geomorphological mapping, usually the raster data are photographs (e.g., aerial photographs), which can be placed in register with points, lines, and areas (polygons), which are all vector data that consist of the user's superimposable annotations or interpretations of the raster data (e.g., feature labels of the landscape) (Smith, 2011). Here, our photomicrographs of Nissl-stained histological material, and those of the adjacent series of immunolabeled tissues from the same subject, were captured in raster format and placed as data layers, with vector-based maps of parcellations superimposed on the photos of immunolabeled data. The simultaneous visualization of multiple data sets in registration with one another affords the investigator with novel views and juxtapositions to fuel the discovery of new spatial relationships among elements of the visualized datasets.

4.3.2 Design features of the choropleth and isopleth maps

For the choropleth maps, a decision was made to produce these by first setting provisional boundaries for the open vector graphics representing the brain regions. At the time of this writing, most of the brain regions represented in BM4.0 vector graphics templates are not closed polygons. Therefore, as noted in *Section 2.5.2*, we first closed these visually apparent vector patterns for the eight levels we analyzed in this dataset. We note in that section how these were provisionally assigned and that future refinements of the *Brain Maps* reference space will no doubt change these boundaries as more data collection and deliberation takes place. The boundaries, therefore, constitute mapped design features that will undergo revision over time and the density scoring that we performed based on their areal measures are also therefore provisional.

The choropleth and isopleth color patterns we used are consistent with older observations, using monochrome LCD monitors, that darker regions on lighter backgrounds, with dark representing greater abundance, is generally most effective in conveying distribution differences (McGranaghan, 1996). Color management of data layers in mapping (Brewer, 2016) also informed our decision to use specific color patterns for our maps. Apart from color, we opted for cartographic generalization and, therefore, the sizes of the glyphs and strokes used to represent perikarya and neurites, respectively, are decidedly not to scale.

4.3.3 Significance of our mapping and spatial averaging methods

We sought to capture — graphically, within our maps — a representation of the variance that occurs when an expert mapper transposes spatial labeling information by eye from the native tissue to the digital atlas map. In our process, by the time the mapper sets out to perform such a

task, they have become familiar with the spatial relationships of the landmarks and territories in relation to their datasets. This includes an understanding of the plane of section and orientation of the tissue (what we could consider here to be a "compass sense", or sense of direction), and the nearest-neighbor relationships of the cytoarchitectonic boundaries of the tissue in relation to the labeling patterns they are observing within it (what we could consider here to be a local "map sense", or sense of location). Thus, when the mapper is setting out to place the labeling patterns within the atlas reference environment, they are already at a stage where the variability in placing such patterns is constrained, where their accuracy in mapping is guided by the bounds imposed by these two senses. The orientation of their vantage point, together with knowledge that they are near the relevant objects in the environment, afford them the correct "field of view" away from the microscope. This is aided by their canvas already being populated as a digital atlas template, containing silhouettes of the regions appearing in their Nissl-stained tissue. Their initial task, therefore, becomes selecting from the appropriate templates and then choosing the correct general location within a single template to begin transferring labeled patterns based on a study of the Nissl series. In most instances, a simple act of placing a filled circle or traced line over the picture of a cell body or neurite, respectively, within the Adobe Illustrator environment preserves its relationship to another labeled cell body or neurite (also see Lingley et al., 2018). In fewer instances, a one-to-one drawn representation of the elements was not attempted for those labeling patterns that were very dense.

4.3.4 Design features of the grid-based maps

Grid-based mapping of the brain can be traced as far back as the invention of the stereotaxic instrument by Horsley and Clarke (1909) (also see Krieg, 1975). Swanson (2000) notes that a drawing of the brain by Eustachius in the 1550s (but published later in 1714), included a pair of rulers, and is a notable early example of a set of coordinates placed in relation to drawn neuroanatomical features. While grids have been used in brain mapping in various ways since these early efforts, our use of grids is based on a different motivation. Specifically, we sought to establish a conceptual framework for the datasets reported by our laboratory that allowed for the recording of spatial locations in atlas-dependent and -independent formats (i.e., locations referring to specific features or entities versus locations referring to an invariant grid or field; see Rigaux et al., 2002). This was born from the "need to compute across *spatial territory*, not just *named variables for territories*, because certain [immunoreactivity] patterns cut across known territories and spill into unlabeled portions" (Khan, unpublished laboratory blog post, 21 May 2020). The reasons for such a need can be parsed into several topics, which are dealt with in greater detail below.

4.3.4.1 Mapping elements that do not conform to cytoarchitectonic criteria. Many neurochemical systems in the hypothalamus and zona incerta do not follow along traditional patterns of cytoarchitecture based on Nissl parcellations. Thus, a named cluster of cells that populates the atlas as a 'part' of a catalog of 'parts', which is largely based on Nissl-delimited cytoarchitectural boundaries, fails to consider patterns that traverse these limits. A grid bypasses such constraints by allowing for its named grid zone to represent everything contained within it regardless of whether the patterns fall within or outside of named brain parts. Thus, 'extra-connectomic' information is also represented and accounted for.

4.3.4.2 Generalizes space without resorting to questions of contents or phenotypes. Grid maps are a useful means to spatially account for, in a systematized fashion, the locations of

labeled elements for neuroanatomical experiments that avoids the complexity of contextualizing location with respect to local features in the tissue, apart from macrolevel landmarks such as white matter tracts or other gross anatomical features. Feature-based maps of the brain have undergone refinements and modifications over their history and are often accompanied by healthy discussion and debate concerning their validity (e.g., debates concerning cortical parcellation and compartmentalization). This is no less true for the hypothalamus and zona incerta, the nomenclature and, indeed, basic organization of which remain vigorous topics of discussion (e.g., Croizier et al., 2015; Puelles & Rubenstein, 2015; Bedont et al., 2015; Kim et al., 2020). The advantage of grid-based mapping is that the essential zoning of labeled chemoarchitecture is independent of and indifferent to varying opinions regarding the location, organization and nomenclature of the brain regions within which such chemoarchitecture resides.

That being said, there is always the option of superimposing the grid zones in our database as a digital overlay over feature-based contours for cytoarchitectonic regions, and counting immunoreactive elements within each grid zone, something we find useful as a hybrid approach, where a composite map (see **Fig. 11**, *top row;* also **Fig. 13**) that includes both features and grids allows for information from both to help orient the user to accurately map elements to the appropriate grid zone. This has been carried out in certain early studies of chemoarchitectural density mapping. For example, Agnati et al., (1985) reported quantitation of perikarya displaying immunoreactivity for the glucocorticoid receptor, where the counts were binned on a grid superimposed over a map of the cytoarchitectural boundaries of the locus coeruleus and paraventicular hypothalamic nucleus in young and aged male rats (see their Fig. 11 on p. 104 and Figs. 14 and 15 on pp. 107–108 of their study, respectively). The main difference in our approach is that the grid zones we use are larger in area and indistinguishable from the areas demarcated by the stereotaxic grid already present within the atlas file in a separate layer.

Thus, the stereotaxic grid, which has traditionally been used to aid neuroscientists in targeting the brain with probes for intracranial chemical or gene-directed manipulations (Khan, 2013), is now being utilized in this instance to map novel chemoarchitecture. At the same time, such mapping efforts – calibrated to what is traditionally a targeting system – automatically renders the newly mapped chemoarchitecture amenable to such targeting once reported to the greater scientific community.

4.3.4.3 Democratization. We also pursued the development and use of a grid-based system as a complement to feature-based mapping because there are unique advantages afforded with each method, much as there are for music referenced as standard notation or as tablature (Pillsbury, 2006, p. xvi), physical processes described in analytic (i.e., Cartesian) vs. geometric (i.e., Euclidean) notation (Feynman, 1964; scrub to 8:53–10:18), longitude measured by timekeeping or astronomical methods (Forbes, 1966; Sobel, 1995), or programs written in machine vs. assembly vs. compiler languages (Hofstadter, 1979, pp. 290–296). In our case, as in all these cases, a key advantage is the larger accessibility and democratization of data reporting that the alternative provides (see also Ramsdale et al., 2017). Specifically, little training is required to use a grid-based system to locate and indeed, even to map, labeled elements of the brain in a standardized way. In fact, apart from a basic understanding of stereotaxic coordinates and the use of a brain atlas, a user of this database could, in principle, map directly onto digital templates of the general atlas section's outline of the brain, without the patterns of parceled brain regions in view (i.e., with the visibility of that digital overlay or data layer toggled off). Much as creators of music and

art do not necessarily require formal training to pursue and successfully create and produce their work and can "approach [the work] conceptually rather than technically" (Eno, 2024), so, too, can neuroscientists untrained in formal atlas-mapping techniques use grids to localize the general position of their labeled elements in an atlas model of the brain.

Thus, the grid should potentially open the atlas to those in the scientific community who seek to incorporate their datasets into a larger community model being built around the *Brain Maps* reference atlas framework, but who do not themselves have the time and/or expertise to rigorously map their labeled elements in the tissue to the underlying cytoarchitecture. At this stage, we do not expect any but the most discerning or motivated of community members to use what we provide here to begin such a process, but also consider this as but a starting point of establishing a more accessible platform where neuroscientists can physically map their own data to the *Brain Maps* atlas and thereby contribute to a larger body of work that models structure-function relationships for the brain in a shareable and registrable manner.

The benefits of such democratization are potentially numerous. For one thing, scientists who have expert training in neuroanatomical techniques outside of mapping, particularly in performing intracranial probe placements, central injections, tract-tracing, viral vector delivery, microdialysis, optogenetics, etc., can now use a relatively straightforward means to map, at a coarse resolution of the 1.0 mm × 1.0 mm stereotaxic grid, the locations of their probe placements. Usually, the practice of reporting stereotaxic coordinates has been to state in the Methods section of papers those coordinates being used to *target* a previously defined set of features, not necessarily to *report* the location of new features. If this practice gains currency – that is, of using grids to <u>map</u> in addition to <u>target</u> – then, suddenly, all probe locations mapped to grid zones by non-expert mappers can be "brought into" the spatial model of atlas reference space and juxtaposed with finer neuroanatomical features mapped by experts. We envision some form of content curation where tiers of quality are assigned to datasets from non-experts vs. experts, and that the system must include lessons learned from similar digital resources who have identified their challenges and best practices, such as the Encyclopedia of Life Project (Rotman et al., 2012). Additionally, the use of this reporting structure (i.e., the grid-based FMRS; *see Section 3.5.4.2*) can be envisioned to serve the needs of those performing microdissections or finer samplings of brain tissue from experimental subjects (e.g., laser-capture microdissection). FMRS annotations can help anchor dissected samples of tissue and their attendant genomic metadata to fixed locations in atlas reference space by grid zone. Such approaches allow for the alignment of genomic information with neuroanatomic information in a more precise way (Khan et al., 2018a).

4.4 Future directions

Below, we note some paths forward for possible future iterations of this resource.

4.4.1 Future directions in data layers and visualization

Colors could in the future be palletized for the user's specific needs (Hodgson, 2016), or a code of colors could universally signify a set of semiotic meanings for the grids or isopleths, producing an essential visual grammar for grids akin to Piet Mondrian's color palettes (Mondiran, 1987; Weber, 2018; Deicher, 2024). In principle, perikarya marked on our maps by a circle glyph could also be color-coded based on cell size and analyzed for spatial patterns, as has been performed for perikarya in the cat and monkey cortex to reveal novel substructure in cytoarchitectonic patterns (Lingley et al., 2018). Our grid-based visualizations could, in principle, also encode more

information by alterations in the appearance of individual tiles, much as Vasarely's paintings so brilliantly achieve (e.g., see Vasarely, 1959–1961, 'Supernovae'), or modify the actual parameters of the grids themselves to create depth in digital overlay space, as so adroitly achieved in other media, such as that found in the works of Christiane Feser (see Feser, 2019, 'Felder 3 (Field 3)') or Charles Biederman (see Biederman, 1939, 'Work No. 3, New York, 1939').

4.4.2 Future validations

There is intriguing evidence that grids in maps facilitate greater recall of features embedded in maps (Edler et al., 2014). It would be interesting to see if this observation holds true for maps of cytoarchitecture, and a test of such a hypothesis could be conducted within a teaching laboratory setting. Work performed in our Brain Mapping & Connectomics teaching laboratory for freshman undergraduates (D'Arcy et al., 2019; Khan et al., 2021) suggests that it could be an ideal setting for such a hypothesis to be tested by student volunteers, a possibility we are now exploring. Grid overlays could also be used to bring separate mapped elements into register in a manner that minimizes specific mapping errors arising from differences in resolution between the elements or from roundoff errors generated by disparities between algorithms and finite-precision mathematical operations, as has been demonstrated in geographic information systems (Magalhães et al., 2015). The overall extent of error in mapping using digital systems, more generally, has been a subject of much discussion in cartography (e.g., Crisman, 1982) and future work will help formalize the sources of error for atlas-based transfer of anatomical information from photomicrographs of histologically processed tissue sections (see the cogent discussion of this topic by Simmons and Swanson, 2009). Aggregation of such data in the form of spatially averaged choropleth and isopleth maps merit additional considerations of error (e.g., MacEachren, 1982; 1985; Sun et al., 2015) which require further exploration for atlas-based mapping.

4.5 Conclusion

Mapping the spatial organization of cells and fibers in the brain is a fundamental challenge in neuroscience. Now in its fourth edition (Swanson, 2018), the *Brain Maps* atlas provides a rigorous anatomical reference for the rat brain and is a valuable resource for the neuroscience community, alongside other excellent brain atlases for the rat (e.g., Paxinos & Watson, 2014; Papp et al., 2014; 2015; Kleven et al., 2023), which have been placed in basic register with the *Brain Maps* framework (Khan et al., 2018; Bjerke et al., 2019).

In this draft report, we have provided a description of a forthcoming spatial database, called *Chemopleth 1.0*, which will furnish freely accessible *Brain Maps 4.0* digital atlas maps of five neurochemical systems in the rat *hypothalamus (Kuhlenbeck, 1927)* and *zona incerta (>1840)* brain regions critically involved in controlling many survival functions. Our efforts to create a spatial database at mesoscale resolution complements efforts to create databases at macroscales based on standardized brain atlases (e.g., Nowinski et al., 1997; 2000; also see Nowinski, 2023) and are meant to be used for the same purpose as they are, particularly with respect to stereotaxic targeting (e.g., see Nowinski et al., 2000). The work also complements efforts for mouse brain to create interactive frameworks to synergize disparate datasets at cellular resolution (Fürth et al., 2018).

Ultimately, we envision future numbered versions of *Chemopleth 1.0* will: (1) contain greater amounts of chemoarchitectural data registered to our existing collection of mapped datasets; (2) incorporate more registered legacy datasets from the published literature; and (3) include *Brain*

Maps base maps that are created for revised versions of the core atlas. Apart from these naturally progressing improvements, we are eyeing the artificial intelligence (AI) landscape for geospatial/archaeological analysis (e.g., the newly emerging field of GeoAI; see Kang, 2020; Kang et al., 2024; see Casini et al., 2023 for archaeological application) to help develop workflows that allow diverse spatial locations of corresponding space on digital overlays to be analyzed for cause-effect biological relationships and inferences drawn about possible interactions, as conceptualized over a decade ago by our laboratory (Khan, 2013, Fig. 8). This will allow for multiscale integration of experimental metadata and would address some issues plaguing top-down and bottom-up approaches (D'Angelo & Jirsa, 2022). They will also bring quickly to the fore the larger challenge of making sense of all spatially registered data within one mapped location, finally shifting our attention in neuroanatomy from data gathering to data intelligence, as we finally "face the mother lode" (Gabriel, 2023a,b): evidence collected from communal data, and finally organized as shared information, waiting to be harnessed for medical treatments, drug discovery, multiscale views of the nervous system, and ultimately, a deeper view of ourselves.

Acknowledgments

Funding. This work was supported by grants awarded to AMK from the National Institute of General Medical Sciences (NIGMS) of the National Institutes of Health (NIH) (GM109817 and GM127251) and a grant from the UTEP Office of Research and Sponsored Projects to the IGNITE group (L. E. O'Dell, A. M. Khan, I. A. Mendez, B. Cushing, S. Iñiguez). Work performed in the Brain Mapping & Connectomics (BMC) Undergraduate Teaching Laboratory was conducted within UTEP PERSIST (Program to Educate and Retain Students in STEM Tracks), a training program funded by Howard Hughes Medical Institute grant 52008125 (PI: S. B. Aley, Co-PIs: L. Echegoyen, A. M. Khan, D. Villagrán, E. Greenbaum). VIN and AA were supported by Doctoral Excellence Fellowships. VIN, ART, and DS are fellows of the UTEP RISE (Research Initiative for Scientific Enhancement) program (NIGMS; R25GM069621; PI: R. Aguilera). AA was also supported by Dodson Research Grants from the UTEP Graduate School and by travel grants from the UTEP Graduate School and the College of Science. This work was also supported by the Border Biomedical Research Center, which is funded by the National Institute on Minority Health and Health Disparities (NIMHD; 2U54MD007592; PI: R. A. Kirken).

Colleagues. The authors thank Patrick Hof, Larry W. Swanson, and the late Anthony N. van den Pol for their support and encouragement of this project. We also thank Suzana Herculano-Houzel and Melissa J. Chee for their feedback on portions of this study. We also thank Claire E. Wells, Christina E. D'Arcy, Briana Pinales, Nicole Dominguez, Richard H. Thompson, Georgina A. Lean, Kristen Pennington, Alexa Escapita, Paola Rojas, and our BMC students for early immunofluorescence efforts on this project. We are grateful to members of the UTEP Systems Neuroscience Laboratory, especially Anais Martinez, Christina E. D'Arcy and Kenichiro Negishi for valuable discussions. AMK expresses his deep gratitude to Vivian-Lee Nyitray for introducing to him Zen aesthetic and tradition, which have contributed greatly to the theoretical underpinnings of this project.

Writing spaces, art installations, live performances. AMK acknowledges several spaces, art installations and live performances influencing the ideas presented in this study including sites where notes for this manuscript were written. These include *Nick Cave:Forothermore* by Nick Cave at the Museum of Contemporary Art, Chicago (Sep 2022); *Maya: The Exhibition* at the California Science Center (Jul 2023); the Robert and Arlene Kogod Courtyard at the Smithsonian American Art Museum/National Portrait Gallery, Washington, D.C. (Jun 2012; Nov 2023; Mar and Apr 2024); *i/o – The Tour*, concert performed by Peter Gabriel at the Kia Forum, Inglewood, California (Oct 2023); *Jennifer Guidi:And so it is* by Jennifer Guidi at the Orange County Museum of Art, Costa Mesa, California (Dec 2023); the Zen Court at the Japanese Garden, The Huntington Library and Botanic Gardens, San Marino, California (Feb 2024); *Where We Belong*, a play performed by Madeline Sayet at the Folger Theatre at the Folger Shakespeare Library, Washington, D.C. (Mar 2024); the Japanese Friendship Garden of Phoenix, Phoenix, Arizona (Jun 2024), *Eno*, a generative documentary directed by Gary Hustwit, screened at the Texas Theatre, Dallas, Texas (Jul 2024), and the collections at the Dallas Museum of Art (Jul 2024) and the Museum of Fine Arts, Boston (Jul 2024).

Trademarks and credits. *BM4.0* atlas maps were modified and/or reproduced with permission under the conditions outlined by a Creative Commons BY-NC 4.0 license. Adobe Illustrator and Adobe Photoshop are either registered trademarks or trademarks of Adobe in the United States and/or other countries.

Resource sharing: Digital maps are forthcoming as part of revised drafts of this study.

References

Abercrombie, M. (1946). Estimation of nuclear population from microtome sections. *The Anatomical Record*, *94*, 239–247. https://doi.org/10.1002/ar.1090940210

Abrahamson, E. E. & Moore, R. Y. (2001). The posterior hypothalamic area: chemoarchitecture and afferent connections. *Brain Research*, *889*, 1–22. https://doi.org/10.1016/s0006-8993(00)03015-8

Adrain, R. (1808). Research concerning the probabilities of the errors which happen in making observations, *Analyst, 1*, 93–109.

Agnati, L. F., Fuxe, K., Calza, L., Giardino, L., Zini, I., Toffano, G., Goldstein, M., *et al*., (1985). Morphometric and microdensitometrical studies on monoaminergic and peptidergic neurons in the aging brain, In: *Quantitative neuroanatomy in transmitter research* (L. F. Agnati; K. Fuxe, eds.), Wenner-Gren International Symposium series, volume 42, pp. 91–112. New York: Plenum Press.

Agostinelli, L. J., Nham, T. A., Zobel, M., Michaels, J. M., & Khan, A. M. (2010). Distribution of neurons expressing nitric oxide synthase, acetylcholinesterase, and hypocretin/orexin in the rat hypothalamus: Relation to basal and stimulated levels of Fos and phospho-ERK. [Program #191.11]. *2010 Abstract Viewer/Itinerary Planner*. San Diego, CA: Society for Neuroscience. Online.

Agostinelli, L. J., & Khan AM. (2011). Distribution of neurons expressing nitric oxide synthase, acetylcholinesterase, and hypocretin/orexin in the rat hypothalamus: relation to basal and stimulated levels of Fos and phospho-ERK. *13th Annual Undergraduate Symposium for Scholarly and Creative Work*, University of Southern California, held on 13 April 2011.

Alpár, A., Benevento, M., Romanov, R. A., Hökfelt, T., & Harkany, T. (2019). Hypothalamic cell diversity: non-neuronal codes for long-distance volume transmission by neuropeptides. *Current Opinion in Neurobiology*, *56*, 16–23. https://doi.org/10.1016/j.conb.2018.10.012

Ambach, G., & Palkovits, M. (1982). Blood supply of the hypothalamus. VII. The lateral hypothalamus (medial forebrain bundle). *Acta Biologica Academiae Scientiarum Hungaricae*, *33*(2–3), 127–137.

Armstrong, W. E., & Stern, J. E. (1997). Electrophysiological and morphological characteristics of neurons in the perinuclear zone of supraoptic nucleus. *Journal of Neurophysiology*, *78*, 2427–2437. https://doi.org/10.1152/jn.1997.78.5.2427

Arnal, A. (2022). *Region detection & segmentation of Nissl-stained rat brain tissue*. Ph.D. dissertation, The University of Texas at El Paso.

Arnal, A., Khan, A. M., & Fuentes, O. (2021). Effects of resolution and scale on segmentation of Nissl-stained rat brain tissue images via convolutional neural networks. Program No. 386.02. Presented at the *SfN Global Connectome Meeting*, held online, Jan 11–13, 2021. Washington, D.C.: Society for Neuroscience.

Argente-Arizón P., Freire-Regatillo, A., Argente, J., & Chowen, J. A. (2015). Role of non-neuronal cells in body weight and appetite control. *Frontiers in Endocrinology*, *6* (Article 42). https://doi.

org/10.3389/fendo.2015.00042

Bäck, S., Necarsulmer, J., Whitaker, L. R., Coke, L. M., Koivula, P., Heathward, E. J., *et al.,* (2019). Neuron-specific genome modification in the adult rat brain using CRISPR-Cas9 transgenic rats. *Neuron*, *102*(1), 105–119. https://doi.org/10.1016/j.neuron.2019.01.035

Banneker, B. (1793). *Banneker's almanack and ephemeris for the year of our Lord 1793*. Philadelphia, Pennsylvania: J. Crukshank.

Bargmann, C. T. & Marder, E. (2013). From the connectome to brain function. *Nature Methods*, *10*(6), 483–490. https://doi.org/10.1038/nmeth.2451

Barnes, J. A. (1978) Control areas and control points in isopleth mapping. *The American Cartographer*, *5*(1), 65–69. https://doi.org/10.1559/152304078784022935

Bedont, J. L., Newman, E. A., & Blackshaw, S. (2015). Patterning, specification, and differentiation in the developing hypothalamus. *WIREs Developmental Biology*, *4*, 445–468. https://doi.10.1002/wdev.187

Bell, J. & Bell, C. (1826) *The Anatomy and Physiology of the Human Body, 6th Edn*., 3 Vols., see Vol. 2 for nervous system (Longmans et al., London). Available online: https://archive.org/details/b24927995_0002/page/n5/mode/2up

Benozzo, D., Baron, G., Coletta, L., Chiuso, A., Gozzi, A., & Bertoldo, A. (2024). Macroscale coupling between structural and effective connectivity in the mouse brain. *Scientific Reports*, *14*, 3142. https://doi.org/10.1038/s41598-024-51613-7

Biederman, C. (1939). Work No. 3, New York, 1939, painted wood, glass, and metal rods, 33 × 27 × 3 1/4 in. (82 × 68 × 8 cm), Dallas Museum of Art, Dallas, TX, USA. Object number 2007.23. https://www.dma.org/art/collection/object/5326379

Biederman, C. (1948). *Art as the evolution of visual knowledge*. [Self-published]: Red Wing, Minnesota. Available online from the Internet Archive: https://archive.org/details/artasevolutionof0000char/mode/2up. Last accessed 16 Jun 2024.

Bjerke, I. E., Schlegel, U., Puchades, M., Bjaalie, J. G., & Leergaard, T. B. (2019). Swanson's "Brain Maps: Structure of the Rat Brain" (4th edition) spatially registered to the Waxholm Space atlas of the rat brain [Data set]. Human Brain Project Neuroinformatics Platform. https://doi.org/10.25493/486N-966

Blacktop, J.M. & Sorg, B. A. (2018). Perineuronal nets in the lateral hypothalamus regulate cue-induced reinstatement of cocaine-seeking behavior. *Neuropsychopharmacology*, *44*, 850–858. https://doi.org/10.1038/s41386-018-0212-8

Bloom, F. (1975). "The gains in brain are mainly in the stain," in *The neurosciences: paths of discovery*, eds. F. G. Worden, J. P. Swazey, and G. Adelman. Cambridge: MIT Press, 211–227.

Bota, M., & Swanson, L. W. (2010). Collating and curating neuroanatomical nomenclatures: Principles and use of the Brain Architecture Knowledge Management System (BAMS). *Frontiers in Neuroinformatics*, *4*, 3. https://doi.org/10.3389/fninf.2010.00003

Bowie, D. (1971). Andy Warhol [song recording]. Recorded at Trident Studios in London, United Kingdom. Released December 17, 1971, as Side 2, Track 2 of the album *Hunky Dory*. Performed by David Bowie. 1971, RCA Records.

Brewer, C. A. (2013). Guidelines for selecting colors for diverging schemes on maps. *The Cartographic Journal*, *33*(2), 79–86. https://doi.org/10.1179/caj.1996.33.2.79

Broberger, C., de Lecea, L., Sutcliffe, J. G., & Hökfelt, T. (1998). Hypocretin/orexin- and melanin-concentrating hormone-expressing cells form distinct populations in the rodent lateral hypothalamus: Relationship to the neuropeptide Y and agouti gene-related protein systems. *The Journal of Comparative Neurology*, *402*(4), 460–474. https://doi.org/10.1002/(SICI)1096-9861(19981228)402:4<460::AID-CNE3>3.0.CO;2-S

Brown, R. A., & Swanson, L. W. (2013). Neural Systems Language: A formal modeling language for the systematic description, unambiguous communication, and automated digital curation of neural connectivity. *The Journal of Comparative Neurology*, *521*, 2889–2906. https://doi.org/10.1002/cne.23348

Bullock, T. H. (1981). Spikeless neurones: where do we go from here? In: *Neurones without impulses: their significance for vertebrate and invertebrate nervous systems* (A. Roberts, B. M. H. Bush, eds.), pp 269–284. Cambridge: Cambridge University Press.

Burdakov, D., & Karnani, M. M. (2020). Ultra-sparse connectivity within the lateral hypothalamus. *Current Biology*, *30*(20), P4063–4070.E2. https://doi.org/10.1016/j.cub.2020.07.061

Burnett, K. A. S., Pinales, B. E., Perez, E. J., Rodarte, D., Cardona, A. M., Galvan, K. J., Hernandez, G. G., Lezama, A. C., Lorenzana, K. T., Vasquez, A., Parada, P., Paz, J. I., Rascon, J., Thomason, R., Bautista, K., Barnes, J., D'Arcy, C. E., & Khan, A. M. (2018). High spatial resolution mapping of anorexigenic neuropeptides expressed in the hypothalamus: A chemoarchitecture study in the adult male rat. Program No. 680.24. *2018 Neuroscience Meeting Planner*. San Diego, CA: Society for Neuroscience, 2018. Online.

Burns, G. A. P. C., Cheng, W.-C., Thompson, R. H., & Swanson, L. W. (2006). The NeuARt II system: a viewing tool for neuroanatomical databased on published neuroanatomical atlases. *BMC Bioinformatics*, *7*, Article 531. https://doi.org/10.1186/1471-2105-7-531

Burns, G. A. P. C., Khan, A. M., Ghandeharizadeh, S., O'Neill, M. A., & Chen, Y.-S. (2003) Tools and approaches for the construction of knowledge models from the neuroscientific literature. *Neuroinformatics*, *1*, 81–109. https://doi.org/10.1385/NI:1:1:081

Burton, C., Hammett, K., Hetfield, J., & Ulrich, L. (1986). Master of Puppets [song recording]. Recorded at Sweet Silence Studios in Copenhagen, Denmark. Released July 2, 1986, as Track 2 of the album *Master of Puppets*. Performed by Metallica. 1986, Elektra Records.

Cajal, S. R. (1912). *La fotografía de los colores. Fundamentos científicos y reglas prácticas*. Madrid: Nicolás Moya.

Casini, L., Marchetti, N., Montanucci, A. *et al.*, (2023). A human–AI collaboration workflow for archaeological sites detection. *Scientific Reports*, *13*, 8699. https://doi.org/10.1038/s41598-023-

36015-5

Chen, Y., McElvain, L. E., Tolpygo, A. S., Ferrante, D., Friedman, B., Mitra, P. P., ...Kleinfeld, D. (2019). An active texture-based digital atlas enables automated mapping of structures and markers across brains. *Nature Methods*, *16*, 341–350. https://doi.org/10.1038/s41592-019-0328-8

Choi, D. C., Furay, A. R., Evanson, N. K., Ostrander, M. M., Ulrich-Lai, Y. & Herman, J. P. (2007). Bed nucleus of the stria terminalis subregions differentially regulate hypothalamic-pituitary-adrenal axis activity: implications for the integration of limbic inputs. *The Journal of Neuroscience*, *27*(8), 2025–2034. https://doi.org/10.1523/jneurosci.4301-06.2007

Cloud, J. (2005). The case of the missing overlays: A strategy for the history of the digital transition in cartography. *Proceedings, AutoCarto 2005*. *The 15th International Research Symposium on Computer-based Cartography*. Las Vegas, Nevada, USA, March 18–25, 2005. Retrieved from https://cartogis.org/autocarto/autocarto-2005/. Last accessed 2 Oct 2024.

Comer, S. C. (2015). *The Tigua Indians of Ysleta del Sur: A Borderlands Community*. PhD dissertation, The University of Texas at El Paso.

Crisman, N. R. (1982). A theory of cartographic error and its measurement in digital databases. *Proceedings of the International Symposium on Computer-Asssisted Cartography*, pp. 159–168. 22–28 Aug 1982, Crystal City, Virginia. Available online: https://cartogis.org/docs/proceedings/archive/auto-carto-5/pdf/a-theory-of-cartographic-error-and-its-measurement-in-digital-databases.pdf. Last accessed 20 Aug 2024.

Croizier, S., Chometton, S., Fellmann, D., & Risold, P.-Y. (2014). Characterization of a mammalian prosencephalic functional plan. *Frontiers in Neuroanatomy*, *8*, 161. https://doi.org/10.3389/fnana.2014.00161

D'Angelo, E., & Jirsa, V. (2022). The quest for multiscale brain modeling. *Trends in Neurosciences, 45*(10), 777–790. https://doi.org/10.1016/j.tins.2022.06.007

D'Arcy, C. E., Martinez, A., Aranda, L. F., Cervantes, H. F. L., Chacon, L. E., Cordero, R. P., Fernandez, V., Garcia, G. A., Holguin, S., Jacquez, A., Miramontes, T. G., Montaño, B., Muñoz, P. C., Valenzuela, I. R., Yu, J. S., & Khan, A. M. (2016). Elaboration of hypothalamic chemoarchitecture of the adult male rat: A high spatial resolution mapping study of melanin-concentrating hormone, hypocretin/orexin, and calbindin immunoreactivities in multiple subjects. Program No. 453.07. *2016 Neuroscience Meeting Planner.* San Diego, CA. Society for Neuroscience, 2016. Online.

D'Arcy, C. E., Martinez, A., Khan, A. M., & Olimpo, J. T. (2019) Cognitive and non-cognitive outcomes associated with student engagement in a novel brain mapping and connectomics course-based undergraduate research experience. *Journal of Undergraduate Neuroscience Education*, *18*(1):A15–A43.

Dashti, A. E., Burns, G. A. P. C., Ghandeharizadeh, S., Jia, S., Shahabi, C., Simmons, D. M., Stone, J., & Swanson, L. W. (2001). The Neuroanatomical Rat Brain Viewer (NeuARt), In: *Computing the Brain: A Guide to Neuroinformatics* (M. A. Arbib, J. S. Grethe, eds.), pp 189–201. San Diego: Academic Press.

Deicher, S. (2024). *Piet Mondrian (1872–1944): structures in space*. Köln, Germany: Taschen.

Devlin, J. T., & Poldrack, R. A. (2007). In praise of tedious anatomy. *NeuroImage*, *37*(1), 1033–1041. https://doi.org/10.1016/j.neuroimage.2006.09.055

Dixon, O. M. (1972). Methods and progress in choropleth mapping of population density. *The Cartographic Journal*, *9*(1): 19–29. https://doi.org/10.1179/caj.1972.9.1.19

Edler, D., Bestgen, A.-K., Kuchinke, L., & Dickmann, F. (2014). Grids in topographic maps reduce distortions in the recall of learned object locations. *PLoS ONE*, *9*(5): e98148. https://doi.org/10.1371/journal.pone.0098148

Elias, C. F., Saper, C. B., Maratos-Flier, E., Tritos, N. A., Lee, C., Kelly, J., ... Elmquist, J. K. (1998). Chemically defined projections linking the mediobasal hypothalamus and the lateral hypothalamic area. *The Journal of Comparative Neurology*, *402*(4), 442–459. https://doi.org/10.1002/(SICI)1096-9861(19981228)402:4<442::AID-CNE2>3.0.CO;2-R

Elmquist, J. K., Elias, C. F., & Saper, C. B. (1999). From lesions to leptin: hypothalamic control of food intake and body weight. *Neuron*, *22*(2):221–232. https://doi.org/10.1016/s0896-6273(00)81084-3

Eno, B. (2024). Interview excerpt from the generative documentary *Eno*, dir. Gary Hustwit, screened live at the Texas Theatre, Dallas, TX, USA, July 20, 2024.

Escapita, A. C., Wells, C. E., & Khan, A. M. (2015). Chemoarchitecture of the mammalian hypothalamus: mapping of three peptidergic neuronal populations (α-MSH, nNOS, and MCH) in rat hypothalamus across multiple animals. *COURI Symposium Abstracts*, Spring 2015.

España, R. A., Baldo, B. A., Kelley, A. E., & Berridge, C. W. (2001). Wake-promoting and sleep-suppressing actions of hypocretin (orexin): Basal forebrain sites of action. *Neuroscience*, *106*(4), 699–715. https://doi.org/10.1016/s0306-4522(01)00319-0

Farriss, A., & Hutchence, M. (1990). The Stairs [song recording]. Recorded at Rhinoceros Studio 2 in Sydney, Australia, and mixed at Air Studios in London, United Kingdom. Released September 25, 1990, as Track 3 on the album *X*. Performed by INXS. 1990, Atlantic Recording Corporation (U.S. release).

Feser, C. (2019) Felder 3 (Field 3), inkjet print with hand additions in lacquer, 55 × 39 1/4 in. (140 × 100 cm), Museum of Fine Arts, Boston. Accession number 2022.1875.

Feynman, R. P. (1964). The motions of the planets around the sun [audio recording of lecture delivered at the California Institute of Technology on March 13, 1964]. On compact disc accompanying text by D. L. Goodstein and J. R. Goodstein, (1996). *Feynman's lost lecture: the motion of the planets around the sun*. New York: Norton.

Fitzgerald, D., & Callard, F. (2015). Social science and neuroscience beyond interdisciplinarity: experimental entanglements. *Theory, Culture & Society*, *32*(1), 3–32. https://doi.org/10.1177/0263276414537319

Flores, C., Arvanitogiannis, & Shizgal, P. (1997). Fos-like immunoreactivity in forebrain regions

following self-stimulation of the lateral hypothalamus and the ventral tegmental area. *Behavioural Brain Research*, *87*, 239–251. https://doi.org/10.1016/s0166-4328(97)02288-2

Flores-Robles, G., Negishi, K., Pacheco, R. A., Enriquez, A., Acevedo, E., Avila, B., Dominguez, E., Hernandez, E. E., Medina, A., Mejia, E., Novoa, M. A., Provencio, A. T., Renteria, F. D., Sifuentes, E., Tellez, Y., & Khan, A. M. (2017). Hypothalamic chemoarchitecture of the adult male rat: Further elaboration of results from a high spatial resolution longitudinal mapping study. Program No. 604.03. *2017 Neuroscience Meeting Planner*. Washington, DC. Society for Neuroscience, 2017. Online.

Foa'i, O., & Miranda, L.-M. (2016). We know the way [song recording]. Released November 18, 2016, as Track 5 on the album *Moana (Original Motion Picture Soundtrack)*. Performed by Opetaia Foa'i and Lin-Manuel Miranda. 2016, Walt Disney Records.

Forbes, E. G. (1966). Tobias Mayer's lunar tables. *Annals of Science*, *22*, 105–116. https://doi.org/10.1080/00033796600203075

Ford, B. J. (1985). *Single lens: the story of the simple microscope*. New York: Harper & Row.

Fordham, J. (2023). An eye for the cameras: Richard Edlund, ASC. *American Cinematographer*, *104*(8). Available online: https://theasc.com/articles/eye-for-cameras-richard-edlund. Last accessed 20 Jan 2024.

Frahm, K. A., Schow, M. J., & Tobet, S. A. (2012). The vasculature within the paraventricular nucleus of the hypothalamus in mice varies as a function of development, subnuclear location, and GABA signaling. *Hormone and Metabolic Research*, *44*, 619–624. https://doi.org/10.1055/s-0032-1304624

Fürth, D., Vaissière, T., Tzortzi, O., Xuan, Y., Märtin, A., Lazaridis, I., *et al*., (2018). An interactive framework for whole-brain maps at cellular resolution. *Nature Neuroscience*, *21*, 139–149. https://doi.org/10.1038/s41593-017-0027-7

Gabriel, P. (2023a). Panopticom [song recording]. Recorded at Real World Studios in Wiltshire and the Beehive in London, United Kingdom. Released January 6, 2023, as the first single from the album *I/O*. Performed by Peter Gabriel. 2023, Republic (US/Canada label).

Gabriel, P. (2023b). "Panopticom: the univerally accessible data globe", in: *i/o: Peter Gabriel, The Tour 2023*. Tour book, p. 42. RealWorld Studios.

Gallistel, C. R., Leon, M., Lim, B. T., Sim, J. C., & Waraczynski, M. (1996). Destruction of the medial forebrain bundle caudal to the site of stimulation reduces rewarding efficacy but destruction rostrally does not. *Behavioral Neuroscience*, *110*(4), 766–790. https://doi.org/10.1037/0735-7044.110.4.766

Gaser, C., Schmidt, S., Metzler, M., Herrmann, K.-H., Krumbein, I., *et al.*, (2012). Deformation-based brain morphometry in rats. *NeuroImage*, *63*(1), 47–53. https://doi.org/10.1016/j.neuroimage.2012.06.066

Gauss, C. F. (1809) Theoria motvs corporvm coelestivm in sectionibvs conicis solem ambientivm. (Hamburg: I. H. Besser). Full text available online:

https://archive.org/details/theoriamotuscor00gausgoog/page/n4/mode/2up

Gauss, C. F. (1857) Theory of the motion of the heavenly bodies moving about the sun in conic sections: A translation of Gauss's "Theoria Motus". Translated from the Latin by Davis, C. H. (Boston: Little, Brown & Co.). Available online at the Biodiversity Heritage Library: https://www.biodiversitylibrary.org/item/58729

Geerling, J. C., Mettenleiter, T. C., & Loewy, A. D. (2003). Orexin neurons project to diverse sympathetic outflow systems. *Neuroscience*, *122*, 541–550. https://doi.org/10.1016/j.neuroscience.2003.07.008

Geser, F., Haybaeck, J., & Yilmazer-Hanke, D.(2022). "Dendroarchitectonics": From Santiago Ramón y Cajal to Enrique Ramón-Moliner or vice versa? *Neuological Sciences*, *43*, 5807–5820. https://doi.org/10.1007/s10072-022-06151-3

Gingerich, O. (2017). The role of ephemerides from Ptolemy to Kepler, In: *The science of time 2016* (E. F. Arias et al., eds.), (*Astrophysics and Space Science Proceedings*, vol. 50), pp. 17–24. https://doi.org/10.1007/978-3-319-59909-0_3

Goaillard, J. M., Moubarak, E., Tapia, M., & Tell, F. (2020). Diversity of axonal and dendritic contributions to neuronal output. *Frontiers in Cellular Neuroscience*, *13*, 570. https://doi.org/10.3389/fncel.2019.00570

Grachev, I. D., Berdichevsky, D., Rauch, S. L., Heckers, S., Kennedy, D. N., Caviness, V. S., & Alpert, N. M. (1999). A method for assessing the accuracy of intersubject registration of the human brain using anatomic landmarks. *NeuroImage*, *9*, 250–268. https://doi.org/10.1006/nimg.1998.0397

Gray, A. G., & Moore, A. W. (2003). Nonparametric density estimation: toward computational tractability. *Proceedings of the 2003 SIAM International Conference on Data Mining (SDM)*, 203–211. https://doi.org/10.1137/1.9781611972733.19

Guidolin, D., Tortorella, C., Marcoli, M., Maura, G., & Agnati, L. F. (2022). Intercellular communication in the central nervous system as deduced by chemical neuroanatomy and quantitative analysis of images: Impact on neuropharmacology. *International Journal of Molecular Sciences*, *23*, 5805. https://doi.org/10.3390/ijms23105805

Guzman, R., Peru, E., Navarro, V., Negishi, K., & Khan AM. (2019). Distributions of axons immunoreactive for α-melanocyte stimulating hormone and neurons immunoreactive for neuronal nitric oxide synthase in the hypothalamus of the adult male rat. *COURI Summer 2019 Symposium Abstracts*, ID=128, The University of Texas at El Paso, El Paso, Texas, USA, 3 August 2019.

Hahn, J. D. (2010). Comparison of melanin-concentrating hormone and hypocretin/orexin peptide expression patterns in a current parceling scheme of the lateral hypothalamic zone. *Neuroscience Letters*, *468*(1), 12–17. https://www.doi.org/10.1016/j.neulet.2009.10.047

Hatton, G. I. (1984). Hypothalamic neurobiology, In: *Brain slices* (R. Dingledine, ed.), pp. 341–374. New York: Plenum Press. https://doi.org/10.1007/978-1-4684-4583-1_14

Hill, H. (1991). *A portfolio of lunar drawings*. Cambridge: Cambridge University Press.

His, W. (1893) Ueber das frontale Ende des Gehirnrohres. *Archiv für Anatomie und Entwickelungsgeschichte*, [no volume indicated] pp. 157–171.

Hodgson, D. O. (2016). Digital color palettes: the essential concepts. Blog entry at teklibri.com. https://www.teklibri.com/digital-color-palettes-tutorial/. Posted on 28 Oct 2016; last accessed 14 Jun 2024.

Hofstadter, D. R. (1979). *Gödel, Escher, Bach: an eternal golden braid*. New York: Basic Books.

Horsley, V., & Clarke, R. H. (1909). The structure and functions of the cerebellum examined by a new method. *Brain*, *31*(1), 45–124. https://doi.org/10.1093/brain/31.1.45

Huber, G. C. (1915/2018). The development of the albino rat, *Mus norvegicus albinus*. *Journal of Morphology*, *26*(2). Reprinted as *Memoirs of the Wistar Institute of Anatomy and Biology, No. 5*, pp. 3–142. Forgotton Books, Ltd., London, UK.

Ingram, W. R. (1939). The hypothalamus: a review of the experimental data. *Psychosomatic Medicine*, *1*, 48–91.

Iwasaki, M., Lefevre, A., Althammer, F., Creusot, E. C., Lapies, O., Petitjean, H., *et al*. (2023). An analgesic pathway from parvocellular oxytocin neurons to the periaqueductal gray in rats. *Nature Communications*, *14*(1), 1066. https://doi.org/10.1038/s41467-023-36641-7

Jansen, A. S. P., Nguyen, X. V., Karpitskiy, V., Mettenleiter, T. C., & Loewy, A. D. (1995). Central command neurons of the sympathetic nervous system: Basis of the fight-or-flight response. *Science*, *270*, 644–646. https://doi.org/10.1126/science.270.5236.644

Kang, Y. (2020). *Integrating artificial intelligence in cartography: Using deep learning for map style transfer and map generalization*. Master of Science thesis, Department of Geography, University of Wisconsin-Madison.

Kang, Y., Gao, S., & Roth, R. E. (2024). Artificial intelligence studies in cartography: a review and synthesis of methods, applications, and ethics. *Cartography and Geographic Information Science*, pp. 1–32. https://doi.org/10.1080/15230406.2023.2295943

Kasdan, L. (director) (2022). *Light & Magic* (Season 1, Episode 3: Just Think About It). Docuseries. Lucasfilm, Ltd. [For a discussion of optical printing of film, see 25:24 – 28:02].

Katz, P. S. (1999). What are we talking about? Modes of neuronal communication, In: *Beyond neurotransmission: Neuromodulation and its importance for information processing* (P.S. Katz, ed.), pp. 1–28. Oxford: Oxford University Press.

Keane, M. P. (2004). *The art of setting stones, and other writings from the Japanese garden*. Berkeley, CA: Stone Bridge Press.

Kelly, A. B., & Watts, A. G. (1998). The region of the pontine parabrachial nucleus is a major target of dehydration-sensitive CRH neurons in the rat lateral hypothalamic area. *The Journal of Comparative Neurology, 394*(1), 48–63. https://doi.org/10.1002/(SICI)1096-9861(19980427)394:1<48::AID-CNE5>3.0.CO;2-H

Kennedy, E. S. (1956). A survey of Islamic astronomical tables. *Transactions of the American Philosophical Society*, *46*(2), 123–177. Available online at the JSTOR Digital Library: https://www.jstor.org/stable/1005726. Last accessed 10 Jun 2021.

Kerman, I. A., Bernard, R., Rosenthal, D., Beals, J., Akil, H., & Watson, S. J. (2007). Distinct populations of presympathetic-premotor neurons express orexin or melanin-concentrating hormone in the rat lateral hypothalamus. *The Journal of Comparative Neurology*, *505*, 586–601. https://doi.org/ 10.1002/cne.21511

Khan, A. M. (2013). Controlling feeding behavior by chemical or gene-directed targeting in the brain: What's so spatial about out methods? *Frontiers in Neuroscience*, *7*, 1–49. http://dx.doi.org/10.3389/fnins.2013.00182

Khan, A. M., D'Arcy, C. E., & Olimpo J. T. (2021) A historical perspective on training students to create standardized maps of novel brain structure: Newly-uncovered resonances between past and present research-based neuroanatomy curricula. *Neuroscience Letters*, *759*:136052. https://doi.org/10.1016/j.neulet.2021.136052

Khan, A. M., Grant, A. H., Martinez, A., Burns, G. A. P. C., Thatcher, B. S., Anekonda, V. T., Thompson, B. W., Roberts, Z. S., Moralejo, D. H., Blevins, J. E. (2018a) Mapping molecular datasets back to the brain regions they are extracted from: Remembering the native countries of hypothalamic expatriates and refugees. *Advances in Neurobiology*, *21*:101–193. https://doi.org/10.1007/978-3-319-94593-4_6

Khan, A. M., Perez, J. G., Wells, C. E., & Fuentes, O. (2018b). Computer vision evidence supporting craniometric alignment of rat brain atlases to streamline expert-guided, first-order migration of hypothalamic spatial datasets related to behavioral control. *Frontiers in Systems Neuroscience*, *12*, 7. https://doi.org/10.3389/fnsys.2018.00007

Khan, A. M., Ponzio, T. A., Sanchez-Watts, G., Stanley, B. G., Hatton, G. I., & Watts, A. G. (2007). Catecholaminergic control of mitogen-activated protein kinase signaling in paraventricular neuroendocrine neurons *in vivo* and *in vitro*: a proposed role during glycemic challenges. *The Journal of Neuroscience*, *27*(27), 7344–7360. https://doi.org/10.1523/jneurosci.0873-07.2007

Khan, A. M., Stanley, B. G., Bozzetti, L., Chin, C., Stivers, C., & Currás-Collazo, M. C. (2000). *N*-methyl-D-aspartate receptor subunit NR2B is widely expressed throughout the diencephalon: An immunohistochemical study. *The Journal of Comparative Neurology*, *428*, 428–449. https://doi.org/10.1002/1096-9861(20001218)428:3<428::AID-CNE4>3.0.CO;2-B

Kim, D. W., Washington, P. W., Wang, Z. Q., Lin, S. H., Sun, C., Ismail, B. T., *et al*., (2020). The cellular and molecular landscape of hypothalamic patterning and differentiation from embryonic to late postnatal development. *Nature Communications*, *11*, 4360. https://doi.org/10.1038/s41467-020-18231-z

King, D. A. & Saliba, G. (eds.) (1987). From deferent to equant: A volume of studies in the history of science in the ancient and medieval Near East in honor of E. S. Kennedy. *Annals of the New York Academy of Sciences*, vol. 500. The New York Academy of Sciences, New York.

King, H. D. (1910). The effects of various fixatives on the brain of the albino rat. *The Anatomical*

Record, *4*(6), 213–244. https://doi.org/10.1002/ar.1090040602

Kleven, H., Bjerke, I., Clascá, F., Groenewegen, H., Bjaalie, J. G., & Leergaard, T. (2023a). Waxholm Space atlas of the rat brain: A 3D atlas supporting data analysis and integration. *Nature Methods*, *20*, 1822–1829. https://doi.org/10.1038/s41592-023-02034-3

Kleven, H., Reiten, I., Blixhavn, C. H., Schlegel, U., Øvsthus, M., Papp, E. A., *et al.*, (2023b). A neuroscientists's guide to using murine brain atlases for efficient analysis and transparent reporting. *Frontiers in Neuroinformatics*, *17*, 1154080. https://doi.org/10.3389/fninf.2023.1154080

Korzybski, A. (1921). *Manhood of humanity: the science and art of human engineering*. New York: E. P. Dutton & Co. Available online at Project Gutenberg. Last accessed on 16 Jun 2024.

Krieg, W. J. S. (1932). The hypothalamus of the albino rat. *The Journal of Comparative Neurology*, *55*(1), 19–89. https://doi.org/10.1002/cne.900550104

Krieg, W. J. S. (1975). *Stereotaxy*. Evanston, IL, USA: Brain Books.

Kosse, C., & Burdakov, D. (2018). Fast and slow oscillations recruit molecularly distinct subnetworks of lateral hypothalamic neurons *in situ*. *eNeuro*, *5*(1) e0012-18.2018 1–9. http://dx.doi.org/10.1523/ENEURO.0012-18.2018

Krisch, B. (1980). Immunocytochemistry of neuroendocrine systems: vasopressin, somatostatin, luliberin. *Progress in Histochemistry and Cytochemistry*, *13*(2), 1–163. https://doi/org/10.1016/s0079-6336(80)80001-5

Kuhlenbeck, H. (1927) *Vorlesungen über das Zentralnervensystem der Wirbeltiere* (Fischer, Jena).

Kundu, S., Sair, H., Sherr, E. H., Mukherjee, P., & Rohde, G. K. (2024). Discovering the gene-brain-behavior link in autism via generative machine learning. *Science Advances*, *10*(24). https://doi.org/doi/10.1126/sciadv.adl5307

Langran, G. & Chrisman, N. R. (1988). A framework for temporal geographic information. *Cartographica*, *25*(3), 1–14. https://doi.org/10.3138/K877-7273-2238-5Q6V

Langran, G. (1993). *Time in Geographic Information Systems*. London: Taylor & Francis.

Larrivée, B., Freitas, C., Suchting, S., Brunet, I., & Eichmann, A. (2009). Guidance of vascular development: lessons from the nervous system. *Circulation Research*, *104*(4), 428–441. https://doi.org/10.1161/CIRCRESAHA.108.188144

Leak, R. K. & Moore, R. Y. (2001). Topographic organization of suprachiasmatic nucleus projection neurons. *The Journal of Comparative Neurology*, *433*, 312–334. https://doi.org/10.1002/cne.1142

Leergaard, T. B., & Bjaalie, J. G. (2022). Atlas-based data integration for mapping the connections and architecture of the brain. *Science*, *378*(6619), 488–492. https://doi.org.10.1126/science.abg2594

Levinthal, C. & Ware, R. (1972). Three dimensional reconstruction from serial sections. *Nature*, *236*, 207–210. https://doi.org/10.1038/236207a0

Lidwell, W., Hoden, K., & Butler, J. (2003). *Universal principles of design*. Beverly, MA: Rockport Publishers.

Lima, M. (2011). *Visual complexity: mapping patterns of information*. New York: Princeton Architectural Press.

Lingley, A. J., Bowdridge, J. C., Farivar, R., & Duffy, K. R. (2018). Mapping of neuron soma size as an effective approach to delineate differences between neuronal populations. *Journal of Neuroscience Methods*, *304*, 126–135. https://doi.org/10.1016/j.jneumeth.2018.04.018

Liu, Z., Brown, A., Fisher, D., Wu, Y., Warren, J., & Cui, X. (2016). Tissue specific expression of Cre in rat tyrosine hydroxylase and dopamine active transporter-positive neurons. *PLoS ONE*, *11*, e0149379. https://doi.org/10.1371/journal.pone.0149379

Lucas, G. (Director). (1980). *Star Wars – Episode V: The Empire Strikes Back*. [Motion Picture]. United States: Twentieth Century Fox.

Ma, Y., Zhang, L., & Huang, X. (2017). Building Cre knockin rat lines using CRISPR/Cas9, In: *Site-specific recombinases: methods and protocols* (N. Eroshenko, ed.), *Methods in Molecular Biology*, *1642*. Springer Science+Business Media. https://doi.org/10.1007/978-1-4939-7169-5_3

MacEachren, A. M. (1982). Choropleth map accuracy: Characteristics of the data. *Proceedings of the International Symposium on Computer-Asssisted Cartography*, pp. 499–507. 22–28 Aug 1982, Crystal City, Virginia. Available online: https://cartogis.org/docs/proceedings/archive/auto-carto-5/pdf/choropleth-map-accuracy-characteristics-of-the-data.pdf. Last accessed 20 Aug 2024.

MacEachren, A. M. (1985). Accuracy of thematic maps: Implications of choropleth symbolization. *Cartographica*, *22*(1), 38–58. https://doi.org/10.3138/Y481-6J14-8802-G755

Mackay, J. R. (1951). Some problems and techniques in isopleth mapping. *Economic Geography*, *27*(1), 1–9. https://doi.org/10.2307/141806

Magalhães, S. V. G., Andrade, M. V. A., Franklin, W. R., & Li, W. (2015). Fast exact parallel map overlay using a two-level uniform grid. *AGM SIGSPATIAL International Workshop on Analytics for Big Geospatial Data*, Seattle, WA, USA. https://doi.org/10.1145.2835185.2835188

Martinez, A., Barraza Escudero, L. M., Castro, D., Chavez, S. A., Coronado, M., Gallegos, S., Pineda Sanchez, A., Ruiz, M. S. P., Ruiz, V. G., Negishi, K., & Khan, A. M. (2018). Hypothalamic chemoarchitecture of the adult male rat: High spatial resolution mapping of copeptin, LIM homeobox 6, and melanin-concentrating hormone. Program No. 680.23. *2018 Neuroscience Meeting Planner.* San Diego, CA: Society for Neuroscience, 2018. Online.

Martinez, A., Navarro, V. I., Arias, K., Barnett, J., Carreon, A., Castaneda, B., Flores, M., Magadan, J., Heredia, D., Hooper, J., Lopez, T., Lozano, A., Mendez, S., Mercer, N., Munoz, A., Rosario Mojica, L., Sanchez, R., Sierra, K., Sotelo, D., Stevens, X., Toccoli, A., Verma, Y., Vizcarra, H., & Khan, A. M. (2019). The Hypothalamic Chemoarchitecture Project, Year 5: High-spatial resolution atlas-based mapping of neuronal populations expressing melanin-concentrating hormone, hypocretin/orexin, and calbindin in the hypothalamus of the adult male rat. Program No. 683.18. *2019 Neuroscience Meeting Planner*. Chicago, IL: Society for Neuroscience, 2019.

Online.

Martínez, M., Espinoza, V. E., Garcia, V., Da Silva, I. E., Carcoba, L. M., Uribe, K., *et al*. (2023). Withdrawal from repeated nicotine vapor exposure increases somatic signs of physical dependence, anxiety-like behavior, and brain reward thresholds in adult male rats. *Neuropharmacology, 240*, 1096812. https://doi.org/10.1016/j.neuropharm.2023.109681

McGranaghan, M. (1996). An experiment with choropleth maps on a monochrome LCD panel, In: *Cartographic design: theoretical and practical perspectives* (C. H. Wood, C. P. Keller, eds.), pp. 177–190. Chichester: John Wiley & Sons.

Mirzadeh, Z., Alonge, K. M., Cabrales, E., Herranz-Pérez, V., Scarlett, J. M., Brown, J. M., *et al.*, (2019). Perineuronal net formation during the critical period for neuronal maturation in the hypothalamic arcuate nucleus. *Nature Metabolism*, *1*, 212–221. https://doi.org/10.1038/s42255-018-0029-0

Mitra, P. P. (2014). The circuit architecture of whole brains at the mesoscopic scale. *Neuron*, *83*, 1273–1283. http://dx.doi.org/10.1016/j.neuron.2014.08.055

Mondrian, P. (1987). *The new art – the new life: the collected writings of Piet Mondrian* (edited and translated by H. Holtzman, M. S. James), London: Thames & Hudson.

Myers, R. D. (1974). *Handbook of drug and chemical stimulation of the brain*. New York, NY: Von Nostrand Reinhold Co.

Nauta, W. J. H., & Haymaker, W. (1969). Hypothalamic nuclei and fiber connections. In, *The Hypothalamus* (W. Haymaker, E. Anderson, W. J. H. Nauta, eds.), pp. 136–209. Springfield, IL: Charles Thomas.

Navarro, V. I. (2020). *An analysis and representation in an atlas reference space of putative appositions from neurons expressing alpha-melanocyte stimulating hormone onto neurons expressing hypocretin/orexin or melanin concentrating hormone.* Master's Thesis, Department of Biological Sciences, The University of Texas at El Paso.

Navarro, V. I., Peru, E., Negishi, K., Ortega, M., & Khan, A. M. (2019). Distributions of immunoreactivities for hypocretin/orexin and neuronal nitric oxide synthase in the male rat hypothalamus: An analysis and representation in an atlas reference space. Program No. 149.18. *2019 Neuroscience Meeting Planner*. Chicago, IL: Society for Neuroscience, 2019. Online.

Negishi, K., & Khan, A. M. (2019). The contribution of axonal projections from infralimbic area neuronal populations to the medial forebrain bundle: analysis of morphology and interactions with hypocretin/orexin neurons in the rat. Program No. 149.24. *2019 Neuroscience Meeting Planner*. Chicago, IL: Society for Neuroscience, 2019. Online.

Nham, T., Khan, A. M. (2009a). Novel co-localization of phospho-ERK1/2 with the hypocretin/orexin system of the lateral hypothalamic area (LHA). *11th Annual Undergraduate Symposium for Scholarly and Creative Work*, University of Southern California, held on 15 April 2009.

Nham, T., Khan, A. M. (2009b). Identification of a novel population of neurons displaying

immunoreactive phosphorylated MAP kinases in the lateral hypothalamic area: histochemical relationship to the hypocretin/orexin system. [Program #866.16]. *2009 Abstract Viewer/Itinerary Planner*. Chicago, IL: Society for Neuroscience. Online.

Nieuwenhuys, R. (1998). Structure and organization of centres, In: (Nieuwenhuys, R. et al., eds.) *The Central Nervous System of Vertebrates, Volume 1*, pp. 25 ff. Berlin: Springer.

Nissl, F. (1913). Die grosshirnanteile des kaninchens. *Archiv für Psychiatrie und Nervenkrankheiten*, *52*, 867–953. https://doi.org/10.1007/BF02160485

Noble, E. E., Hahn, J. D., Konanur, V. R., Hsu, T. M., Page, S. J., Cortella, A. M., *et al.*, (2018). Control of feeding behavior by cerebral ventricular volume transmission of melanin-concentrating hormone. *Cell Metabolism*, *28*, 55–68. https://doi.org/10.1016/j.cmet.2018.05.001

Nowinski, W. L.(2023). Advances in neuroanatomy through brain atlasing. *Anatomia*, *2*(1), 28–42. https://doi.org/10.3390/anatomia2010004

Nowinski, W. L., Fang, A., Nguyen, B. T., Raphel, J. K., Jagannathan, L., Raghavan, E., *et al.*, (1997). Multiple brain atlas database and atlas-based neuroimaging system. *Computer Aided Surgery*, *2*, 42–66. https://doi.org/10.3109/10929089709149082

Nowinski, W. L., Yang, G. L., & Yeo, T. T. (2000). Computer-aided stereotactic functional neuosurgery enhanced by the use of the multiple brain atlas database. *IEEE Transactions on Medical Imaging*, *19*(1), 62–69. https://doi.org/10.1109/42.832961

Oglivie, M. B. (2007). Inbreeding, eugenics, and Helen Dean King (1869–1955). *Journal of the History of Biology*, *40*, 467–507. https://doi.org/10.1007/s10739-006-9117-1

Oguchi, T., Hayakawa, Y. S., & Wasklewicz, T. (2011). Data sources, In: *Geomorphological mapping: methods and applications (Developments in Earth surface processes, vol. 15)*, (M. J. Smith, P. Paron, J. S. Griffiths, eds.), pp 189–224. Amsterdam: Elsevier. https://doi.org/10.1016/B978-0-444-53446-0.00007-0

Papp, E., Leergaard, T. B., Calabrese,E., Johnson, G. A., & Bjaalie, J. G. (2014). Waxholm Space atlas of the Sprague Dawley rat brain. *NeuroImage*, *97*, 374–386. https://doi.org/10.1016/j.neuroimage.2014.04.001

Papp, E., Leergaard, T. B., Calabrese, E., Johnson, G. A., & Bjaalie, J. G. (2015). Addendum to "Waxholm Space atlas of the Sprague Dawley rat brain" [*NeuroImage 97* (2014) 374-386]. *Neuroimage*, *105*, 561–562. https://doi.org/10.1016/j.neuroimage.2014.10.017

Paxinos, G. & Watson, C. (1986). *The rat brain in stereotaxic coordinates, 2nd edition*. San Diego: Academic Press.

Paxinos, G., Watson, C., Carrive, P., Kirkcaldie, M., & Ashwell, K. W. S. (2009). *Chemoarchitectonic atlas of the rat brain, 2nd ed*. Elsevier, Amsterdam.

Paxinos, G., Kassem, M. S., Kirkcaldie, M., & Carrive, P. (2022). *Chemoarchitectonic atlas of the rat brain, 3rd ed*. Elsevier, London.

Pennington, K., Wells, C. E., & Khan A. M. (2014). Chemoarchitecture of the mammalian hypothalamus: Mapping of three peptidergic neuronal populations (α-MSH, nNOS, and MCH) in the lateral hypothalamic area and surrounding regions. *COURI Symposium Abstracts*, Spring 2014, The University of Texas at El Paso.

Perez, J., Fuentes, O., & Khan, A. M. (2018). Automatic derivation of atlas plate correspondences between rat brain atlases using feature-based matching and dynamic programming. Program No. 680.22. *2018 Neuroscience Meeting Planner*. San Diego, CA: Society for Neuroscience, 2018. Online.

Peru, E. (2020). *Distributions of axons immunoreactive for alpha-melanocyte-stimulating hormone and neurons immunoreactive for neuronal nitric oxide synthase in the hypothalamus of the adult male rat: An analysis of interactions and their representation in an atlas reference space.* Doctoral Dissertation, Department of Biological Sciences, The University of Texas at El Paso.

Peru, E., Navarro, V. I., Negishi, K., Guzman, R., & Khan, A. M. (2019). Distributions of axons immunoreactive for α-melanocyte stimulating hormone and neurons immunoreactive for neuronal nitric oxide synthase in the hypothalamus of the adult male rat: An analysis of interactions and their representation in an atlas reference space. Program No. 149.23. *2019 Neuroscience Meeting Planner*. Chicago, IL: Society for Neuroscience, 2019. Online.

Pillsbury, G. T. (2006). *Damage incorporated: Metallica and the production of musical identity*. New York: Routledge.

Pinales, B. E., Dominguez, N., & Khan, A. M. (2012). Chemoarchitecture of the lateral hypothalamic area: Contiguous mapping and distribution of six biomarkers in the adult male rat. COURI Symposium Abstracts, Spring 2012. Paper 44.

Pinales, B. E., Rojas, P., Dominguez, N., Wells, C. E., & Khan, A. M. (2013a). Chemoarchitecture of the lateral hypothalamic area: determinations of forebrain and hindbrain contributions of the Neuropeptide Y system. *COURI Symposium Abstracts*, Spring 2013, The University of Texas at El Paso.

Pinales, B. E., Lean, G. A., Wells, C. E., Silva, N. D., Walker, E. M., Rojas, P., Dominguez, N., Martinez, A., Thompson, R. H., & Khan, A. M. (2013b). The Hypothalamic Chemoarchitecture Project: High resolution mapping of neuronal populations involved in pre-autonomic, neuroendocrine, and feeding control. Poster P301. *21st Annual Meeting of the Society for the Study of Ingestive Behavior (SSIB)*; New Orleans, LA; Jul 30–Aug 3, 2013.

Pinales, B. E., Wells, C. E., Pennington, K., & Khan, A. M. (2014). Identifying feeding control circuits in the brain by phenotyping, imaging and mapping the neurons of the lateral hypothalamic area in the adult rat brain. *2014 Annual Biomedical Research Conference for Minority Students (ABRCMS)*, San Antonio, Texas; Nov 12–15, 2014.

Puelles, L., & Rubenstein, J. L. R. (2015). A new scenario of hypothalamic organization: rationale of new hypotheses introduced in the updated prosomeric model. *Frontiers in Neuroanatomy*, *9*, 27. https://doi.org/10.3389/fnana.2015.00027

Quintana, M. L., Navarro, V. I., Balivada, S., & Khan, A. M. (2024). Evaluating suitable proxies for

Nissl staining to identify rat hypothalamic cytoarchitecture in light sheet fluorescent microscopy: the region-defining ability of Neuronal Nuclei (NeuN) in 3-D. 2024 Annual Meeting of the Society for Neuroscience, Chicago, IL, Oct 5–9.

Radley, J. J., Arias, C. M., & Sawchenko, P. E. (2006). Regional differentiation of the medial prefrontal cortex in adaptive responses to acute emotional stress. *The Journal of Neuroscience*, *26*(50), 12967–12976. https://doi.org/10.1523/jneurosci.4297-06.2006

Rámon-Moliner, E. (1969). The leptodendritic neuron: its distribution and significance. In: Petras, J. M., Noback, C. R. (eds.), Comparative and evolutionary aspects of the vertebrate central nervous system. *Annals of the New York Academy of Sciences*, *167*:65–70.

Ramsdale, J. D., *et al*., (2017). Grid-based mapping: A method for rapidly determining the spatial distributions of small features over very large areas. *Planetary and Space Science*, *140*, 49–61. https://doi.org/10.1016/j.pss.2017.04.00

Rigaux, P., Scholl, M., & Voisard, A. (2002). *Spatial databases with application to GIS*. San Francisco: Morgan Kaufmann Publishers/Elsevier. https://doi.org/10.1016/B978-1-55860-588-6.X5000-3

Riviére, D., Leprince, Y., Labra, N., Vindas, N., Foubet, O., Cagna, B., *et al.*, (2022). Browsing multiple subjects when the atlas adaptation cannot be achieved *via* a warping strategy. *Frontiers in Neuroinformatics*, *16*, Article 803934. https://doi.org/10.3389/fninf.2022.803934

Rotman, D., Procita, K., Hansen, D., Parr, C. S., & Preece, J. (2012). Supporting content curation communities: The case for the Encyclopedia of Life. *Journal of the American Society for Informationn Science and Technology*, *63*(6), 1092–1107. https://doi.org/10.1002/asi.22633

Roy, R. K., Althammer, F., Seymour, A. J., Du, W., Hamm, J. P., Filosa, J. A., *et al.*, (2021). [Preprint] Inverse neurovascular coupling contributes to positive feedback excitation of vasopressin neurons in response to systemic homeostatic challenge. Available at SSRN: https://ssrn.com/abstract=3773611 or http://dx.doi.org/10.2139/ssrn.3773611

Saint-Marc, C., Davoine, P. A., & Villanova-Oliver, M. (2014). Methods for mapping volcanic events overlaid across time. *Journal of Maps*, *10*(2), 249–256. https://doi.org/10.1080/17445647.2014.888376

Santarén, J. F. (2014). Santiago Ramón y Cajal and three-dimensional cinema. *Journal of the History of the Neurosciences*, *24*(2), 111–122. https://doi.org/10.080/0964704X.2014.896410

Sayet, M. (2022). *Where we belong*. London: Bloomsbury Publishing Place.

Sayet, M. (2024). *Where we belong*, written by Madeline Sayet, directed by Mei Ann Teo. The Folger Shakespeare Library in association with the Woolly Mammoth Theatre Company. Performed at The Folger Theatre, Washington, DC, March 10, 2024.

Schmid, C. F., & MacCannell, E. H. (1955). Basic problems, techniques, and theory of isopleth mapping. *Journal of the American Statistical Association*, *50*(269), 220–239. Available online at: http://www.jstor.com/stable/2281108

Sergejeva, M., Papp, E. A., Bakker, R., Gaudnek, M. A., Okamura-Oho, Y., Boline, J., Bjaalie, J. G., & Hess, A. (2015). Anatomical landmarks for registration of experimental image data to volumetric rodent brain atlasing templates. *Journal of Neuroscience Methods*, *240*, 161–169. http://dx.doi.org/10.1016/j.jneumeth.2014.11.005

Shepherd, G. M. (1981). Introduction: the nerve impulse and the nature of nervous function. In: *Neurones without impulses: their significance for vertebrate and invertebrate nervous systems* (A. Roberts, B. M. H. Bush, eds.), pp 1–28. Cambridge: Cambridge University Press.

Silva, N. D., & Khan, A. M. (2012). Angioarchitecture of the adult rat neuroendocrine hypothalamus. *COURI Symposium Abstracts*, Spring 2012. Paper 41.

Simerly, R. B. (2015). Organization of the hypothalamus, In: *The Rat Nervous System, 4th Edition* (G. Paxinos, ed.), pp. 267–294. Amsterdam: Academic Press.

Simmons, D. M., & Swanson, L. W. (2009). Comparing histological data from different brains: Sources of error and strategies for minimizing them. *Brain Research Reviews*, *60*, 349–367. https://doi.org/10.1016/j.brainresrev.2009.02.002

Simmons, J. M., Ackermann, R. F., & Gallistel, C. R. (1998). Medial forebrain bundle lesions fail to structurally and functionally disconnect the ventral tegmental area from many ipsilateral forebrain nuclei: Implications for the neural substrate of brain stimulation reward. *The Journal of Neuroscience*, *18*(20), 8515–8533. https://doi.org/10.1523/JNEUROSCI.18-20-08515.1998

Singh, M. K., & Singh, K. K. (2021). A review of publicly available automatic brain segmentation methodologies, machine learning models, recent advancements, and their comparison. *Annals of Neurosciences*, *28*(1–2), 82–93. https://doi.org/10.1177/0972753121990175

Smith, M. J. (2011). Digital mapping: visualisation, interpretation and quantification of landforms, In: *Geomorphological mapping: methods and applications (Developments in Earth surface processes, vol. 15)*, (M. J. Smith, P. Paron, J. S. Griffiths, eds.), pp 225–251. Amsterdam: Elsevier. https://doi.org/10.1016/B978-0-444-53446-0.00008-2

Smith, R. C., & Cheeseman, P. (1986). On the representation and estimation of spatial uncertainty. *The International Journal of Robotics Resarch*, *5*(4), 56–58. https://doi.org/10.1177/027836498600500404

Sobel, D. (1995). *Longitude: the true story of a lone genius who solved the greatest scientific problem of his time*. New York: Walker.

Song, A. J., & Palmiter, R. D. (2018). Detecting and avoiding problems when using the Cre/lox system. *Trends in Genetics*, *34*(5), 333–340.

Sotelo, D., Guevara, A., Peru, E., Navarro, V. I., Toccoli, A., Szilvásy-Szabó, A., Magdolna, R. Y., Farkas, E., Guerra-Ruiz, J., Arzate, L. S., Negishi, K., Balivada, S., Arnal, A., Fekete, C., & Khan, A. M. (2020/21). Mesoscale and microscale interactions of fibers immunoreactive for α-melanocyte-stimulating hormone and hypocretin/orexin with somata immunoreactive for neuronal nitric oxide synthase: A representation in an atlas reference space of the adult male rat, with supporting ultrastructural evidence. Program No. 263.08. *Presented at the Global Connectome Meeting of the*

Society for Neuroscience. Online, Jan 11–13.

Stahl, S. (2006). The evolution of the normal distribution. *Mathematics Magazine*, *79*, 113–196. https://doi.org/10.1080/0025570X.2006.11953386

Straathof, M., Sinke, M. R. T., Roelofs, T. J. M., Blezer, E. L. A., Sarabdjitsingh, R. A., *et al*., (2020). Distinct structure-function relationships across cortical regions and connectivity scales in the rat brain. *Scientific Reports*, *10*, 56. https://doi.org/10.1038/s41598-019-56834-9

Strathern, L. (2021). Getting graded: Teaching principles of chemical synaptic transmission without action potentials. *Journal of Undergraduate Neuroscience Education*, *19*(2), R28–R30.

Streeter, G. L. (1905). The development of the cranial and spinal nerves in the occipital region of the human embryo. *American Journal of Anatomy*, *4*(1), 83–116. https://doi.org/10.1002/aja.1000040106

Sun, C., Shrivastava, A., Singh, S., & Gupta, A. (2017). Revisiting unreasonable effectiveness of data in deep learning era. *Proceedings of the IEEE International Conference on Computer Vision (ICCV)*, 2017, 843–852. *arXiv*:1707.02968. https://doi.org/10.48550/arXiv.1707.02968

Sun, M., Wong, D. W., & Kronenfeld, B. J. (2015). A classification method for choropleth maps incorporating data reliability information. *The Professional Geographer*, *67*(1), 72–83. https://doi.org/10.1080/00330124.2014.888627

Swanson, L. W. (1987). The hypothalamus, In: *Handbook of chemical neuroanatomy, vol. 5: integrated systems of the CNS, part I*, (A. Björklund, T. Hökfelt, L. W. Swanson, eds.), pp. 1–124. Amsterdam: Elsevier.

Swanson, L. W. (1992). *Brain maps: structure of the rat brain*. Elsevier, Amsterdam.

Swanson, L. W. (1993). *Brain maps: computer graphics files, professional version 1.0*, with 4 floppy diskettes (Elsevier, Amsterdam).

Swanson, L. W. (1998). *Brain maps: structure of the rat brain. A laboratory guide with printed and electronic templates for data, models and schematics, 2nd edition* [with 2 CD-ROMs] (Elsevier, Amsterdam).

Swanson, L. W. (2000). A history of neuroanatomical mapping, In: *Brain mapping: the systems* (A. W. Toga, J. C. Mazziotta, eds.), pp. 77–109. San Diego: Academic Press. https://doi.org/10.1016/b978-012692545-6/50005-2

Swanson, L. W. (2001). Interactive brain maps and atlases, In: *Computing the brain: A guide to neuroinformatics*, (M. A. Arbib, J. S. Grethe, editors), pp. 167–177. San Diego: Academic Press. Available online: https://archive.org/details/computingbraingu0000unse/page/166/mode/2up

Swanson, L. W. (2004). *Brain maps: structure of the rat brain. A laboratory guide with printed and electronic templates for data, models and schematics, 3rd edition*. Amsterdam: Elsevier, 215 pp. with CD-ROM, *Brain maps: computer graphics files 3.0*.

Swanson, L. W. (2007). Quest for the basic plan of nervous system circuitry. *Brain Research*

Reviews, *55*, 356–372. https://doi.org/10.1016/j.brainresrev.2006.12.006

Swanson, L. W. (2018). *Brain maps 4.0—Structure of the rat brain*: An open access atlas with global nervous system nomenclature ontology and flatmaps. *The Journal of Comparative Neurology*, *526*(6), 935–943. https://doi.org/10.1002/cne.24381

Swanson, L. W. & Bota, M. (2010). Foundational model of structural connectivity in the nervous system with a schema for wiring diagrams, connectome, and basic plan architecture. *Proceedings of the National Academy of Sciences of the United States of America*, *107*(48), 20610–20617. https://doi.org/10.1073/pnas.1015128107

Swanson, L. W., Sanchez-Watts, G., & Watts, A. G. (2005). Comparison of melanin-concentrating hormone and hypocretin/orexin mRNA expression patterns in a new parceling scheme of the lateral hypothalamic zone. *Neuroscience Letters*, *387*(2), 80–84. https://doi.org/10.1016/j.neulet.2005.06.066

Thompson, C. (2019). *Sea people: the puzzle of Polynesia*. New York: Harper.

Thompson, D. W. (1917). *On growth and form*. Cambridge: Cambridge University Press. Available online at the Internet Archive: https://archive.org/details/ongrowthform1917thom/page/n7/mode/2up

Toccoli, A., Arzate, L. S., Navarro, V. I., Peru, E., Sotelo, D., Szilvásy-Szabó, A., Magdolna, R. Y., Farkas, E., Guevara, A., Guerra-Ruiz, J., Negishi, K., Balivada, S., Arnal, A., Fekete, C., & Khan, A. M. (2020/21). An analysis and representation in an atlas reference space of synaptic interactions between alpha-melanocyte stimulating hormone-immunoreactive axonal fibers and neurons expressing hypocretin/orexin or melanin-concentrating hormone: light and electron microscopic evidence. Program No. 263.05. *Presented at the Global Connectome Meeting of the Society for Neuroscience*. Online, Jan 11–13.

Toga, A. W., Goo, R. L., Murphy, R., & Collins, R. C. (1984). Neuroscience application of interactive image analysis. *Optical Engineering*, *23*(2), 279–282. https://doi.org/10.1117/12.7973278

Uschakov, A., Gong, H., McGinty, D., & Szymusiak, R. (2007). Efferent projections from the median preoptic nucleus to sleep- and arousal-regulatory nuclei in the rat brain. *Neuroscience*, *150*, 104–120. https://doi.org/10.1016/j.neuroscience.2007.05.055

Van Rossum, G. (1993). An introduction to Python for UNIX/C programmers. Proceedings of the NLUUG najaarsconferentie (Netherlands local UNIX users group).

Van Rossum, G. (2009–2018). A history of Python. [Blog]. https://python-history.blogspot.com. Last accessed 21 Jun 2024.

Vasarely, V. (1959–1961). Supernovae, oil on canvas, 95¼ × 60 in. (242 × 152 cm), Tate Modern, London, Ref. T00676, https://www.tate.org.uk/art/artworks/vasarely-supernovae-t00676

Veening, J. G., Swanson, L. W., Cowan, W. M., Nieuwenhuys, R., & Geeraedts, L. M. G. (1982). The medial forebrain bundle of the rat. II. An autoradiographic study of the topography of the major descending and ascending components. *The Journal of Comparative Neurology*, *206*(1),

82–108. https://doi.org/10.1002/cne.902060107

Virtanen, P., Gommer, R., Oliphant, T. E., Haberland, M., Reddy, T., Cournapeau, D., *et al*., (2020). SciPy 1.0: fundamental algorithms for scientific computing in Python. *Nature Methods*, *17*, 261–272. https://doi.org/10.1038/s41592-019-0686-2

Weber, N. F. (2018). *Piet Mondrian's early years: The winding path to straight abstraction*. [Thesis fully internal (DIV), University of Groningen]. University of Groningen.

Weinstein, B. M. (2005). Vessels and nerves: marching to the same tune. *Cell*, *120*, 299–302. https://doi.org/10.1016/j.cell.2005.01.010

Wells, C. E. (2017). *Method & madness – advanced techniques for characterizing rat hypothalamic chemoarchitecture and for modernizing legacy data*. Doctoral Dissertation, Department of Biological Sciences, The University of Texas at El Paso.

Wells, C. E., Pinales, B. E., Farkas, E., Lean, G. A., Walker, E. M., Rojas, P., Dominguez, N., Martinez, A., Fekete, C., Thompson, R. H., & Khan AM. (2014a). The Hypothalamic Chemoarchitecture Project: High resolution mapping of neuronal populations involved in pre-autonomic, neuroendocrine, and feeding control. *2nd Annual Interdisciplinary Research Symposium at UTEP*, April 24–25, 2014. The University of Texas at El Paso.

Wells, C. E, Pennington, K., & Khan A. M. (2014b). Hypothalamic chemoarchitecture in the adult male rat: Creating canonical atlas maps for three co-visualized neuronal populations and their fiber systems from a single brain. Program No. 256.17. *2014 Neuroscience Meeting Planner*. Washington, DC: Society for Neuroscience, 2014. Online.

Wells C. E., Pinales, B. E., Lean, G. A., Farkas, E., Pennington, K., Fekete, C., Thompson, R. H., & Khan, A. M. (2015a). Creating a multi-scale chemoarchitectural reference atlas of optogenetic targets in the mammalian hypothalamus. *Keystone Symposium on Molecular and Cellular Biology, 2015 Conference on Optogenetics*, March 12–16, 2015; Denver, Colorado.

Wells, C. E., Acosta, A., Aldrete, D., Carrion, A., Castro, L., Escapita, A. C., Espinoza, E., De La Fuente, K., Garrett, A., Gomez, A., Gomez, N., Hernandez-Casner, C., Luevano, M., Lopez, A., Martinez, D., Mendoza, E., Ortega, M., Perez, M., Rangel, E., Reza, E., Rivera, J., Roman, C., Rosas, A., Seade-Galindo, C., Teran, J., Unpingco, J., Valdez, S., & Khan, A. M. (2015b). Next generation interaction maps of hypothalamic circuits controlling survival behaviors. *Hypothalamic Circuits for Control of Survival Behaviors Workshop*; 2015 Sep 27; Janelia Farm Research Campus, Ashburn, Virginia.

Wells, C. E., Acosta, A., Aldrete, D., Carrion, A., Castro, L., Escapita, A. C., Espinoza, E., De La Fuente, K., Garrett, A., Gomez, A., Gomez, N., Hernandez-Casner, C., Luevano, M., Lopez, A., Martinez, D., Mendoza, E., Ortega, M., Perez, M., Rangel, E., Reza, E., Rivera, J., Roman, C., Rosas, A., Seade-Galindo, C., Teran, J., Unpingco, J., Valdez, S., & Khan, A. M. (2015c). Hypothalamic chemoarchitecture in the adult male rat: Creating canonical atlas maps for co-visualized immunoreactive peptidergic neuronal populations (α-MSH, nNOS, MCH) and their fiber systems in multiple brains. Program No. 616.08. *2015 Neuroscience Meeting Planner*. Chicago, IL. Society for Neuroscience, 2015. Online.

West, G. (2017). *Scale: the universal laws of life, growth, and death in organisms, cities, and companies*. New York: Penguin Books.

Wicks, R. (2004). Being in the dry Zen landscape. *The Journal of Aesthetic Education*, *38*(1), 112–122. https://www.jstor.org/stable/3527367

Wirfs-Brock, A., & Eich, B. (2020). JavaScript: the first 20 years. *Proceedings of the ACM on Programming Languages*, *4*, HOPL, Article 77 (June 2020), 189 pages. https://doi.org/10.1145/3386327

Witten, I. B., Steinberg, E. E., Lee, S. Y., Davidson, T. J., Zalocusky, K. A., Brodsky, M., *et al*. (2011). Recombinase-driver rat lines: Tools, techniques, and optogenetic application to dopamine-mediated reinforcement. *Neuron*, *72*, 721–733. https://doi.org/10.1016/j.neuron.2011.10.028

Wood, M., Adil, O., Wallace, T., Fourman, S., Wilson, S. P., Herman, J. P., *et al*. (2019). Infralimbic prefrontal cortex structural and functional connectivity with the limbic forebrain: a combined viral genetic and optogenetic analysis. *Brain Structure and Function*, *224*, 73–97. https://doi.org/10.1007/s00429-018-1762-6

Woodward, D. J., Smith, W. K., Schlusselberg, D. S., Azizi, S. A., & Chapin, J. K. (1985). Tasks in computer-assisted neuroanatomy: Data acquisition, imaging and database, In: *Quantitative neuroanatomy in transmitter research* (L. F. Agnati; K. Fuxe, eds.), Wenner-Gren International Symposium series, volume 42, pp. 25–39. New York: Plenum Press.

Yao, S. T., Gouraud, S., Paton, J. F., & Murphy, D. (2005). Water deprivation increases the expression of neuronal nitric oxide synthase (nNOS) but not orexin-A in the lateral hypothalamic area of the rat. *The Journal of Comparative Neurology*, *490*(2), 180–193. https://doi.org/10.1002/cne.20662

Yao,Y., Taub, A. B., LeSauter, J., & Silver, R. (2021). Identification of the suprachiasmatic nucleus venous portal system in the mammalian brain. *Nature Communications*, *12*, 5643. https://doi.org/10.1038/s41467-021-25793-z

Xie, Y., & Dorsky, R. I. (2017). Development of the hypothalamus: conservation, modification and innovation. *Development*, *144*, 1588–1599. https://doi.org.10.1242/dev.139055

Zallar, L. J., Tunstall, B. J., Richie, C. T., Zhang, Y. J., You, Z. B., Gardner, E. L., *et al*. (2019). Development and initial characterization of a novel ghrelin receptor CRISPR/Cas9 knockout Wistar rat model. *International Journal of Obesity*, *43*, 344–354. https://doi.org/10.1038/s41366-018-0013-5

Zoghby, M. M., Erickson, B. J., & Conte, G. M. (2024). Generative Adversarial Networks for brain MRI synthesis: impact of training set size on clinical application. *Journal of Imaging Informatics in Mediccine*, *37*, 1228–1238. https://doi.org/10.1007/s10278-024-00976-4

Zoli, M., Agnati, L. F., Tinner, B., Steinbusch, H. W. M., & Fuxe, K. (1993). Distribution of dopamine-immunoreactive neurons and their relationships to transmitter and hypothalamic hormone-immunoreactive neuronal systems in the rat mediobasal hypothalamus. A morphometric and microdensitometric analysis. *Journal of Chemical Neuroanatomy*, *6*(5), 293–310. https://doi.

org/10.1016/0891-0618(93)90034-2

Zséli, G., Vida, B., Martinez, A., Lechan, R. M., Khan, A. M., & Fekete, C. (2016). Elucidation of the anatomy of a satiety network: Connectivity of the parabrachial nucleus in the adult rat. *The Journal of Comparative Neurology*, *524*, 2803–2827. https://doi.org/10.1002/cne.23992